1988

Boundary layer response to an unsteady turbulent environment.

Renoud, Robert W.

Monterey, California. Naval Postgraduate School

NAVAL POSTGRADUATE SCHOOL
Monterey, California

THESIS

BOUNDARY LAYER RESPONSE TO AN UNSTEADY TURBULENT ENVIRONMENT

by

Robert W. Renoud

December 1988

Thesis Advisor Richard M. Howard

REPORT DOCUMENTATION PAGE

Report Security Classification Unclassified		1b Restrictive Markings	
Security Classification Authority		3 Distribution Availability of Report Approved for public release; distribution is unlimited.	
Declassification Downgrading Schedule			
Performing Organization Report Number(s)		5 Monitoring Organization Report Number(s)	
Name of Performing Organization aval Postgraduate School	6b Office Symbol *(if applicable)* 31	7a Name of Monitoring Organization Naval Postgraduate School	
Address *(city, state, and ZIP code)* onterey, CA 93943-5000		7b Address *(city, state, and ZIP code)* Monterey, CA 93943-5000	
Name of Funding Sponsoring Organization	8b Office Symbol *(if applicable)*	9 Procurement Instrument Identification Number	
Address *(city, state, and ZIP code)*		10 Source of Funding Numbers	
		Program Element No / Project No / Task No / Work Unit Accession No	

Title *(include security classification)* BOUNDARY LAYER RESPONSE TO AN UNSTEADY TURBULENT ENVIRON-ENT

Personal Author(s) Robert W. Renoud

a Type of Report	13b Time Covered	14 Date of Report *(year, month, day)*	15 Page Count
aster's Thesis	From To	December 1988	123

Supplementary Notation The views expressed in this thesis are those of the author and do not reflect the official policy or po-ion of the Department of Defense or the U.S. Government.

Cosati Codes			18 Subject Terms *(continue on reverse if necessary and identify by block number)*
eld	Group	Subgroup	Low Reynolds Number, Boundary Layer, Turbulence, Transition, Laminarization, Unsteady Aerodynamics.

Abstract *(continue on reverse if necessary and identify by block number)*

An experimental investigation of a wing boundary layer subjected to periodic turbulent flow at a Reynolds number of 0,000 was conducted. Non-thrusting turbulence pulses were generated at a rate of 50 pulses per second with a turbulence tensity near 10% by spinning a rod in the free stream flow upwind of the test airfoil.

Time-varying velocity measurements were made at three representative chord locations (laminar, transitional turbulent, lly turbulent) at one angle of attack using single-element hot-wire anemometry. The characteristics of the boundary layer locity profiles, turbulence intensity profiles, and velocity spectra and total spectral power were documented.

The time-varying boundary layer response could be characterized by three flow regimes: undisturbed flow: turbulence lse; and recovery period. The boundary layer exhibited a cyclic transition response varying from the undisturbed flow re-me to the turbulence pulse regime back to the undisturbed flow regime. The turbulence pulse was found to penetrate into e entire boundary layer. The turbulence pulse prompted laminarization of the flow during the recovery period. aminarization apparently resulted from rapid acceleration of the near-surface flow within the boundary layer due to turbu-nce induced momentum transfer down through the boundary layer and local flow acceleration following the velocity deficit the turbulence pulse. The effects of the periodic turbulence pulse were most noticeable in the recovery period at the nsitional/turbulent and fully turbulent regions of the wing. Recovery was generally characterized by lowered turbulence vels and reduction in boundary layer thickness, indicating a stabilizing effect of the external turbulence pulse.

Distribution Availability of Abstract unclassified unlimited ☐ same as report ☐ DTIC users	21 Abstract Security Classification Unclassified	
a Name of Responsible Individual chard M. Howard	22b Telephone *(include Area code)* (408) 646-2870	22c Office Symbol 67HO

FORM 1473,84 MAR 83 APR edition may be used until exhausted
All other editions are obsolete

security classification of this page

Unclassified

Approved for public release; distribution is unlimited.

Boundary Layer Response to an Unsteady Turbulent Environment

by

Robert W. Renoud
Lieutenant Commander, United States Coast Guard
B.B.A., Northwood Institute, 1980

Submitted in partial fulfillment of the
requirements for the degree of

MASTER OF SCIENCE IN AERONAUTICAL ENGINEERING

from the

NAVAL POSTGRADUATE SCHOOL
December 1988

ABSTRACT

An experimental investigation of a wing boundary layer subjected to periodic turbulent flow at a Reynolds number of 500,000 was conducted. Non-thrusting turbulence pulses were generated at a rate of 50 pulses per second with a turbulence intensity near 10% by spinning a rod in the free stream flow upwind of the test airfoil.

Time-varying velocity measurements were made at three representative chord locations (laminar, transitional/turbulent, fully turbulent) at one angle of attack using single-element hot-wire anemometry. The characteristics of the boundary layer velocity profiles, turbulence intensity profiles, and velocity spectra and total spectral power were documented.

The time-varying boundary layer response could be characterized by three flow regimes: undisturbed flow; turbulence pulse; and recovery period. The boundary layer exhibited a cyclic transition response varying from the undisturbed flow regime to the turbulence pulse regime back to the undisturbed flow regime. The turbulence pulse was found to penetrate into the entire boundary layer. The turbulence pulse prompted laminarization of the flow during the recovery period. Laminarization apparently resulted from rapid acceleration of the near-surface flow within the boundary layer due to turbulence induced momentum transfer down through the boundary layer and local flow acceleration following the velocity deficit of the turbulence pulse. The effects of the periodic turbulence pulse were most noticeable in the recovery period at the transitional/turbulent and fully turbulent regions of the wing. Recovery was generally characterized by lowered turbulence levels and reduction in boundary layer thickness, indicating a stabilizing effect of the external turbulence pulse.

TABLE OF CONTENTS

LIST OF FIGURES

NOMENCLATURE

c	wing chord
F	tunnel calibration factor
f_c	cutoff frequency
f_n	Nyquist frequency
f_s	sampling frequency
K	acceleration parameter $\frac{\nu}{U^2}\frac{dU}{dx}$
p_t	total pressure
p	static pressure
Δp	differential static pressure
q	test section dynamic pressure
R_c	chord Reynolds number $\frac{U_\infty c}{\nu}$
T_u	turbulence intensity $\sqrt{\frac{\overline{u'^2}}{U_e}}$
U	streamwise mean velocity or ensemble average velocity
u	streamwise instantaneous velocity
v	test section velocity
x	streamwise coordinate
y	coordinate direction normal to and away from surface
δ	boundary layer thickness
ν	kinematic viscosity
ρ	density

subscripts

e	boundary layer edge value
∞	free stream value

superscripts

$'$	fluctuating quantity
$-$	time mean value

ACKNOWLEDGEMENT

This work was funded by the Aircraft Division, Research and Technology, Naval Air Systems Command, under the supervision of Thomas Momiyama and Harry Berman.

I wish to thank the following NPS Aeronautical Engineering Department engineers and technicians whose contributions made this investigation possible:

Pat Hickey - Laboratory Supervisor

Alan McGuire - Laboratory Aeronautical Engineer

Jim Nageotte - Composites and Structures Technician

Ron Ramaker - Wood and Plastics Model Shop Technician

John Moulton - Metal Model Shop Technician

Ronald Harvey - Metal Model Shop Technician

Jack King - Electronics Shop Technician

I wish also to thank Dr. Rick Howard for his guidance, support, and help throughout each stage of this project.

Finally, I wish to thank my wife, Ashley, and my children, Keli and Christina. Together we undertook the challenge of graduate education; and together, with God's help and guidance, we were found equal to the task.

I. INTRODUCTION

A. BACKGROUND

Airfoil experimental research at low chord Reynolds numbers has become a major field of academic, military, and civil interest in the last few years due to the current development of low-speed remotely piloted vehicles (RPVs), manned and unmanned ultra-light aircraft, human-powered aircraft, and high altitude station keeping aircraft. Low Reynolds number flight ($R_c < 500{,}000$) is generally considered as very low speed flight, or flight with a short wing chord. Low Reynolds number flight also occurs at high altitudes where the air density is low. Most low Reynolds number data in the past have come from experiments on gliders and model airplanes. [Ref. 1]

The aerodynamic response of a wing at low Reynolds numbers is considerably different than for Reynolds numbers greater than about 500,000. At low Reynolds numbers, laminar flow exists for a distance downstream from the leading edge. As such, the laminar to turbulent transition occurs much further back on the wing, often in the adverse pressure gradient region. The transition area is often quite broad and not well defined. In addition, the transition process is very sensitive to free stream disturbances, external turbulence, and surface imperfections.

Laminar flow tends to separate easily at low Reynolds numbers especially in the presence of an adverse pressure gradient. Leading and trailing edge separation is frequently observed as well as separation along the airfoil. Separation along the airfoil is commonly referred to as the "laminar separation bubble". Laminar separation bubbles greatly affect the performance of the wing. The most efficient low Reynolds number airfoils are designed to obtain maximum benefit from the separation bubble; but only because the separation bubble cannot be completely eliminated at low Reynolds numbers. Numerous factors also affect the size, shape, and character of the separation bubble including free stream disturbances, vibration, surface condition, angle of attack, etc.

The critical nature of the boundary layer and the many factors that influence it have prompted many recent investigations in the characteristics of airfoils and wings at low Reynolds numbers. Although investigations under steady state conditions provide important lift, drag, and airfoil performance data, they may not reliably predict the laminar to turbulent transition, leading and trailing edge separation, and formation and reat-

tachment of the separation bubble as these phenomena may be influenced to a high degree by unsteadiness in the flow. [Ref. 1]

Unsteady low Reynolds number aerodynamic research has recently been undertaken on three fronts:

Airfoil response to high steady-state free stream turbulence

Airfoil response to low to moderate frequency sinusoidal modulation of the free stream

Airfoil response to transient free stream disturbances

Meier and Kreplin [Ref. 2], Potter et al. [Ref. 3], and Kindelspire [Ref. 4], among others, have investigated airfoil performance and boundary layer development and behavior in the presence of high free stream turbulence. Meier and Kreplin found that both the intensity and spectral distribution (length scale) of the free stream turbulence affected airfoil performance. The most significant changes were noted when the length scales were on the order of the boundary layer thickness. Potter et al. also found that the free stream turbulence intensity spread into the entire boundary layer, but the effect was dependent on length scale. They also noted that the free stream turbulence has to penetrate and alter the velocity profile before producing any significant change in the boundary layer detachment location. Kindelspire found that increasing levels of free stream turbulence caused correspondingly earlier laminar to turbulent transition. He also confirmed that turbulence length scales on the order of the boundary layer thickness had the most influence on boundary layer thickness.

Brendel [Ref. 5] performed a wind tunnel study with unsteady flow consisting of a streamwise sinusoidal velocity variation. Brendel found that, in general, the imposed unsteadiness had little effect on the mean boundary layer thickness. The unsteadiness did, however, reduce the thickness and length of the separation region associated with the separation bubble. He also found that lower frequencies (large length scales) had no effect on the overall flow.

Howard [Ref. 6] most recently investigated the time varying characteristics of the boundary layer of an airfoil immersed in a propeller slipstream (see Figure 1). The propeller wake subjected the airfoil to a transient free stream disturbance. Howard found that the wing boundary layer varied from laminar to turbulent in response to the passage of the propeller wake. He also found, in general, that the effects of the propeller slipstream tended to enhance the stability of the boundary layer and reduced the drag coefficient in the laminar portion of the slipstream cycle below its undisturbed value.

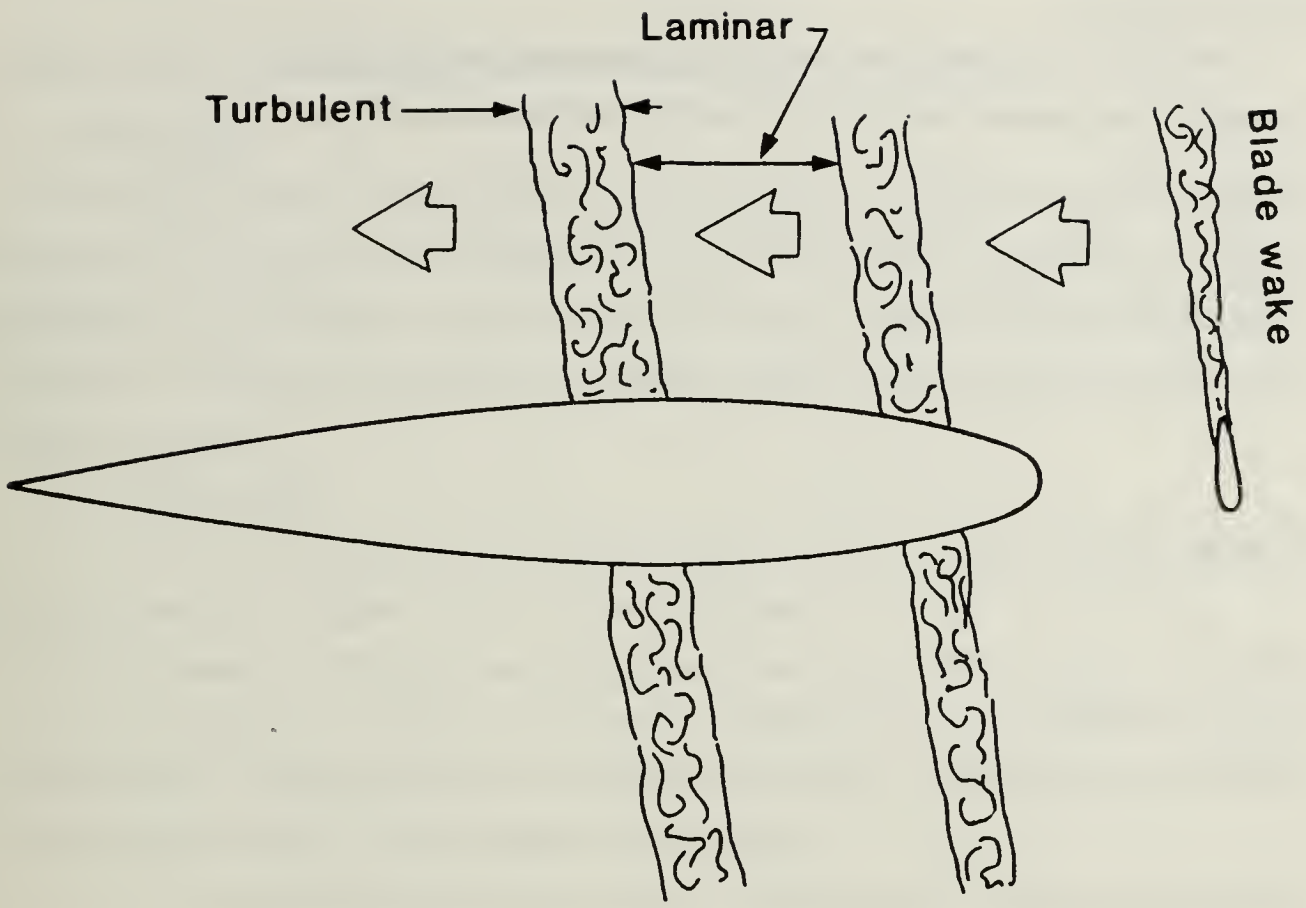

Figure 1. Wing Immersed in Propeller Slipstream: [Ref. 6: p. 17]

In particular, Howard noted a distinct relaminarization process at work during the transition from turbulent to laminar flow as evidenced by a decrease in turbulence and an increase in velocity near the surface.

B. THESIS OBJECTIVES

The goal of this study is to thoroughly investigate the boundary layer response over a wing to periodic free stream disturbance at the laminar, transitional, and turbulent portions of the wing.

This thesis describes the design, fabrication, and testing of a non-thrusting periodic turbulence generating device to simulate transient phenomena such as wind gust or turbulent wake disturbances. The investigation consists of wind tunnel tests of an airfoil operating in a periodically disturbed free stream at a chord Reynolds number of approximately 500,000. Measured data are presented in the form of non-stationary mean velocity and turbulence time histories at various heights above the surface; as

ensemble-average velocity profiles and turbulence profiles; and as velocity spectra and total power plots.

These data will form a base for follow-on research at high angles of attack and for work within the separation region of low Reynolds number airfoils.

II. EXPERIMENTAL EQUIPMENT

A. APPARATUS

The major hardware items utilized in this investigation included the wind tunnel, the wing section and wing mount assembly, the periodic turbulence generator, the hot-wire anemometer, the traversing mechanism, and the data acquisition and processing system. This chapter presents the specifications, design, setup, and operating characteristics of all equipment used.

1. Wind Tunnel

The Naval Postgraduate School low speed horizontal wind tunnel was employed for this experiment. Figure 2 shows the tunnel layout.

The tunnel is of single return design and measures 64 feet in length, 25.5 feet in width, and supports a 32-inch by 45-inch by 4-foot test section. The tunnel was designed by Aerolab Development Company of Pasadena, California and has been in continuous use at the Navy School since the middle 1950's. [Ref. 7]

The tunnel consists of five basic units: the fan section; diffusers; settling chamber; contraction cone; and test section. The tunnel is constructed of wood throughout and recently received a coat of fire resistant paint on the interior surface to meet OSHA standards. The paint roughened the surface somewhat; however, the level of free-stream turbulence was not significantly worsened due to the numerous anti-turbulence features built into the tunnel.

The tunnel is powered by a 100-horsepower electric motor driving a three-bladed variable-pitch propeller. Tunnel velocity is controlled by electrically setting blade pitch angle at the control unit located adjacent to the test section. A four-speed Dodge transmission is installed between the motor and the fan to provide greater tunnel velocity control over the design range of the tunnel (up to 290 ft/sec). The transmission was left in 3rd gear for all data runs with a fan shaft speed of 750 RPM.

Eight radial stator blades are mounted directly downstream of the fan on the drive shaft housing. These stator blades serve to straighten the flow and remove the swirl generated by the fan. These are the first of the installed anti-turbulence devices.

The diffuser sections are located on either side of the fan section. The gradual increase in cross-sectional area and the long length of the diffuser sections gradually slow

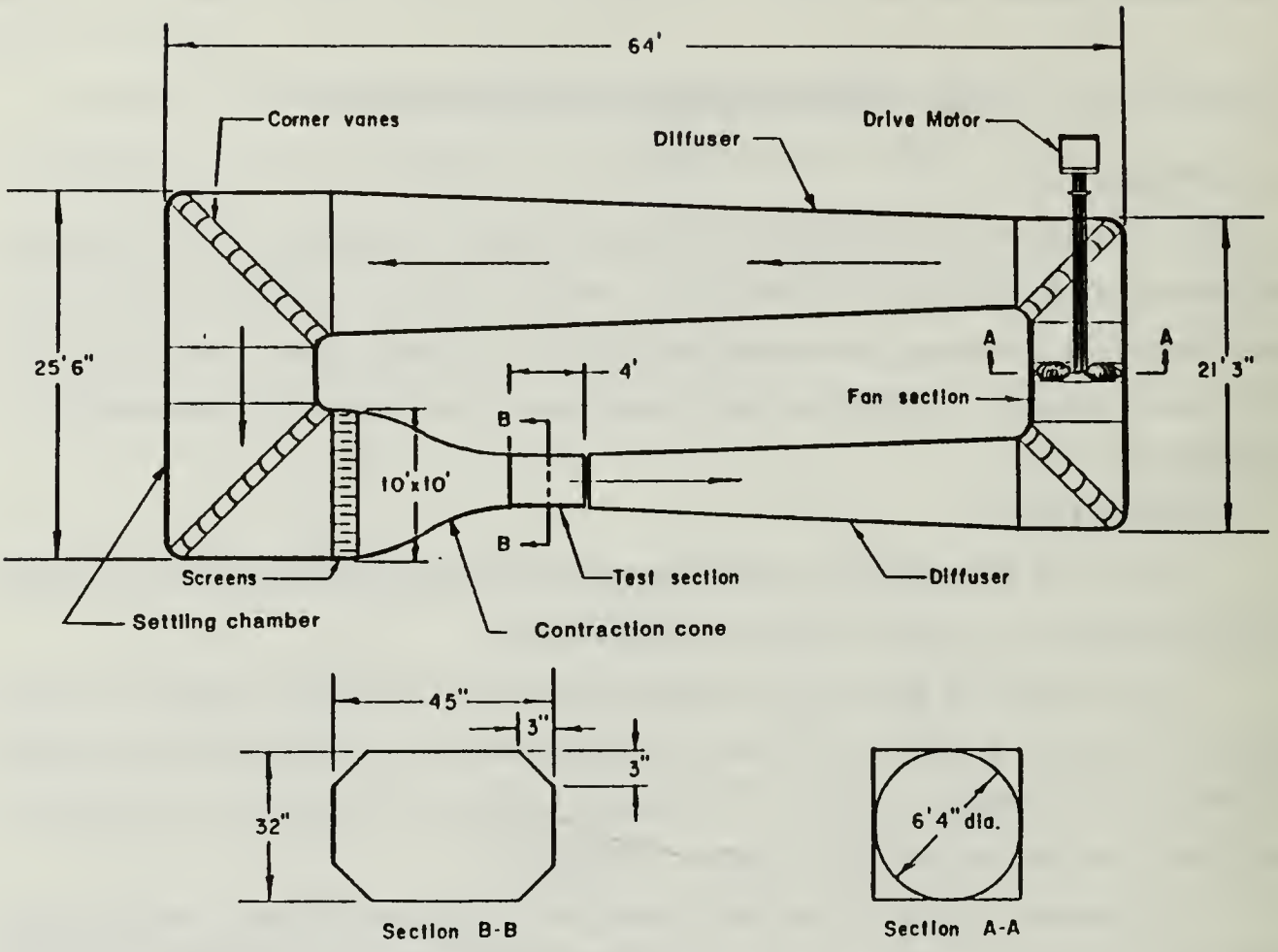

Figure 2. NPS Low Speed Wind Tunnel

the air while introducing little additional turbulence and keeping friction losses to a minimum.

The large settling chamber, located at the left of Figure 2, damps any remaining flow unsteadiness. In addition, two fine wire screens are mounted six inches apart in the settling chamber. These serve to further break up turbulent fluctuations in the flow prior to the air entering the test section.

The contraction cone accelerates the air and delivers it to the test section. The large contraction ration of 10:1 helps assure low turbulence in the test section.

The test section of the low speed wind tunnel is equipped with a full size reflection plane mounted 4 inches above the tunnel floor. The reflection plane is permanently mounted and has an electrically-driven turntable mechanism in the center (not used in this investigation). The test section is additionally equipped with full length lighting located in the corner fillets and has a hinged window on either side. The walls of the test section are slightly divergent to counteract the contraction resulting from

boundary layer growth. Breather slots are installed immediately downstream of the test section to maintain the test section at atmospheric pressure and to allow the tunnel to breath as necessary on start up and shutdown.

Two sets of static pressure port rings are installed in the tunnel and used to measure the tunnel speed. One ring set is installed just upstream of the contraction cone and the other set is installed at the test section entrance. The pressure differential across the two ring sets is measured on a water micro-manometer. This pressure differential, once calibrated, corresponds to the velocity in the test section. The wind tunnel velocity calibration procedure is covered in Chapter III.

2. Wing Section and Wing Mount Assembly

The wing section and wing mount assembly are shown in Figure 3. This installation was designed by Kindelspire [Ref. 4: pp. 11-15] and a complete description of the apparatus is contained in his work. The following paragraphs highlight the pertinent aspects of the wing and wing mount system.

The airfoil tested was a section of a Bell helicopter tail rotor (model and type unknown) having a 10-inch chord and 24-inch span. The airfoil shape is shown in Figure 4 and the section coordinates are given in Appendix A.

The airfoil section was stripped to bare metal, filled, sanded, and finished with high gloss black lacquer prior to installation. The lacquer finish was polished using fine polishing compound and given a final coat of automobile wax to bring it to the highest possible gloss. A glossy, reflective surface was important as the hot-wire anemometer probe was positioned to within 0.0032 inches of the surface by viewing the probe and its reflection through a sighting level. The probe positioning procedure is discussed in Chapter III.

The wing mount assembly consists of two 8-in wide machined aluminum endplates mounted vertically between the reflection plane and the top of the test section. The wing section is mounted between the endplates on rotatable inserts that allow the angle of attack (AOA) to be varied from +35 degrees to -15 degrees. Graduated markings on the rotatable inserts are used for coarse setting of AOA. The acutal AOA is determined by measuring the height of the leading and trailing edges above the reflection plane and solving analytically for AOA.

All data collected during this experiment were taken 1-inch left of mid-span (looking from the rear) due to the presence of several mars in the wing surface at the mid-span line which were caused by the measuring micrometer when the wing section coordinates were documented. The 1-inch offset was sufficient to remain free of dis-

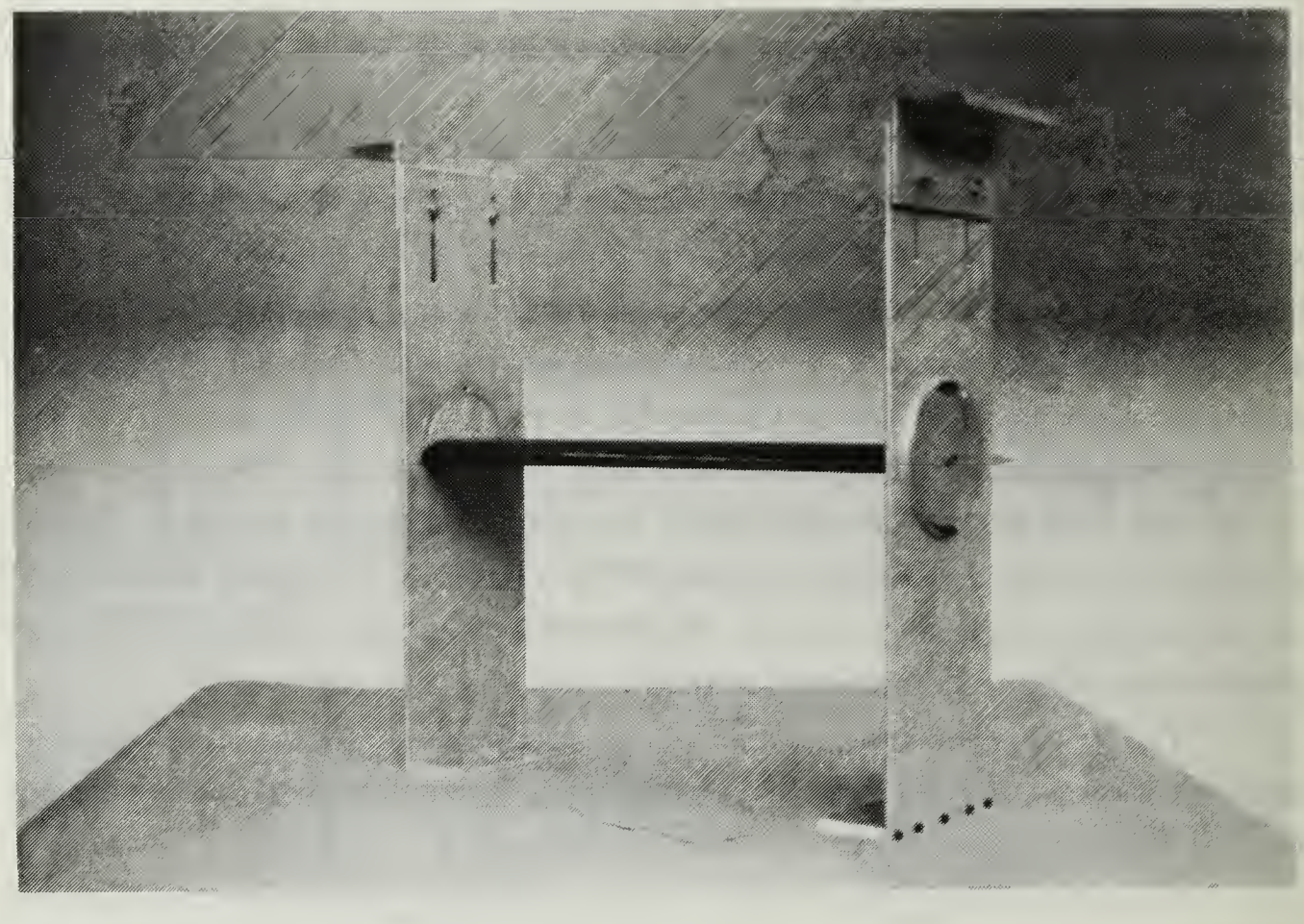

Figure 3. Wing and Wing Mount Assembly

turbances generated by the surface imperfections[1] while also remaining clear of any end plate effects [Ref. 4: pp. 13-14]. The wing was set at 0 degrees angle-of-attack (AOA) on the inscribed end plate graduations. This resulted in an actual measured AOA of 0.71 degrees. All data were collected at this AOA.

3. Periodic Turbulence Generator

Periodic turbulence pulses were generated by spinning a cylindrical metal rod in the freestream just upwind of the wing section. The turbulence generating assembly, which resembles a propeller, is shown in Figure 5. The mechanism consists of the base support assembly, cylindrical bar and hub, flexible drive shaft, and motor and timing/position sensor. The support assembly and cylindrical bar/ hub were manufactured in the NPS Department of Aeronautics and Astronautics machine shop facilities.

---

1 A general rule-of-thumb is that disturbance propagation is confined to a 15-degree arc downstream of a surface imperfection.

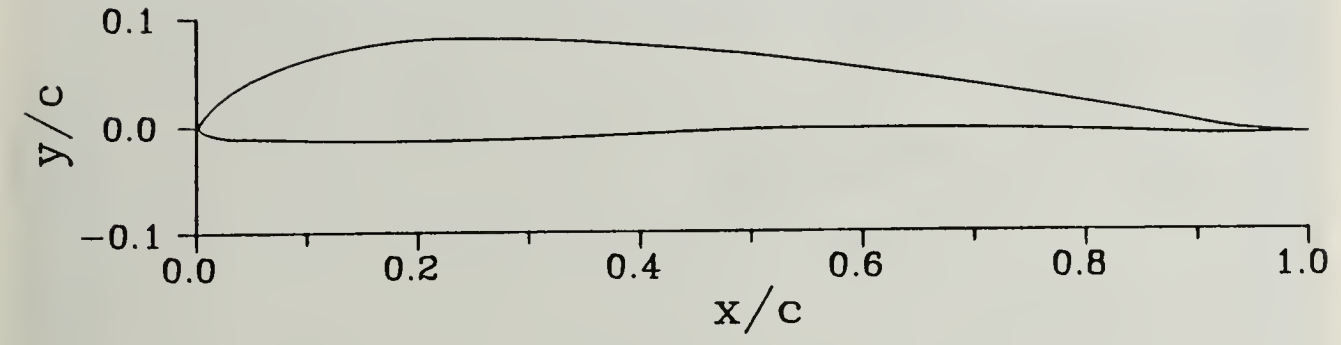

Figure 4. Experimental Airfoil Section

The support assembly was constructed out of aluminum stock and designed to bolt to the reflection plane such that the hub was position 2.5 inches below and 1 inch ahead of the wing at center span. The hub was placed well below the wing in order to allow the disturbances generated by the hub section to pass under the wing. The leading edges of the mount were also rounded and/or beveled to minimize drag and free stream disturbances. Figure 6 shows the wing/wing mount and periodic turbulence generator installed in the NPS wind tunnel.

The vertical strut of the support assembly was bored to accept the output end of the flexible drive shaft. The drive shaft was held firmly in place by a bracket mounted on the backside of the vertical strut.

The bar and hub were both machined out of stainless steel. The 18-inch by 3/8-inch diameter bar was secured to the hub by a standard 1/8-inch roll pin. The hub was bored and tapped to screw onto the threaded end of the flexible drive shaft extending from the support assembly. The hub was secured in place on the threaded shaft by a locknut. In addition, the counterclockwise direction of rotation was chosen such that the hub would tend to tighten during operation.

The 38-inch flexible drive shaft used to couple the motor and the bar/hub was purchased at a local hardware store as an electric drill extension. As noted previously, the output end had a 3/8-inch threaded shaft onto which the hub assembly was mounted. The input end of the flexible shaft was made to fit a 1/4-inch drill chuck. Use of the flexible drive shaft, rather than direct drive, reduced the size, weight, and complexity of the support assembly as it did not have to support the heavy drive motor.

The drive motor and position sensor are shown in Figure 7. The motor was mounted on the tunnel floor well clear of the wing environment at the downwind end

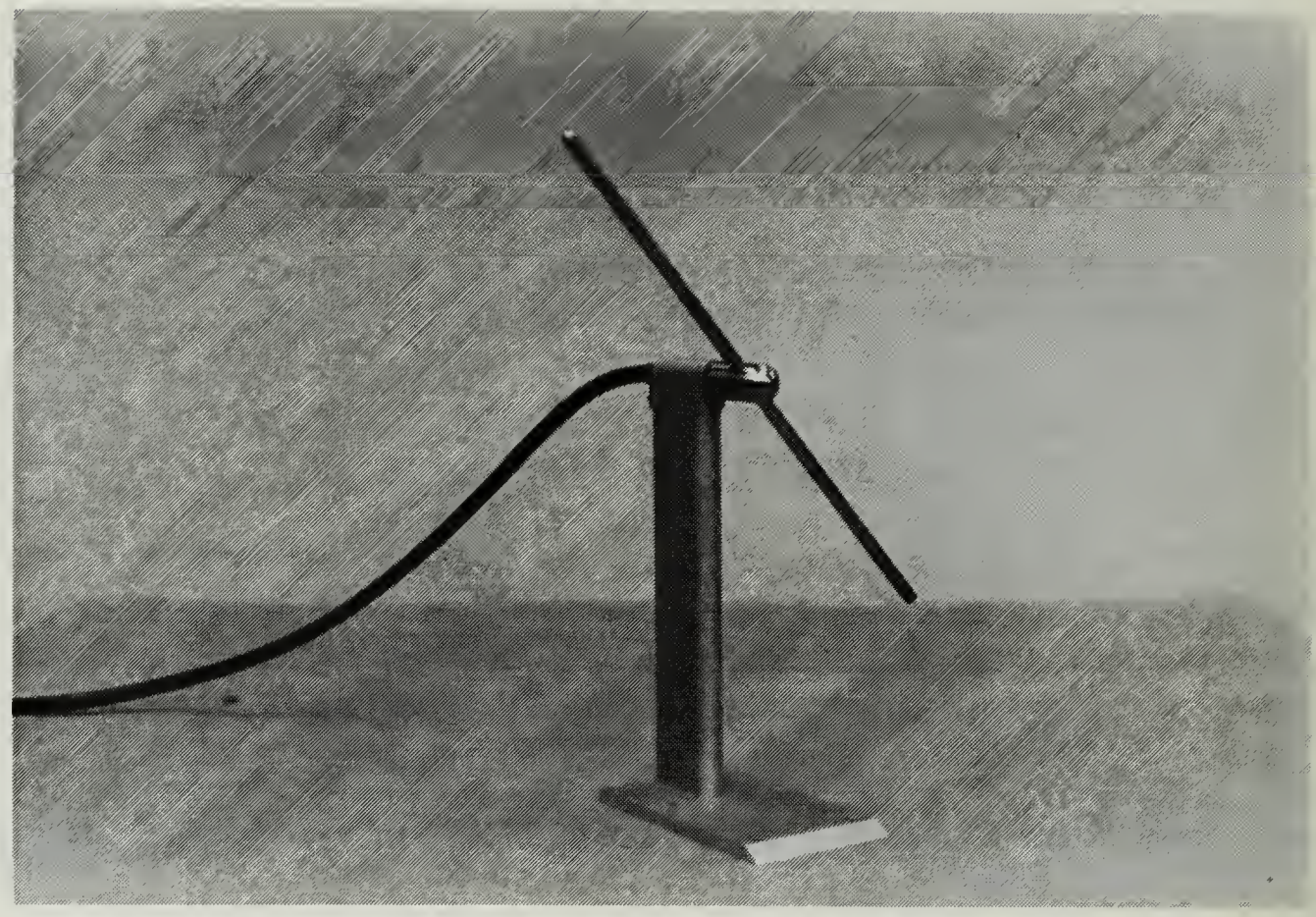

Figure 5. Periodic Turbulence Generating Assembly

of the test section. The motor is a 1 4-horsepower permanent magnet variable speed motor. Motor speed could be controlled over the range 60-2500 RPM. An adapter with a 3/8-inch threaded output shaft was manufactured to fit the 1/2-inch motor shaft. A 1/4-inch drill chuck was threaded on the adapter and used to drive the flexible shaft in this installation. A ferro-magnetic transducer was installed adjacent to the motor shaft to sense shaft speed and shaft position from a toothed steel disk mounted on the motor shaft. The toothed steel disk, seen in Figure 7, was modified by removing all but two of the original 30 teeth. Thus modified, an electrical pulse was generated twice each revolution corresponding to each passage of the bar in front of the wing section. This signal was used to drive an electronic RPM counter and provided timing information for the data acquisition system and data analysis software.

4. Hot-Wire Anemometer

Velocity and turbulence measurements were made using a Thermo System, Inc (TSI) IFA-100 System Model 150 Constant Temperature Anemometer and Model 157

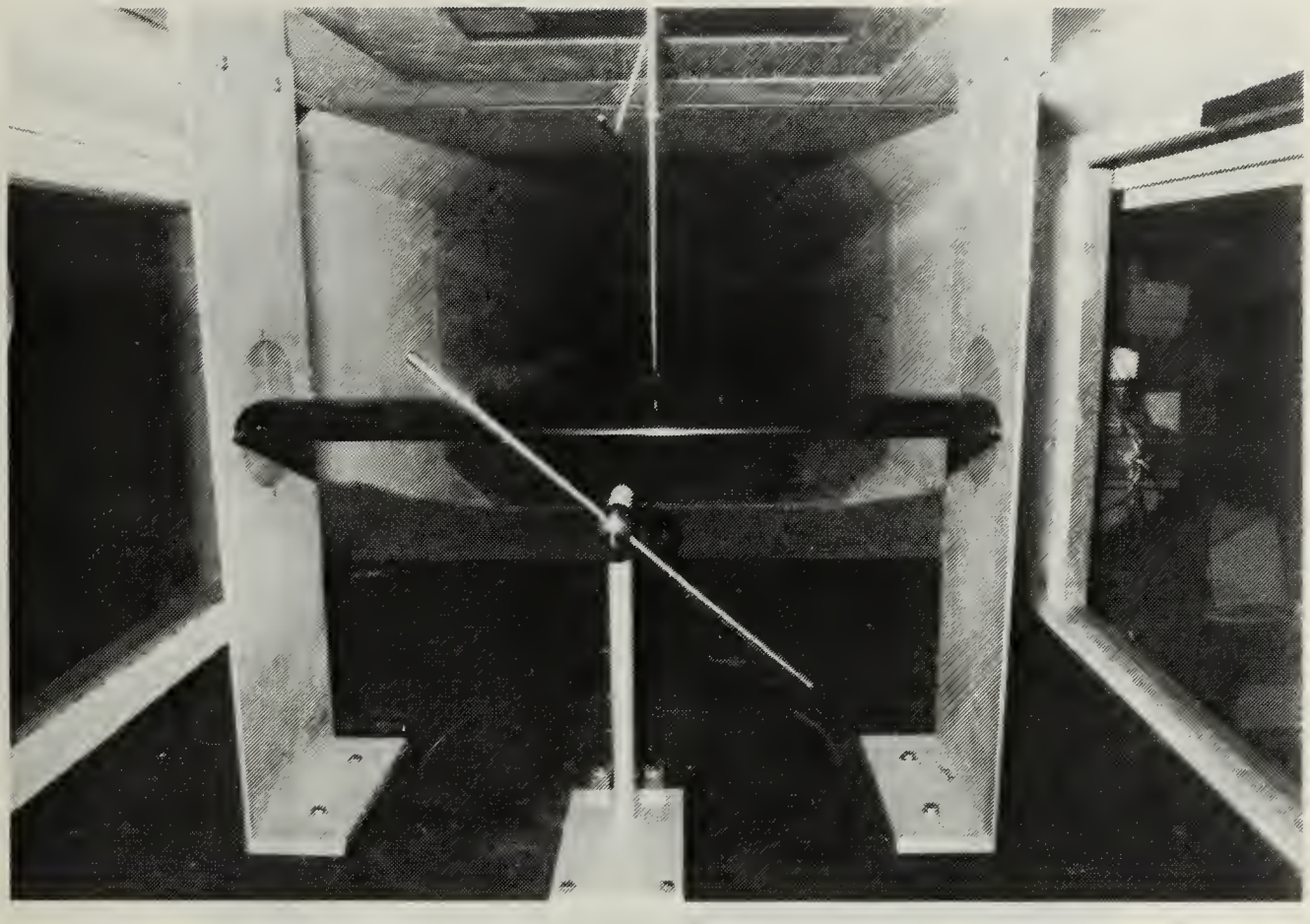

Figure 6. Wing/Wing Mount and Periodic Turbulence Generator Installed in NPS Wind Tunnel

Signal Conditioner. Figure 8 shows the IFA-100 system installation. The IFA-100 system is used with touch panel entry of all anemometer and signal conditioner settings and digital panel readouts.

The Model 150 Anemometer module was operated in the standard bridge configuration with a standard 15-foot RG-58A U probe cable. This configuration provided extremely low noise output signals with a typical frequency response of DC to 150 KHz [Ref. 8: pp. 8-3 to 8-4]. These parameters were important in order to accurately measure the low level, high frequency turbulence components of the velocity signal.

The hot-wire signal was processed using the Model 157 Signal Conditioner to improve the velocity resolution of the measurement system and to provide low pass filtering. The unconditioned hot-wire output voltage over the calibration velocity range varied from 1.5 volts at a flow rate of 40 ft/sec to 1.8 volts at 140 ft sec. With the given analog to digital voltage resolution of 2.44 millivolts, the resulting velocity resolution

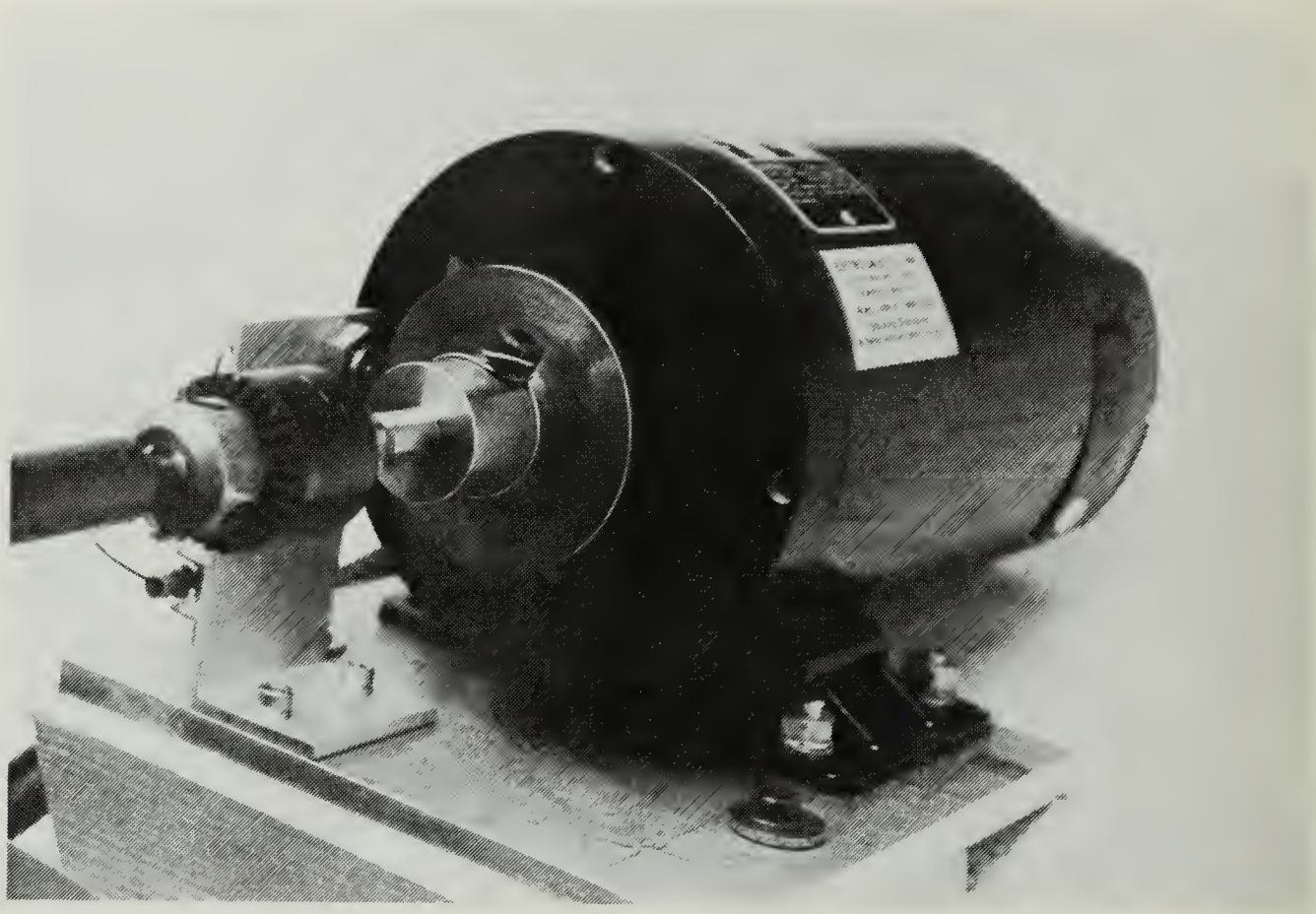

Figure 7. Drive Motor and Position Sensor

was, at best, 0.8 ft sec. By applying a -1.0 volt offset and gain of 5 to the raw signal with the signal conditioner, the output voltage over the calibration range was made to vary from 2.5 to 4.0 volts giving a velocity resolution of 0.16 ft sec--the improvement in resolution being directly related to the gain setting.

The low pass filter of the Model 157 Signal Conditioner was set as close as possible to the Nyquist cutoff frequency. The Nyquist cutoff frequency, f_n , is defined by the formula:

$$f_n = \frac{f_s}{2} \tag{1}$$

where f_s is the digital sampling rate in Hertz (Hz). To avoid serious errors in the data, it is important that the signal have no significant components in the frequency range above f_n prior to digital conversion [Ref. 9: pp. 68-69]. Setting the low pass filter to f_n effectively removes all the unwanted high frequency components.

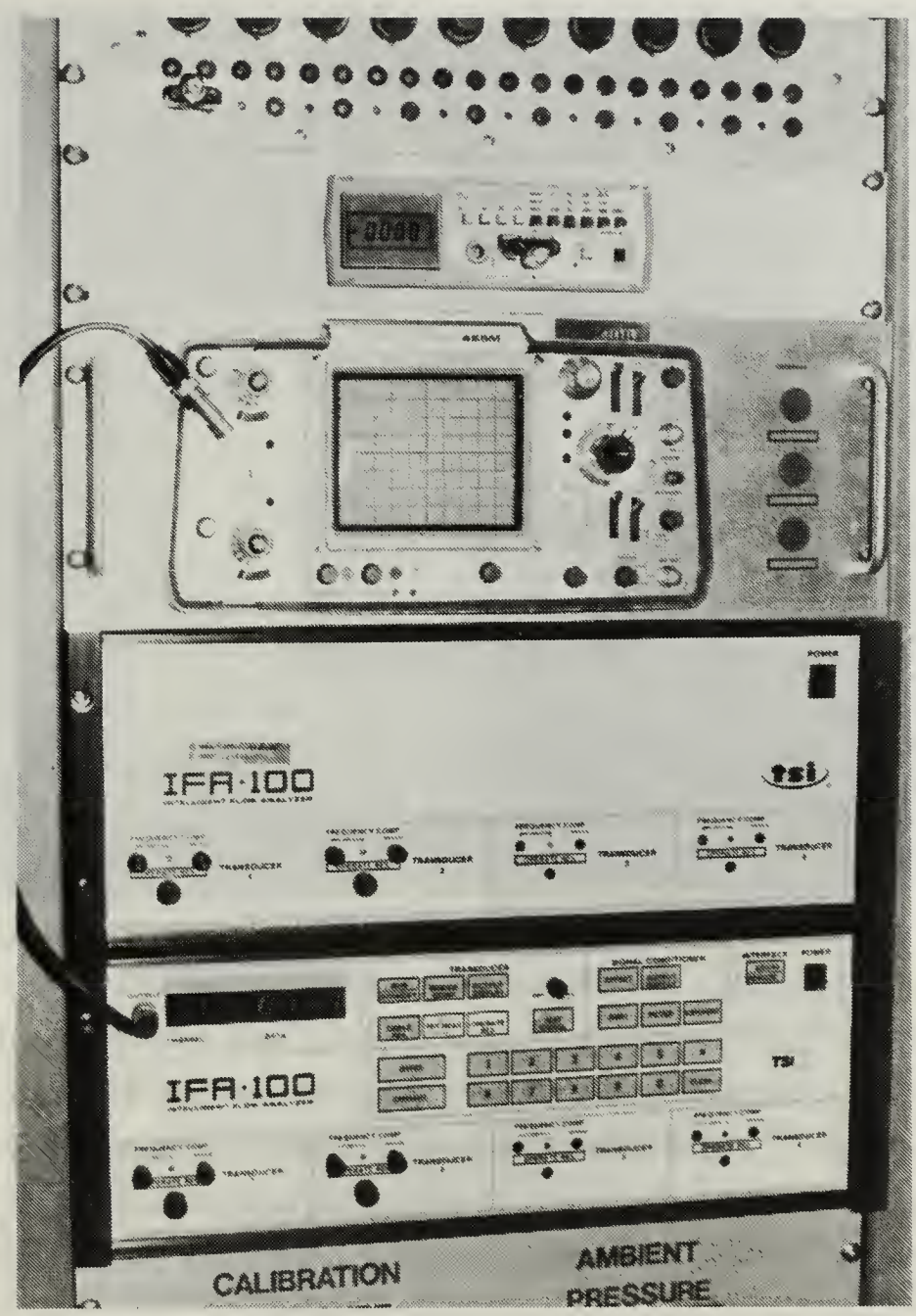

Figure 8. IFA-100 Anemometer System

A Dantec 55p11 straight general purpose hot-wire probe with a 5-micron diameter platinum plated tungsten wire was used for all measurements.

The oscilliscope and digital voltmeter, also mounted on the IFA-100 equipment rack (Figure 8), were used to monitor the hot-wire signal during each run. The digital voltmeter was set to read the mean DC, or steady state, component of the signal and

served to monitor the steady state velocity. The oscilliscope displayed the AC, or turbulent, component of the signal and served to monitor turbulence in the flow.

The calibration procedures for the anemometer are covered in Chapter III of this report.

5. Three Dimensional Traverser

Figure 9 shows the Velmex 8300 Control/Driver 3-D traversing system employed to position the hot-wire probe through the boundary layer. The traverser configuration used by this investigator was identical to that utilized and described by Kindelspire [Ref. 4: pp. 21-24].

The traverser was mounted above the test section, thus allowing the hot-wire probe to be positioned spanwise, chordwise, and vertically in relation to the wing section. Minimum incremental movement in any of the three directions was 0.000125 inches. The traverser could be controlled either manually or by software command from a personal computer interface. An IBM PC/AT was used to control the traverser in this installation. The software routine used to drive the traverser is explained in a later section of this chapter.

6. Analog-to-Digital Data System

Data collection was accomplished using a PC/AT-type personal computer coupled to a Metrabyte Model DAS-16F analog-to-digital converter.

The PC/AT-type personal computer used for data collection and analysis was configured with a 40 megabyte hard disk, two high density disk drives, and operated at a throughput speed of 12 MHz. The computer was additionally equipped with 1 megabyte of random access memory. The large storage capacity was necessary to handle the volume of data collected in this investigation. Each sample point yielded close to 1 megabyte of raw data and over 150 points were sampled.

The Metrabyte DAS-16F is a 12-bit very high speed analog to digital interface designed for use with IBM and IBM compatible personal computers. The board fits directly in an expansion slot in the computer. The analog inputs were brought in through an external interface junction box. The board operates at a maximum rate of 100,000 samples/sec (Hz) with up to 16 single ended or 8 differential analog input channels. The DAS-16F offers a wide range of operating parameters including four triggering options, three data transfer options, nine selectable input voltage ranges, and various other input/output modes.

The DAS-16F was configured to read two differential channels (hot-wire voltage and timing pulse) over the input range of 0-5 volts. This resulted in an analog-to-digital

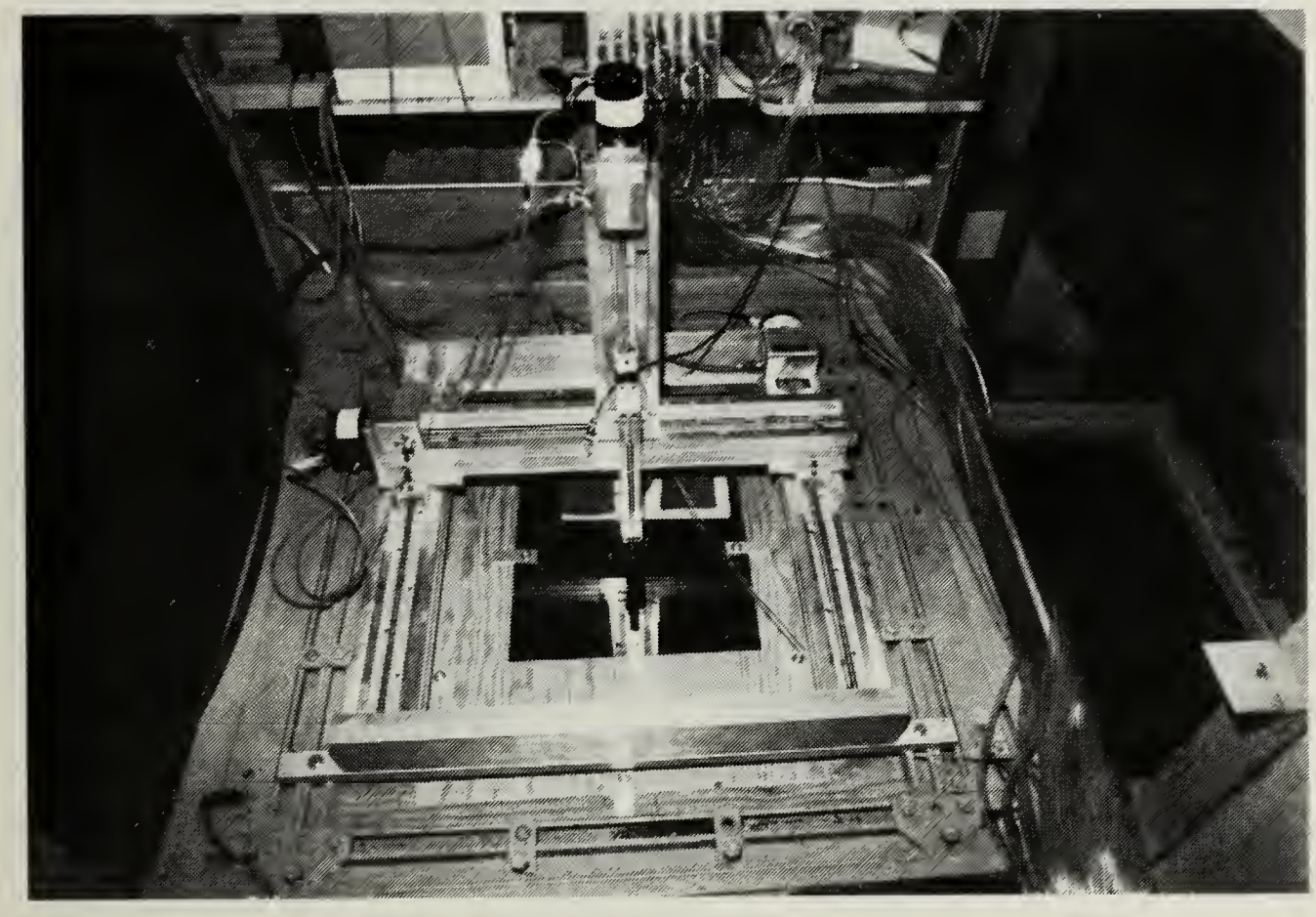

Figure 9. 3-D Traverser

resolution of 2.44 millivolts. The board was operated at its maximum sample rate of 100.000 Hz (50.000 Hz per channel) during this experiment.

B. SOFTWARE

The computer played an important role in all phases of data collection and analysis in this investigation. The entire experiment was conducted using two PC AT-type computers. The software programs created for each phase of the investigation are detailed in this section. The computer code for each of the programs developed by this author is contained in Appendix C through Appendix F.

1. Data Collection Software

The programs in this section facilitated data collection and performed the following control functions:

3-D Traverser Control (TRAVERSE.BAS)

Hot-Wire Calibration (HWCAL.BAS)

Analog-to-Digital Board control (LABTECH NOTEBOOK)

Data Acquisition in the Boundary Layer (BLDATA.BAS)

a. Program TRAVERSE.BAS

The program TRAVERSE.BAS provides discrete or automated motor movement control of the VELMEX 8300 traverser through interactive keyboard commands from an IBM PC/AT computer. The TRAVERSE.BAS program written by Kindelspire [Ref. 4: pp. 27-30] was modified by this author to remove manual data entry routines and to improve the accuracy of the motor stepping routines.

Program TRAVERSE gives the operator the option to input individual discrete step commands from the keyboard or to elect automated movement sequences. Discrete inputs were generally used to position the hot-wire in the boundary layer prior to each investigation. Discrete movements could be entered for any or all of the three directions with the minimum movement being 0.000125 inches in any one direction. Once the hot-wire was positioned, the operator then selected computer controlled movement to advance the probe through the boundary layer during the data acquisition process.

The computer stepped the hot-wire through the boundary layer according to the positioning algorithm of Equation 2:

$$z(j) = BL\left\{1 - \left[\sin\left(\frac{\pi}{2}\right)\right]\left[1 + \frac{(j-1)}{(n-1)}\right]\right\} \tag{2}$$

z(j) = Position in the boundary layer
BL = Estimated boundary layer thickness
n = Number of data points desired
j = Incremental data point

The sine function based algorithm of Equation 2 is designed to concentrate many smaller incremental steps at the bottom of the boundary layer and gradually increase the increment size toward the top of the layer. Special care was taken in writing the actual stepping routine to ensure motor movement commands were given in multiples of the motor step interval (0.000125 inches) to preclude cumulative roundoff errors throughout the boundary layer.

b. Program HWCAL.BAS

This program, written by the author, is used to calibrate the hot-wire

anemometer. The program was written in Microsoft[2] QuickBasic and compiled to generate a stand alone executable program.

The hot-wire is calibrated against a reference pitot-static probe located in the test section free stream adjacent to the hot-wire. Pitot-static input is in centimeters (cm) of water as read on a micro-manometer. These data are manually entered on the keyboard by the operator for each calibration point while the corresponding hot-wire voltage from the IFA-100 Anemometer is digitally read by the Metrabyte DAS-16F analog-to-digital converter board. The operator also enters the ambient temperature and pressure at the conclusion of each run. One thousand hot-wire samples are read and averaged at each calibration point[3]. The hot-wire was generally calibrated at 1, 2, 3, 4, 6, 8, and 10 cm of water providing accurate calibration data over the velocity range 40-140 ft/sec. Program output consists of five columns of data suitable for plotting using most current graphing software packages:

Pitot-static pressure (cm of water)

Hot-wire voltage (volts)

Free-stream velocity (ft/sec)

(Hot-wire voltage) ** 2

Velocity ** .5

The hot-wire calibration procedures are covered in Chapter III of this report.

c. LABTECH NOTEBOOK

The commercial software package *LABTECH NOTEBOOK (Version 4.3)* marketed by Laboratory Technologies Corporation[4] provided set up and operating control of the DAS-16F analog-to-digital board. Using the NOTEBOOK menus, the operator was able to enter all the operating parameters including sample rate, channels to sample, run duration, start mode, output data file name and output device, and data output format. NOTEBOOK allowed this investigator to take and store up to 130,000 data samples during any one run while operating at the 100,000 Hz rate. Other software control programs appeared to be limited to 32,000 samples under the same operating conditions. This feature was paramount, as a minimum data capability of 92,000 discrete samples was required at each point.

---

2 Microsoft is a registered trademark of Microsoft Corporation

3 The suggested analog to digital sample rate is 1000 Hz with a run period of 1.01 seconds.

4 LABTECH is a registered trademark of Laboratory Technologies Corporation.

d. Program BLDATA.BAS

This driver program controls the analog-to-digital data acquisition process. Program BLDATA.BAS was written in QuickBasic and compiled to generate a stand alone executable program. The user inputs the number of data points desired in the boundary layer and a common output file name. BLDATA then calls NOTEBOOK which in turn initiates data collection. Once the data are collected and the output file written by NOTEBOOK, BLDATA renames the output file giving it a sequentially numbered tag and prepares for another data point in the boundary layer. At the completion of the run, the investigator has a directory of sequentially named files relating to each data point.

2. Data Analysis Software

The author used the data analysis software routines specifically developed by Johnson [Ref. 10] to analyze the periodic, non-steady velocity and turbulence data obtained in this investigation. These programs are not reproduced here due to their length and considerable documentation. A summary, however, of Johnson's main programs as well as those written by the author is provided.

a. Program CONVERT.FOR

This program was written by the author to convert the raw hot-wire voltage and position sensor voltage into velocity data and a synchronization pulse. Input data was in ASCII integer form with the integer values 0 to 4095 representing 0 to 5 volts. The bar sensor voltage was processed to return a 2 at the exact center of the position sensor pulse and a 0 elsewhere. The hot-wire voltage to velocity conversion constants are obtained from the hot-wire calibration data from program HWCAL discussed previously.

b. Program MEANSMU.FOR

This program, written by Johnson [Ref. 10: pp. 158-166], computes the time varying mean of a non-stationary, periodic time series. The data are first ensemble averaged in the time domain and then transformed into the frequency domain via a Fast Fourier Transform (FFT). The ensemble is then smoothed by applying a low pass digital filter to the ensemble. The ensemble is then transformed back into the time domain by an inverse FFT and written to the output file. The amount of smoothing is a function of the low pass filter cutoff frequency. The lower the cutoff frequency, the greater the smoothing and vice versa. The amount of smoothing can be specified by the user through keyboard input. The methodology of selecting the low pass cutoff frequency is detailed in Chapter IV.

c. Program TURBIN.FOR

Written by Johnson [Ref. 10: pp. 173-181], this program computes the instantaneous turbulence intensity of a non-stationary, periodic time series. It is the turbulence intensity counterpart of the non-stationary mean program MEANSMU. TURBIN first calculates the time varying mean velocity of each ensemble by low pass filtering in the frequency domain. TURBIN then determines the instantaneous turbulent (fluctuating) component at each point on each ensemble. The turbulence components are then ensemble averaged and and written to the output file. As in MEANSMU, the user can specify the cutoff frequency of the low pass filter used to smooth the individual ensembles.

d. Program PSD.FOR

This program, written by Johnson [Ref. 10: pp. 182-190], computes the power spectral density of a real discrete steady time series. This program was for spectral analysis of the free stream flow in the test section.

e. Program ENSPSDAV.FOR

This program, written by Johnson [Ref. 10: pp. 191-202], performs spectral analysis on a short time segment of an ensemble of non-stationary, periodic, turbulent velocity data. Whereas program PSD performs spectral analysis on a steady state signal, ENSPSDAV investigates the time varying spectrum on selected portions of the ensemble itself. As such, the author was able to separately investigate the undisturbed flow segment, the turbulence pulse, and the laminar flow/recovery period and characterize the power spectrum and power content of each.

III. EXPERIMENTAL PROCEDURE

A. WIND TUNNEL TEST SECTION CALIBRATION

The purpose of wind tunnel test section calibration was to determine the relationship between the actual free stream dynamic pressure (q) in the test section and the measured static pressure differential (Δp) across the contraction cone. This relationship is used to indirectly determine test section free stream velocity by measuring Δp.

For this calibration, a reference pitot-static probe was inserted in the center of the test section. A differential micro-manometer was connected across the total and static ports of the pitot-static probe to measure q. The relationship between the pitot-static probe differential pressure, q, and test section velocity is given by Equation 3:

$$q = (p_t - p) = \frac{\rho v^2}{2} \tag{3}$$

p_t = Total pressure measured by the pitot tube
p = Static pressure in the test section
q = Test section dynamic pressure
ρ = Density of air
v = Velocity in the test section

The static pressure differential across the contraction cone, Δp, was measured by a second differential micro-manometer connected across the two static port ring assemblies mounted in the wind tunnel walls just before and after the contraction cone. In most cases q is linearly related to Δp and can be written:

$$q = F(\Delta p) \tag{4}$$

where F is a constant called the Tunnel Calibration Factor [Ref. 7: pp. A1-1 to A1-5]. F is determined experimentally by plotting the measured values of q and Δp. The slope F is given at every point by:

$$F = \frac{q}{\Delta p} = \text{Tunnel Correction Factor} \tag{5}$$

Once F has been determined, test section velocity can be calculated from Δp by:

$$v = \sqrt{\frac{2\Delta pF}{\rho}} \tag{6}$$

Calibration measurements were taken at numerous velocities over the range of 40 - 140 ft/sec. The two differential pressures were recorded at each calibration point. Figure 10 shows the plot of q versus Δp for this calibration. The relationship is observed to be linear and the tunnel correction factor is 1.126. This value differed significantly from the calibration factor of 1.075 which has been in common use at NPS since 1982. The author speculates that the original 1982 calibration was made prior to installation of the reflection plane. Another possibility is that the new calibration factor reflects the numerous small changes made to the tunnel over the years.

B. HOT-WIRE ANEMOMETER CALIBRATION

The purpose of hot-wire anemometer calibration was to determine the equation relating hot-wire output voltage to velocity. This equation was used in the data conversion program CONVDAT.FOR described earlier in Chapter III. The hot-wire was calibrated before and after each data run. Hot-wire calibration consists of three steps:

IFA-100 system setup and initialization

Calibration data acquisition

Curve plotting and least squares fit

Initialization procedures for the IFA-100 system followed the steps for routine operation outlined in the instruction manual [Ref. 8: pp. 3-19]. The setup parameters for the IFA-100 were as follows:

Bridge	Standard Bridge Configuration
High Pass Filter	Not used
Low Pass Filter	20 KHz
Voltage Offset	-1 volt
Voltage Gain	5

As mentined in Chapter II, the low pass filter was set to the Nyquist cutoff frequency calculated by Equation 1. The Nyquist cutoff frequency for this investigation was 25 KHz. The low pass filter could only be set in increments of 10 KHz, however, so the filter was set to 20 KHz--the closest lower frequency. Voltage offset and gain were used to improve the measurement resolution of the analog-to-digital converter by expanding the output voltage range of the hot-wire anemometer, as discussed in Chapter II.

The hot-wire was calibrated against a reference pitot-static probe located near the top of the test section. The hot-wire was traversed to a position adjacent to the pitot-static probe for each calibration.

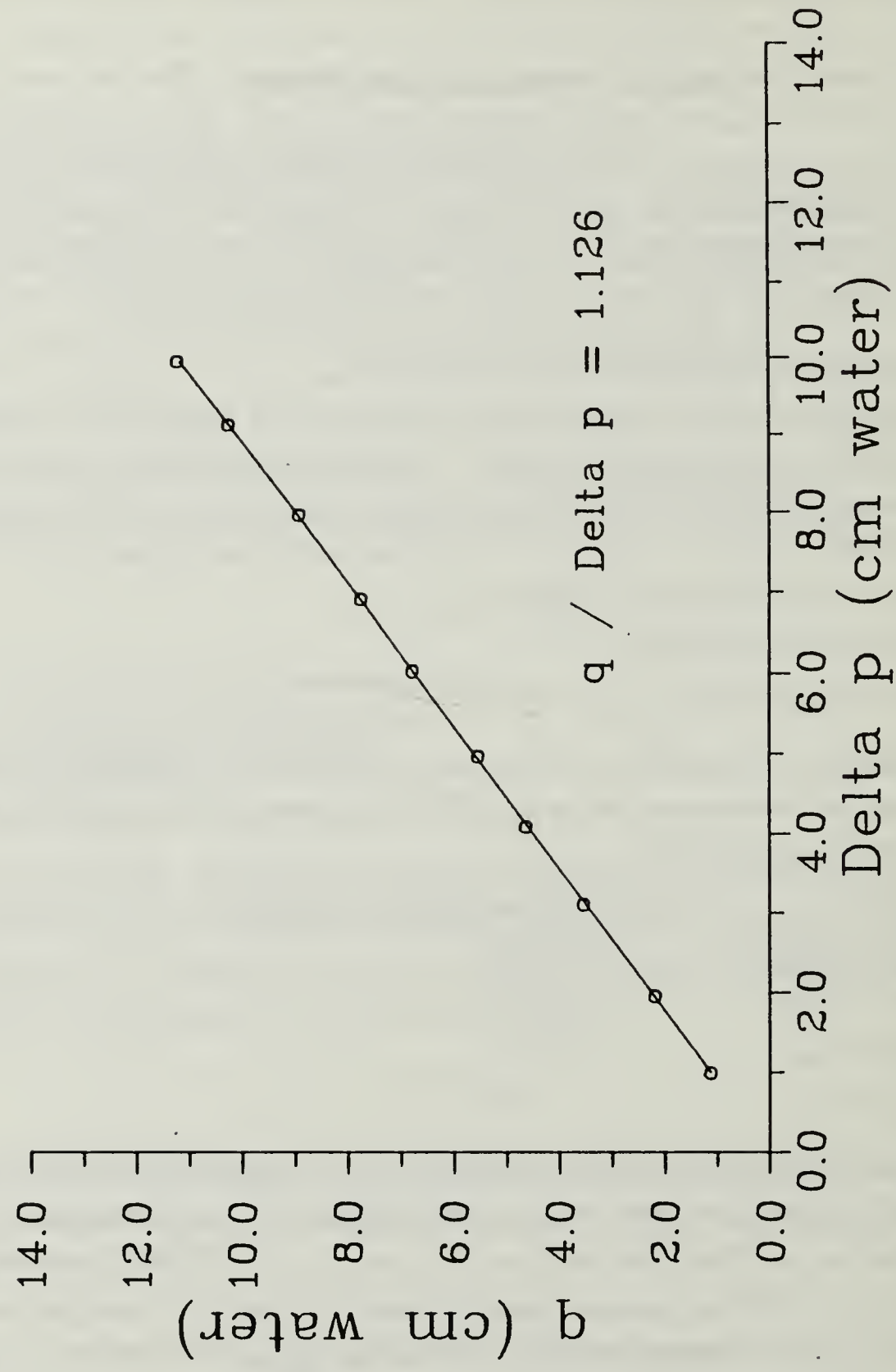

Figure 10. Wind Tunnel Test Section Calibration

The hot-wire was calibrated at or near seven selected velocities (1, 2, 3, 4, 6, 8, and 10 centimeters Δp across the contraction cone) using the software routine HWCAL.BAS described in Chapter II. The calibration velocities are centered about the expected operating speed of 95 ft/sec and extended over the range 40 - 140 ft/sec.

The final calibration curve was obtained by plotting hot-wire voltage squared versus the square root of velocity. A nearly straight line relationship results for this fourth order fit. Most graphing routines will plot the data and provide the equation of the linear least squares best fit line. This linear equation is of the form:

$$y = Ax + B \tag{7}$$

where $y = \sqrt{\text{velocity}}$ and $x = (\text{hot-wire voltage})^2$. Using the constants A and B from Equation 7, the hot-wire calibration equation becomes:

$$\text{velocity} = [A(\text{voltage})^2 + B]^2 \tag{8}$$

This relationship can readily be used in any data conversion program such as DATCONV.FOR (Chapter II) to calculate velocity.

C. HOT-WIRE POSITIONING

Great attention was given to the task of positioning the hot-wire in the boundary layer adjacent to the wing. The objective was to accurately position the hot-wire as close as possible to the wing surface while not damaging either the wing or the hot-wire.

Vaught and Fernholz provide an excellent summary of the various methods in use today [Ref. 11]. The optical sighting method was used for this investigation. Kindelspire also used this technique in prior work at NPS [Ref. 4: pp. 12-13].

Several modifications to Kindelspire's methods were made by this investigator to improve positioning accuracy and repeatability. The techniques employed are described below.

The height of the hot-wire above the wing surface was measured by observing the hot-wire and its reflection in the wing through a surveyor's sighting level. The sighting level was positioned approximately six feet behind and to the left of the tunnel test section. Figure 11 shows the sighting level in position adjacent to the NPS low speed wind tunnel.

As noted previously in Chapter II, the wing was finished in high gloss black lacquer to enhance the reflected image of the hot-wire probe. The distance between the hot-wire probe and its image was determined by using the horizontal cross-hair and vertical offset

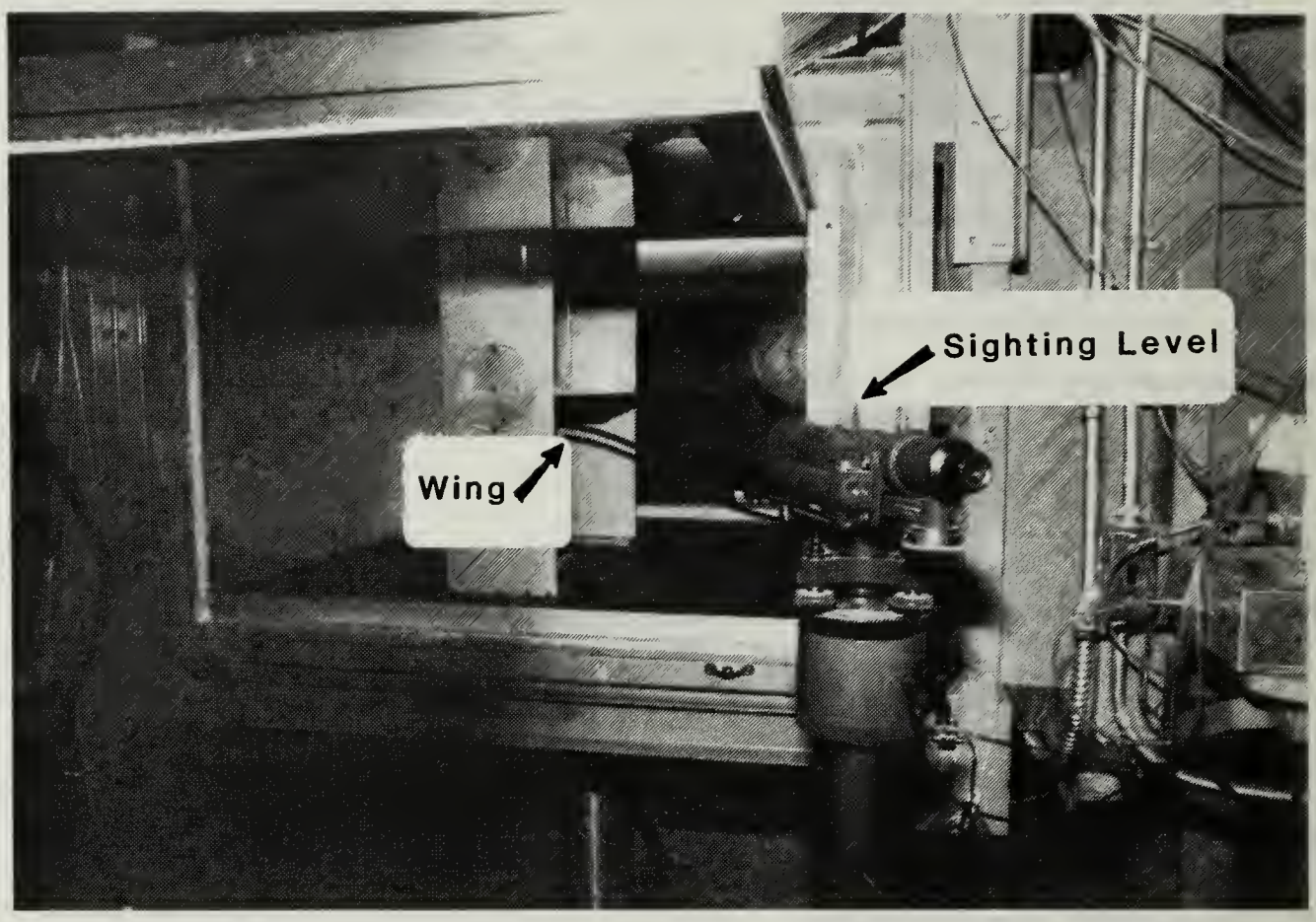

Figure 11. Surveyor's Sighting Level

vernier on the sighting level. The vertical vernier was adjustable over a range of ± 45 vernier units from the center position. One vernier unit was determined to be 0.0032 inches of vertical probe displacement using the traverser, with 0.000125 inches stepping accuracy, as a calibration reference. The sighting level could be repeatedly set and read to 1 2 vernier unit resulting in a positioning accuracy of 0.0016 inches.

The actual probe to wing distance is 1.2 the distance observed between the two images. The hot-wire images were brought to within three vernier units separation for data collected at the 70% chord location resulting in an initial hot-wire distance of 0.0048 ± 0.0008 inches. The probe was brought to two vernier units separation for all other wing positions (50% and 30% chord) which equated to an initial distance of 0.0032 ± 0.0008 inches.

An external flood light was directed at the wing section and the hot-wire probe during the sighting process to enhance the image in the wing. The polished high gloss black finish on the wing provided a clear and sharp reflected image comparable in qual-

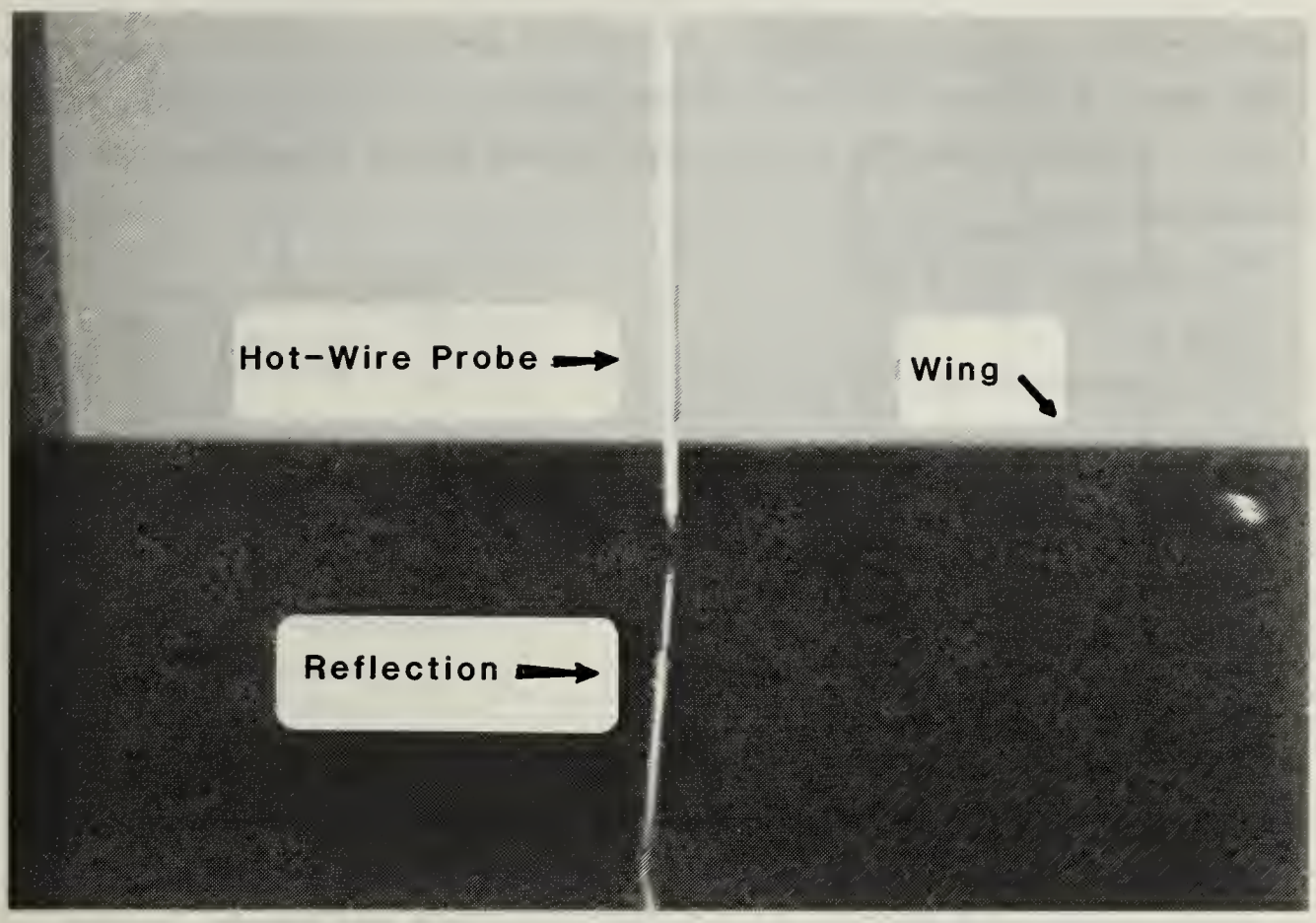

Figure 12. Hot-Wire Probe and Reflection

ity to the actual probe as shown in Figure 12. No correction was made for the slight angle of the wing surface due to camber as this angle was less than five degrees at the points examined resulting in a positioning error of less than three percent.

D. ACQUISITION OF EXPERIMENTAL DATA

1. Test Environment Conditions and Setup Parameters

All test were conducted at a chord Reynolds number of 500,000. Tunnel velocity for a given Reynolds number is given by:

$$v = \frac{R_c \mu}{\rho c} \tag{9}$$

R_c = Chord Reynolds Number
μ = Viscosity
ρ = Density
c = Chord Length

Solving Equation 9 using typical NPS ambient conditions (temperature = 68 degrees F, pressure = 29.95 inches Hg) where $R_c = 500{,}000$ and $c = 10$ inches yields a tunnel operating velocity of 95 ft/sec. All data runs were made at this reference free stream velocity.

The setup parameters that remained constant throughout the investigation are summarized below:

Wing Angle of Attack (AOA)	0.71 degrees
Wing Chord	10 inches
Free Stream Reference Velocity	95 ft/sec
Chord Reynolds Number	500,000
Turbulence Generator Motor Speed	1,500 RPM
Frequency of Turbulence Pulses	50 Hz
Period Between Turbulence Pulses	20 milliseconds
Free Stream Distance between Pulses	22.8 inches
Analog Channels Sampled	2 channels
Hot-Wire Voltage	Channel 1
Timing Data	Channel 2
Analog-to-Digital Rate	50 KHz per Channel
Sample Period	0.92 seconds
Number of Pulse Periods Sampled	45
Number of Samples per Pulse period	1000
Period Between Each Sample	20 microseconds

2. Equipment Configuration

Figure 13 shows the equipment configuration used for this investigation. As noted previously, two personal computers were used during the data acquisition phase. One computer was dedicated to controlling the traverser mechanism while the other managed data collection and processing. Two computers were necessary as the operating programs and data (92,000 samples) entirely filled the free memory of the data acquisition computer.

Data collection was quite routine once the hot-wire anemometer was set up and calibrated, and the hot-wire probe initially positioned in the boundary layer. From that point, the operator had only to monitor the operating environment (tunnel velocity, tunnel temperature, turbulence generator motor speed, and hot-wire output), step the hot-wire through the boundary layer using one computer, and collect data with the other

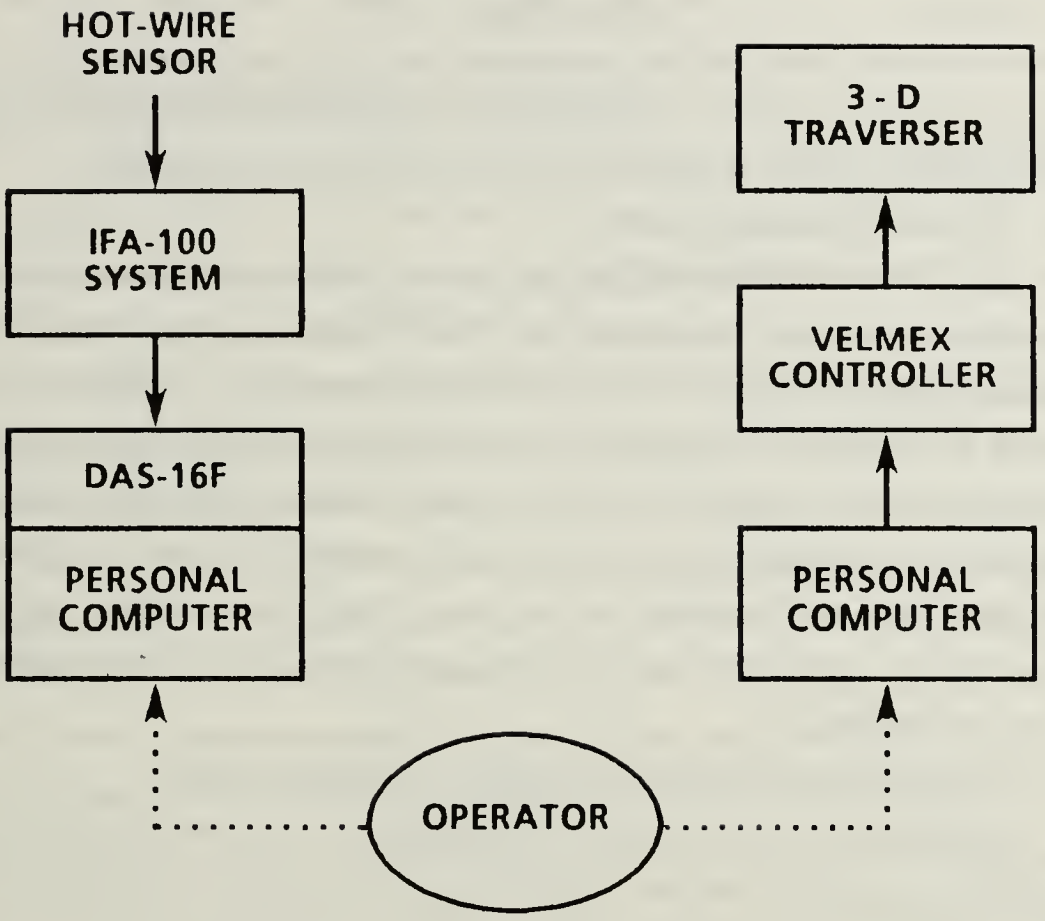

Figure 13. Equipment Configuration

computer. Approximately seven minutes were needed to collect and store the data at any one position in the boundary layer. While the actual data sampling period was less than one second, the computer took over 5 minutes to transfer the data from random access memory to permanent disk storage.

3. Flow Characterization

Data were collected to characterize the flow in the following regions of interest:

Test Section Free Stream

Periodic Turbulence Pulses

Boundary Layer Response to Periodic Turbulence Pulses

a. Test Section Free Stream

Data were collected in the free stream of the test section with all equipment removed to determine the intensity and spectral content of the flow. This step served to document the steady state baseline characteristics of the free stream flow at 95 ft/sec and also allowed this investigator to compare the free stream turbulence data obtained in this investigation with that obtained previously by other investigators.

b. Periodic Turbulence Pulses

Data were collected with just the periodic turbulence generator installed and operating in the test section. The tunnel and the turbulence generator were set at their normal operating parameters of 95 ft/sec and 50 Hz respectively. The hot-wire was positioned at the approximate vertical position of the upper wing surface (approximately half way between the hub and the rod tip). Measurements were taken four, six, and eight inches downstream from the rotating rod. These three positions coincided with the 30%, 50%, and 70% chord locations on the wing. These tests served to document the time-varying velocity, turbulence, and spectral characteristics of the turbulence pulse generated by the rotating bar.

c. Boundary Layer Response to Periodic Turbulence Pulses

Measurements were made in the boundary layer at the 30%, 50%, and 70% chord locations on the upper surface of the wing with the periodic turbulence generator operating at 50 Hz. The wing AOA was measured at 0.71 degrees and the free stream velocity was set at 95 ft/sec. Data were taken at up to 50 points over the estimated boundary layer thickness at each chord location. The spacing of the sample points taken at each of the three chord locations is given in Appendix B.

All data measurements were taken over a four day period. One additional day of tunnel operation was needed following the data collection runs in order to investigate the hot-wire drift problems addressed in Chapter IV.

IV. RESULTS

A. HOT-WIRE ANEMOMETER CALIBRATION

Hot-wire calibration was conducted before and after each boundary layer investigation[5] to confirm the stability of the hot-wire anemometry system and to ensure the accuracy of the data. Roane [Ref. 12: pp. 40-41] experienced some calibration curve drift in previous hot-wire work in the NPS low speed wind tunnel. As such, a minor amount of drift was expected. This investigator planned to average the initial and final calibration curves and use the resulting average to convert each day's data. The tabulated data from the calibrations runs on each day tended to confirm the expectation of only *slight* drift and, therefore, the data acquisition runs were completed as planned. Subsequent detailed analysis of the calibration data for day three, however, showed that the initial and final curves differed by approximately 14%. The drift for day two was less but still significant at approximately 8%. The drift for day one could not be determined as the final calibration data were lost. The results of the calibration runs for day three, presented in Figure 14, show the divergence between the initial and final calibration data. The magnitude of the error was too great to resolve by averaging. In addition, the cause of the drift and its characteristics were unknown.

This investigator planned and conducted an additional six-hour tunnel run on the following day in order to document and characterize the observed hot-wire drift. The tunnel was run at 95 ft/sec with just the pitot-static and hot-wire probes installed in the test section. Calibrations were conducted at the start and every hour thereafter. The results of this run, plotted in Figure 15, show the shift of the calibration curve over time. The drift rate is greatest at the beginning and becomes very small after six hours. The effects of the drift and the induced error are greatest at the higher velocities due to the fourth order relationship that exists between hot-wire voltage and velocity.

The drift rate was graphically analyzed at a reference velocity of 100 ft/sec and expanded by extrapolation to cover an eight-hour period. Figure 16 shows the change in calibration of the hot-wire over eight hours. Notice that nearly 50% of the drift occurs in the first two hours of operation.

---

5 The final calibration data for day one was not saved due to operator error.

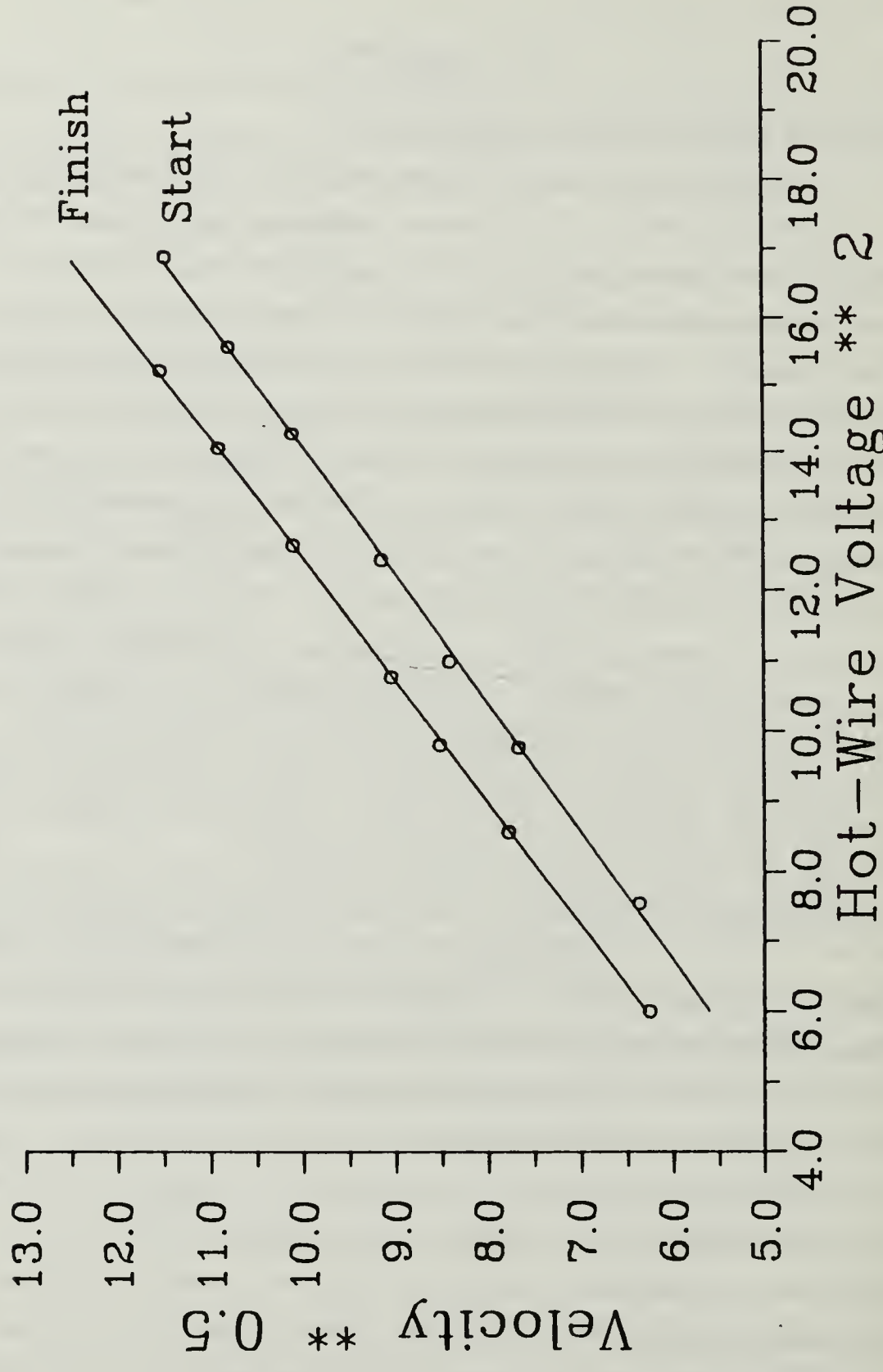

Figure 14. Hot-Wire Calibration Results, Day Three

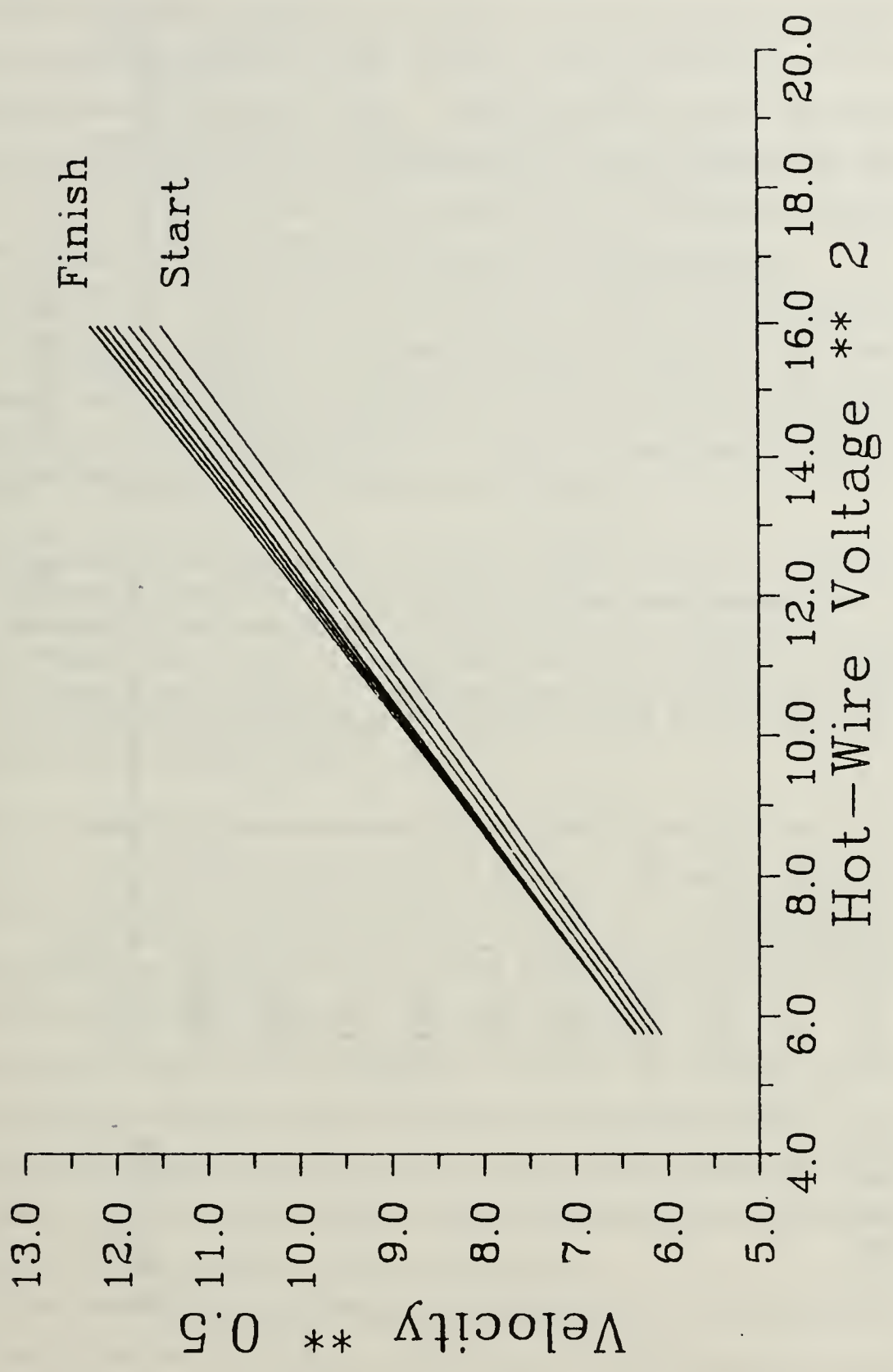

Figure 15. Hot-Wire Drift Analysis

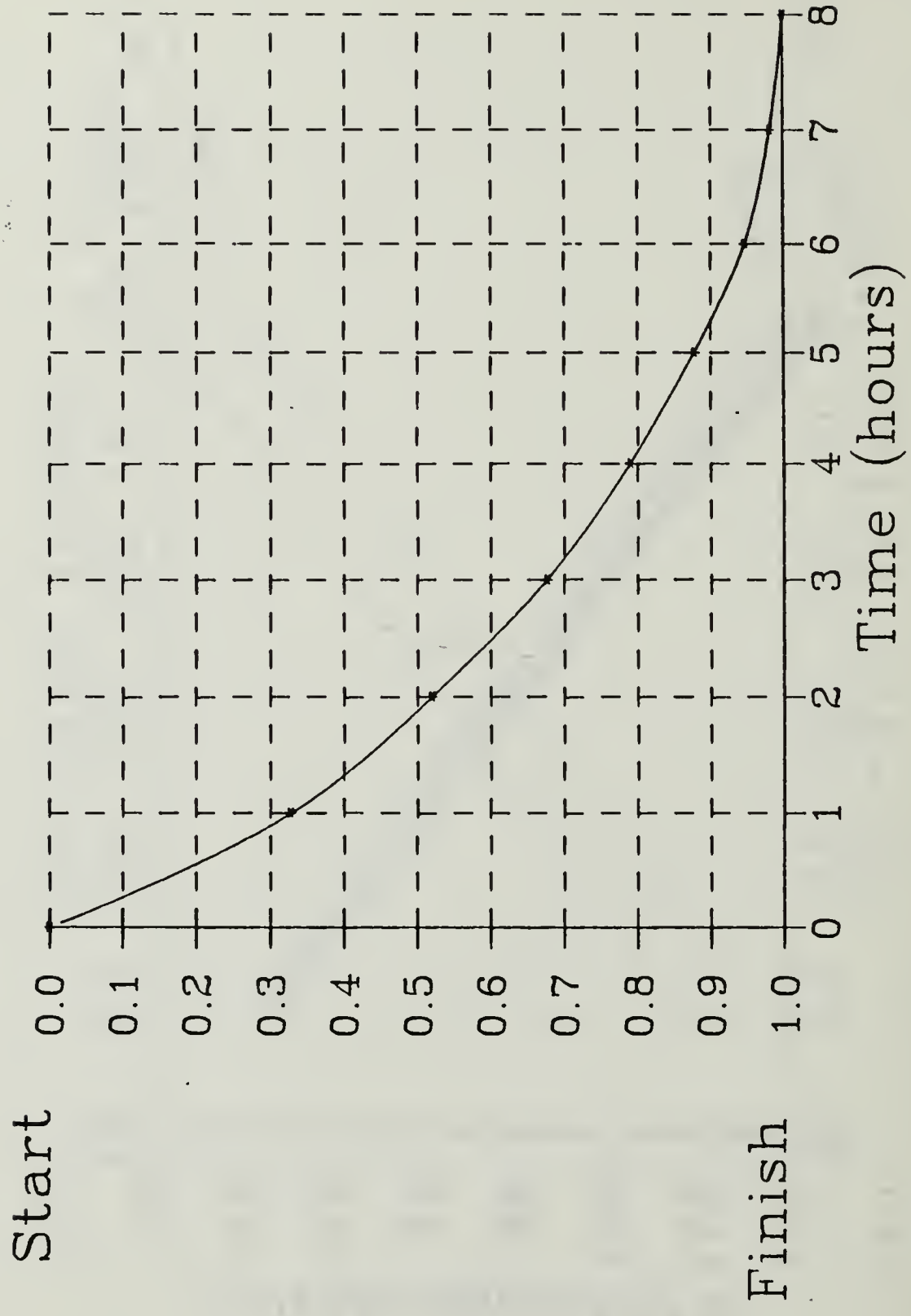

Figure 16. Hot-Wire Calibration Drift Over Eight Hour Period

The author applied the drift vs. time relationship of Figure 16 to each day's calibration data in order to generate a set of time varying calibration equations. The equations were staggered such that the maximum velocity difference between sequential calibration curves was one ft/sec or less. These corrections assumed that the drift rate determined during the test run was representative of the drift experienced on each day and that the run duration for each days was eight hours. Corrections were applied only to the data taken on day two (50% chord) and day three (30% chord).

This investigator believes the hot-wire drift is a result of environmental contamination of the hot-wire probe. Hot-wire contamination appears to be a well known phenomenon among experienced researchers, but a subject about which little is printed in current hot-wire operating manuals or in fluid flow measurement texts. An older publication by TSI has this to say about hot-wire stability:

> For a mean flow measurement to be useful it must maintain its calibration over long time periods. Hot wires are notoriously troublesome in this regard due to their small size making them susceptible to picking up small contaminants . . . . The larger hot film sensor has been a great improvement in this regard. The effects of surface contamination tend to be a function of sensor size and a ceramic coating on the sensor surface prevents corrosion and erosion. Hence, the hot film is far superior for mean measurements. [Ref. 13: p. 91]

Figure 17, reprinted from the above TSI publication, shows the typical change in calibration of a hot-wire sensor and a hot-film sensor vs. time when subjected to an artificially dirty flow stream. The drift vs. time curve for this investigation (Figure 16) is remarkably similar to the TSI drift curve. With this knowledge, it was not difficult to pinpoint the source of contamination to the wind tunnel itself.

For the month prior to this investigation, the tunnel was used for a series of flow visualization studies using an oil-based smoke as a visualization medium. This type of medium tends to produce a certain amount of contaminants which, due to the closed circuit design of the tunnel, were trapped in the tunnel environment. This oil residue is the likely contaminant and cause of the observed drift.

Little can be done about the tunnel contamination, but one likely solution to the drift problem is the use of a hot-film sensor instead of a hot-wire probe. As noted previously, the hot-film is virtually impervious to particulate contamination. A second solution would be to pre-run the tunnel prior to taking data for six to eight hours to allow the hot-wire to stabilize.

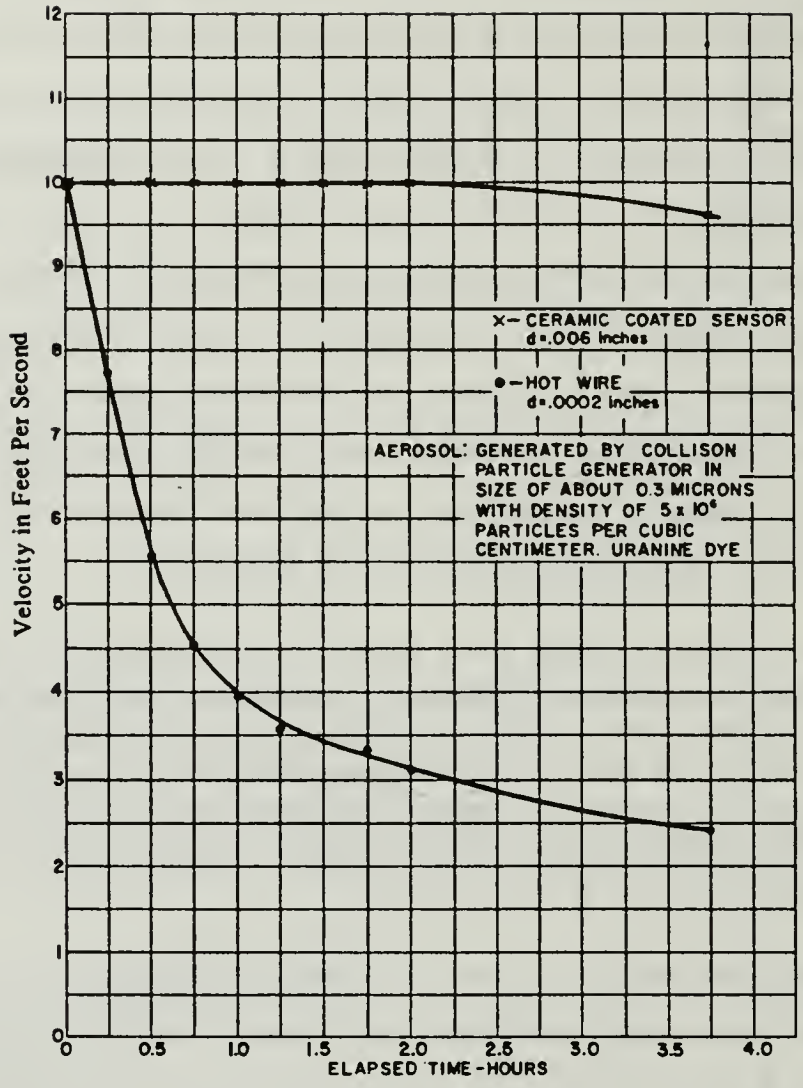

Figure 17. Change in Calibration of Hot-Wire vs. Hot-Film When Subjected to a Dirty Flow Stream: [Ref. 13: p. 92]

B. ANALYSIS OF TIME VARYING DATA

Ensemble averaging methods were employed to characterize the non-stationary, periodic data acquired during this investigation. The periodic nature of the data made it possible to collect a series of repetitive time histories, or pulse passage cycles, each associated with the passage of one turbulence pulse. This series of time histories is called an ensemble. A typical ensemble consisted of a series of 45 pulse passage cycles. The number of passage cycles in one ensemble was essentially limited by available computer memory. For this investigation, 45 cycles was the upper limit. Howard [Ref. 6: pp.

114-115] showed that 20 or more pulses were needed in each ensemble to accurately portray the actual mean values, substantiating that 45 pulses were sufficient in this case.

1. Ensemble Characteristics

Each of the 45 pulse passage cycles making up the typical ensemble for any one data point is slightly different due to the random nature of the turbulent components of the signal. Figure 18 and Figure 19 show two sequential pulse passage cycles (instantaneous velocity vs. sample number) from a typical ensemble (Test Case A) taken near the wing surface at 70% chord. These data were collected using a single hot-wire sensor. The velocity data were sampled, or digitized, at 50 KHz with the turbulence generator operating at 50 Hz. This digitizing rate results in approximately 1000 data points per passage cycle. The period of each passage cycle being 20 milliseconds, each sample represents 20 microseconds in time. Time is not recorded explicitly but can be calculated from the digitizing rate and sample number. The data are plotted with straight line segments between each of the sample points.

Each passage cycle is typically made up of three representative flow regimes as depicted in Figure 18:

Undisturbed Flow

Turbulence Pulse

Recovery Period

The specific characteristics of these regimes are very dependent on chord location and position in the boundary layer; but the following general characteristics hold true for each. The undisturbed flow segment is representative of the natural steady-state flow for the wing when operated in an undisturbed free stream. Howard [Ref. 6: p. 81] confirmed this relationship experimentally by comparing the drag of the undisturbed segment with that for natural flow and finding the two equal. The turbulence pulse is clearly identified as a highly turbulent velocity deficit. The recovery period is broadly defined as the period from the end of the turbulence pulse to the point where the flow returns to the undisturbed state.

2. Mean Velocity Determination

The author employed program MEANSMU.FOR described in Chapter II to extract the slowly varying mean velocity from the ensemble of instantaneous velocities. In principle, MEANSMU filters out the high frequency turbulence components while leaving the low frequency variations of the signal mean intact. The amount of smooth-

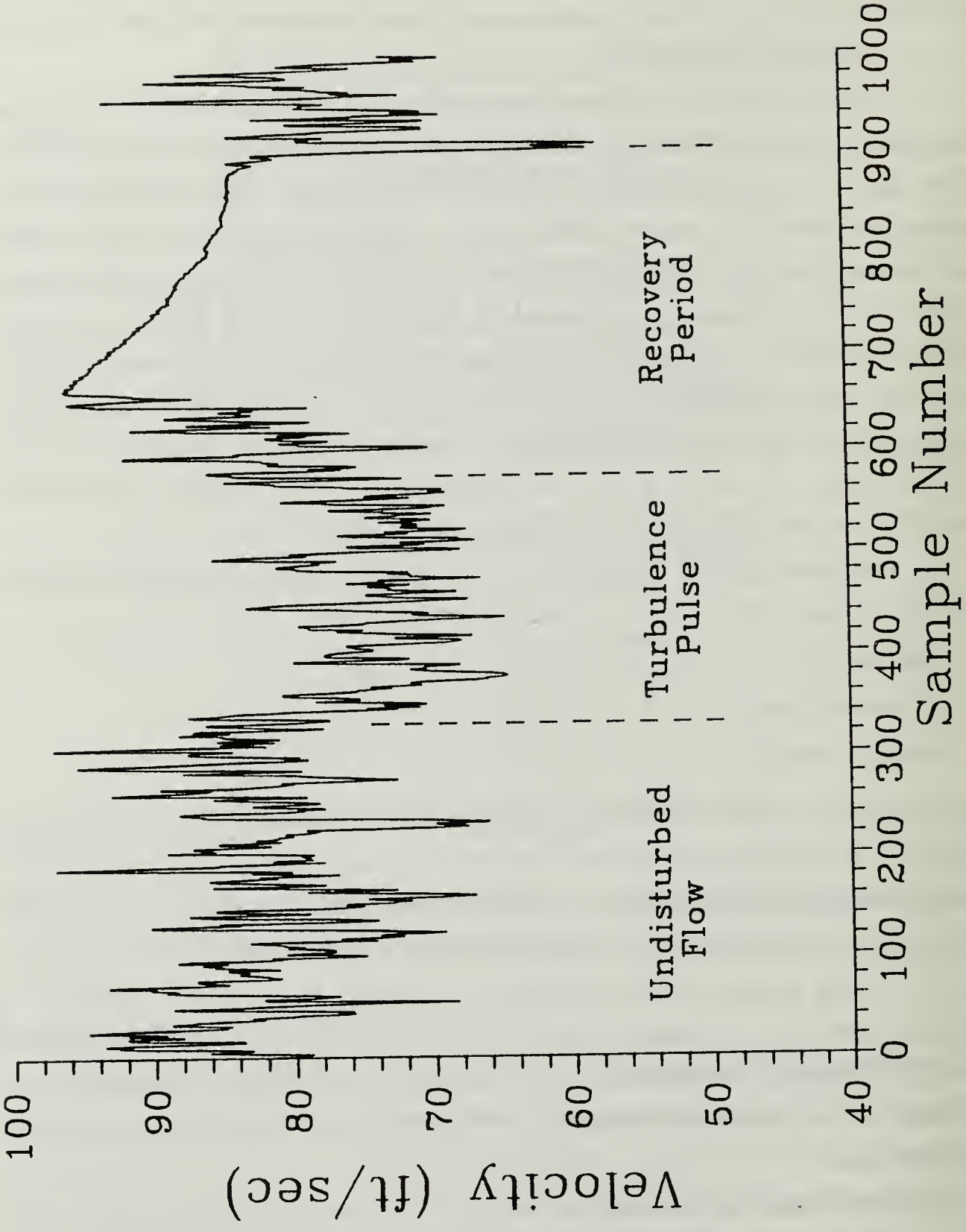

Figure 18. Pulse Cycle Number One for Test Case A: (Fs = 50 KHz)

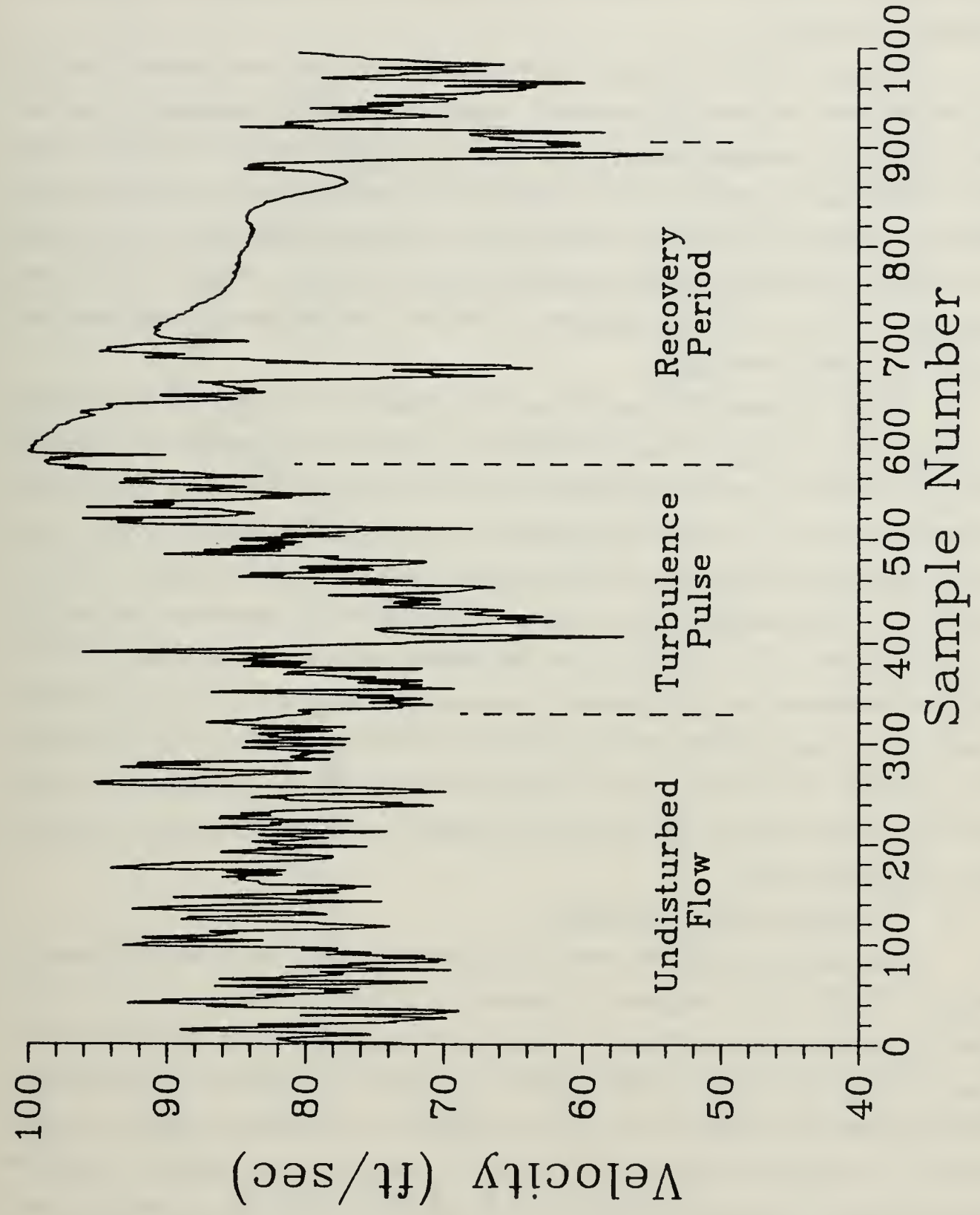

Figure 19. Pulse Cycle Number Two for Test Case A: (Fs = 50 KHz)

ing is determined by the user selectable cutoff frequency of the digital low pass filter in program MEANSMU.

Program MEANSMU extracts the mean through a two step process. First, the 45 time histories are ensemble averaged to generate a single "representative" time history. Ensemble averaging consists of simply stacking the 45 time histories one on another and taking the average of the 45 values at each sample point in the time history. Figure 20 presents the ensemble average of the 45 pulse passage cycles for Test Case A. Note that the large turbulent fluctuations observed in Figure 18 and Figure 19 have been reduced but not entirely eliminated. The three flow regimes are also quite pronounced and easily identifiable.

Figure 21 through Figure 24 show the application of digital low pass filtering to the ensemble average of Figure 20 with low pass filter cutoff frequencies (f_c) of 1082 Hz, 541 Hz, 360 Hz, and 267 Hz respectively. Note that the amount of smoothing is directly related to f_c ; the lower f_c the greater the smoothing. 360 Hz was choosen as the optimal cutoff frequency based on the findings of Landrum and Macha [Ref. 14] in their analysis of the spectra documenting the growth of turbulent disturbances through the transition process. They found that the free stream energy is contained below 200 Hz while the turbulence energy is generally contained above 550 Hz in the early transition stages. The cutoff frequency was choosen to lie between these two frequencies. Coincidentially, the f_c = 360Hz curve is relatively smooth and flat throughout the undisturbed flow regime and displays good peak response over both the turbulence pulse and recovery period regimes.

3. Turbulence Level Determination

Turbulence values of the time-varying, periodic signals were calculated using the program TURBIN.FOR described in Chapter II. TURBIN accomplishes this by calculating the instantaneous turbulence at each point in each of the 45 time histories and then ensemble averaging the instantaneous turbulence magnitudes. The result is a time-varying representation of the mean turbulence at each sample point in the pulse period. It is important to note that TURBIN also employs user selectable digital low pass filtering in its routines. The author used 360 Hz in this routine to maintain continuity among the various output data.

Figure 25 shows the turbulence trace for Test Case A. Note that the representative flow regimes (undisturbed flow, turbulence pulse, and recovery period) are as clearly identifiable here as in the mean velocity traces in the previous section.

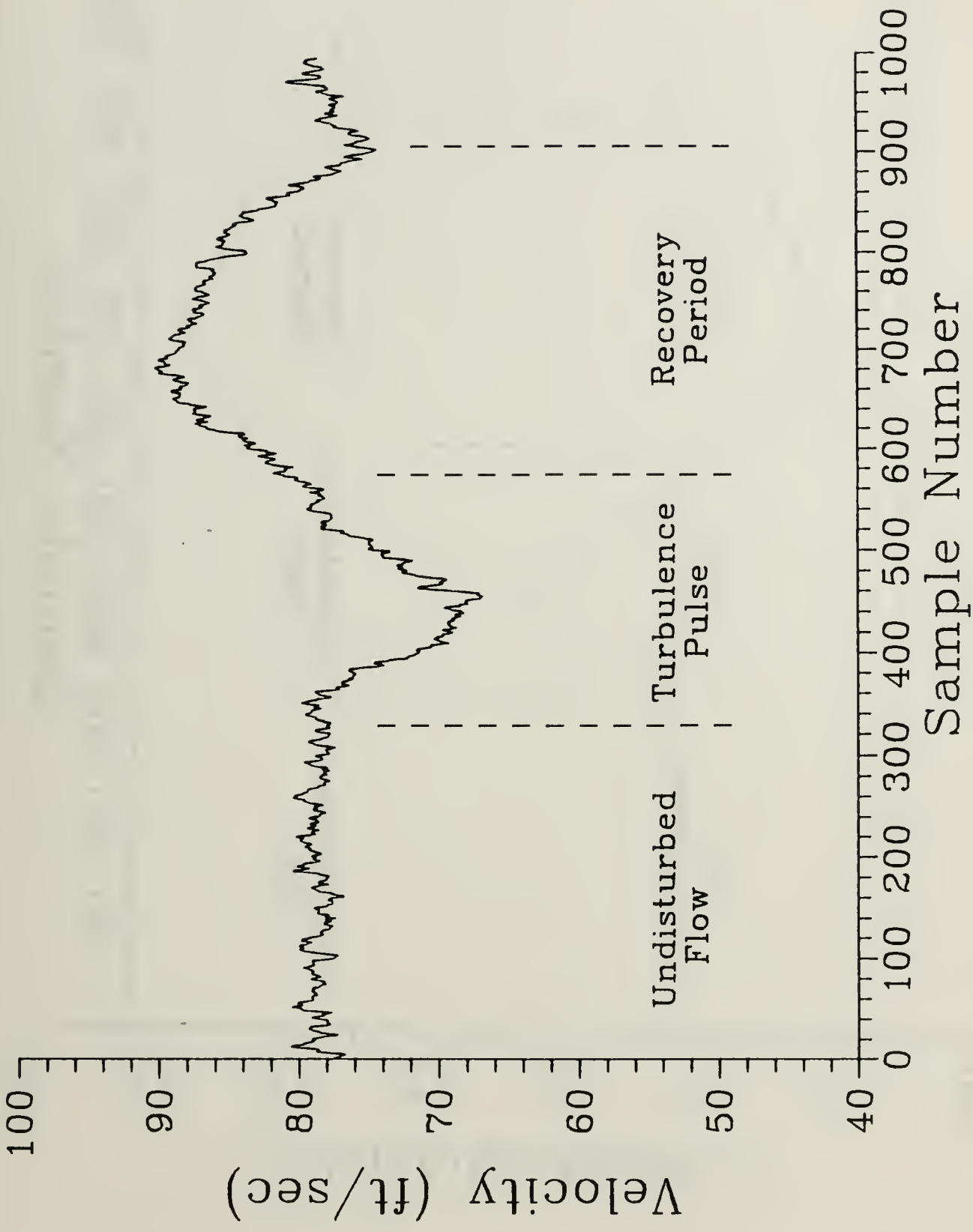

Figure 20. Ensemble Average for Test Case A: (Fs = 50 KHz)

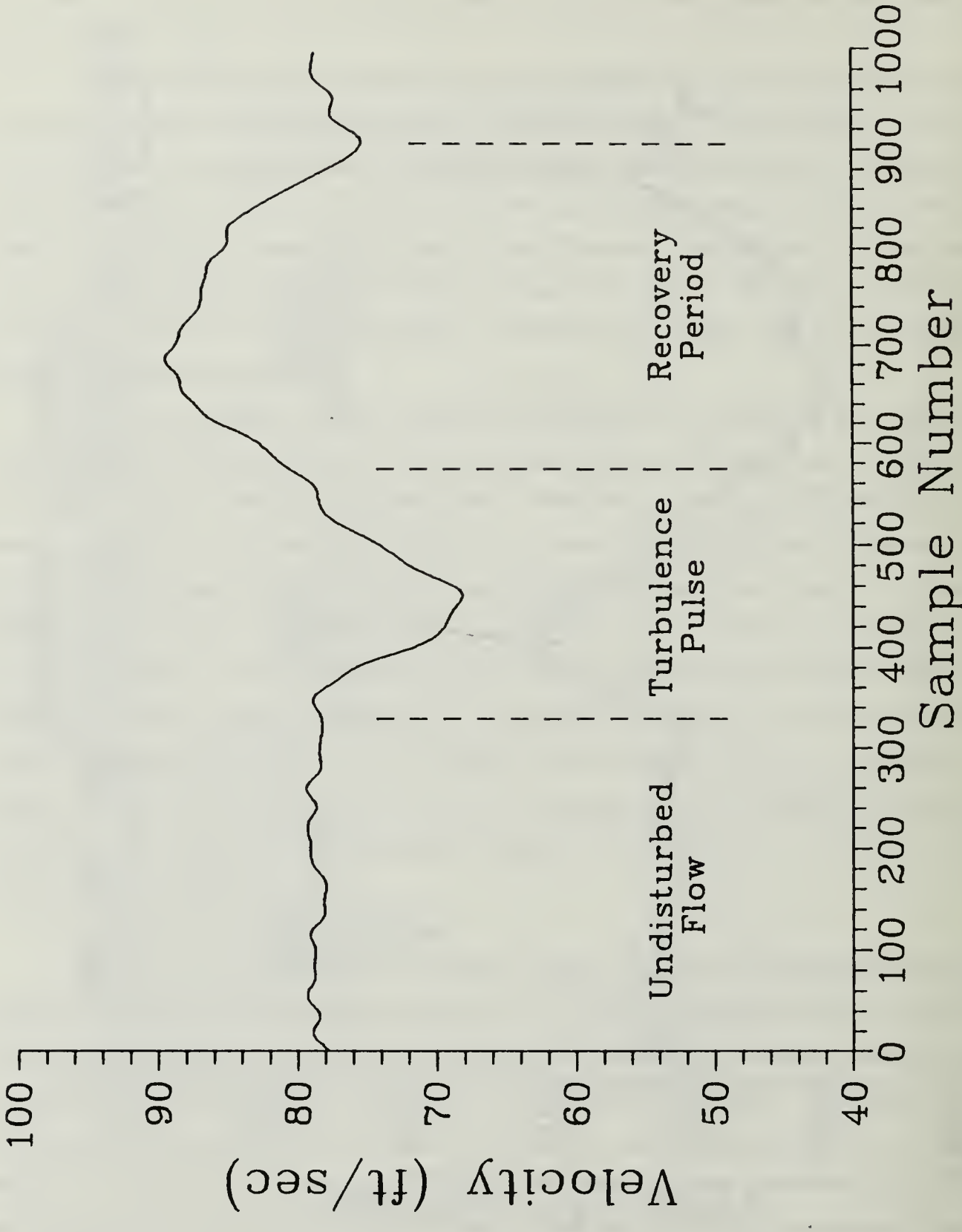

Figure 21. Smoothed Ensemble Average for Test Case A, Fc = 1082 Hz: (Fs = 50 KHz)

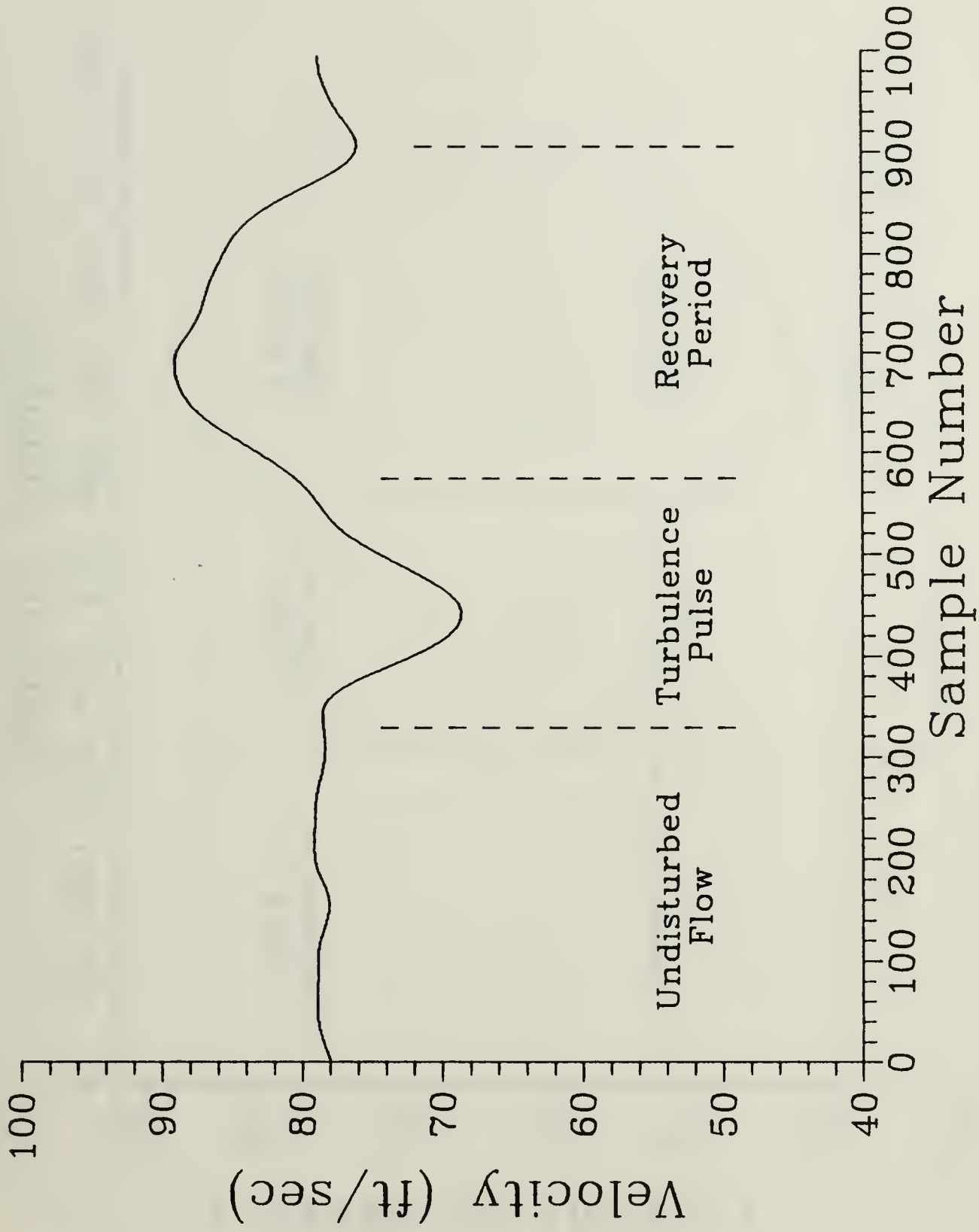

Figure 22. Smoothed Ensemble Average for Test Case A, Fc = 541 Hz: (Fs = 50 KHz)

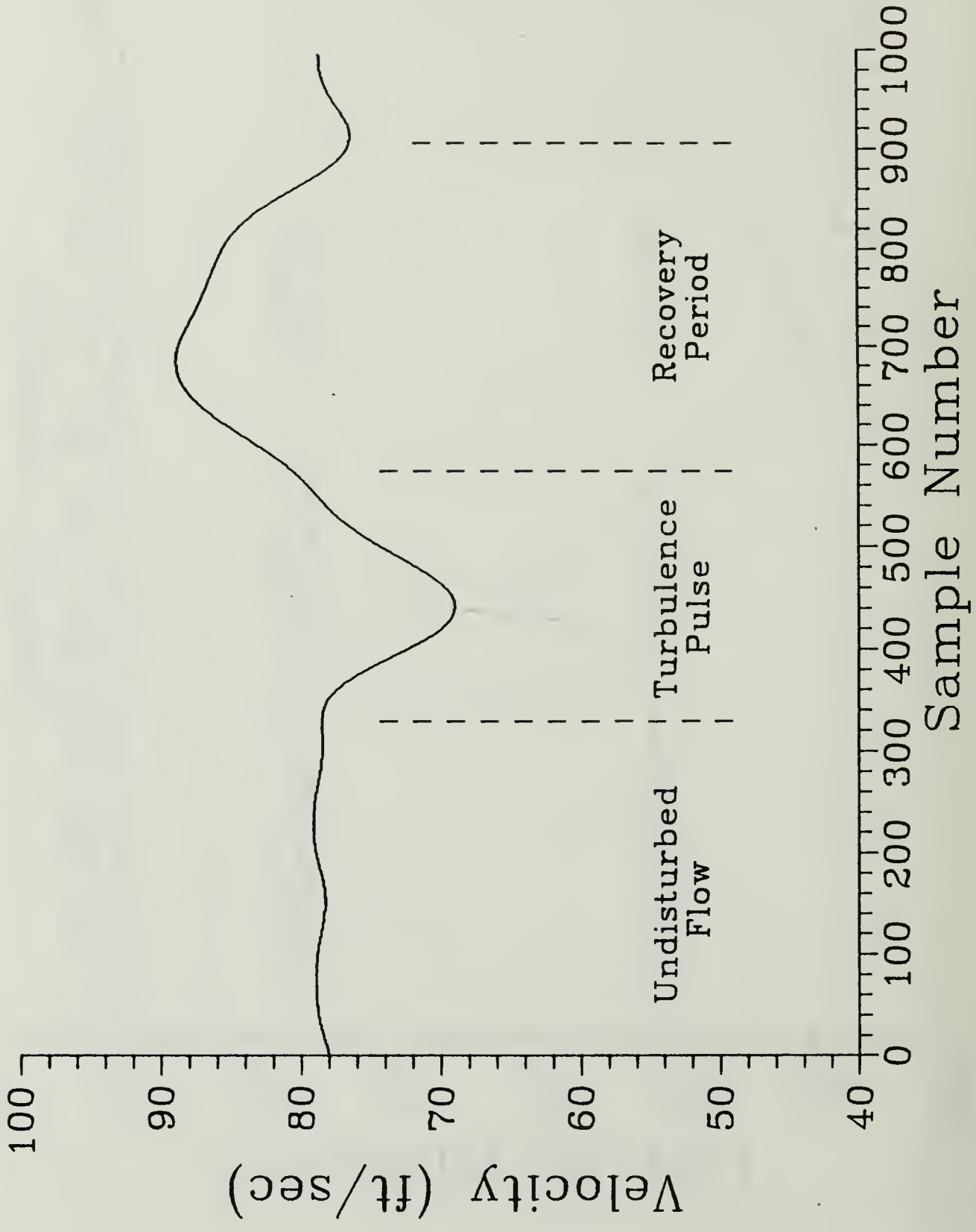

Figure 23. Smoothed Ensemble Average for Test Case A, Fc = 360 Hz: (Fs = 50 KHz)

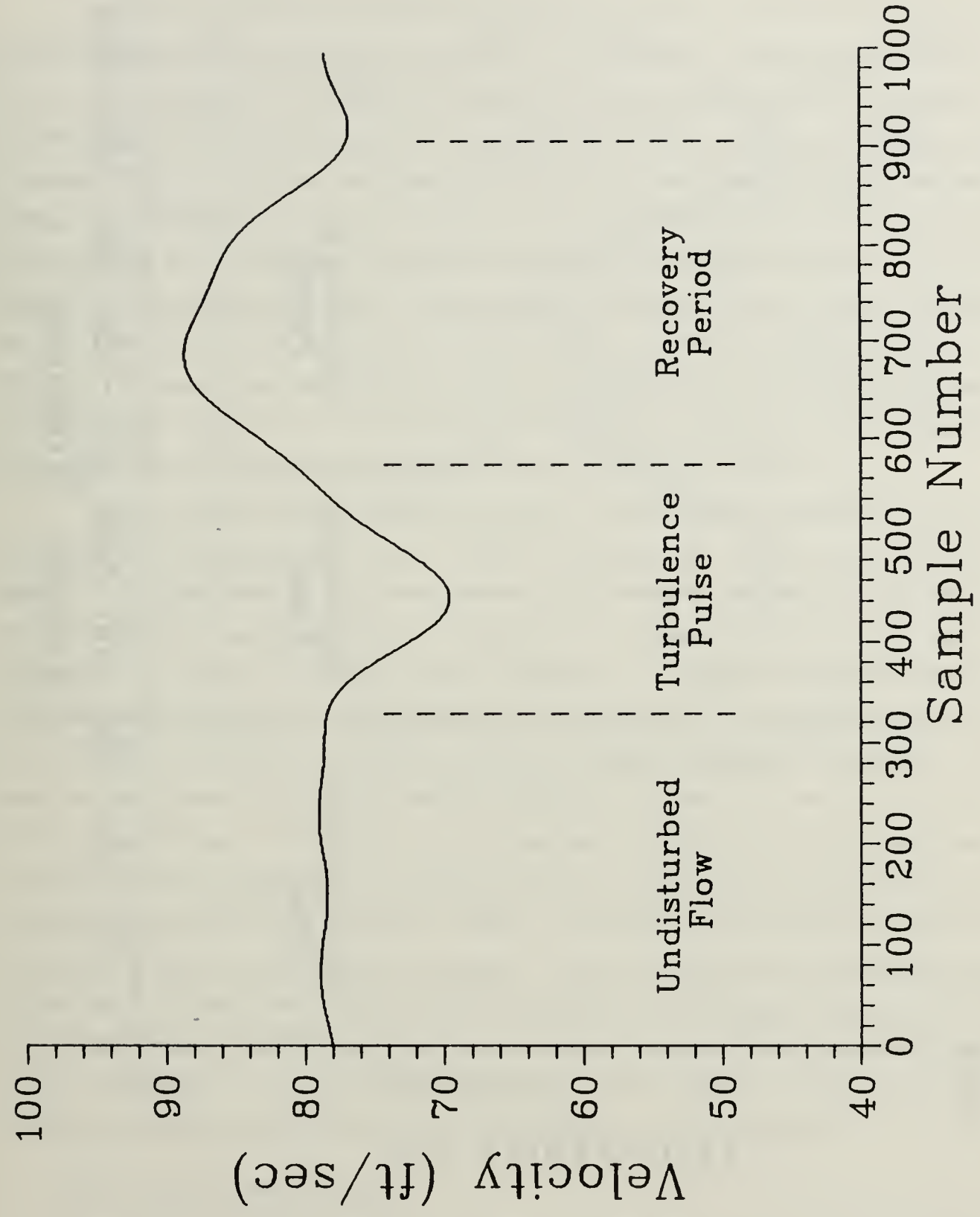

Figure 24. Smoothed Ensemble Average for Test Case A, Fc = 267 Hz: (Fs = 50 KHz)

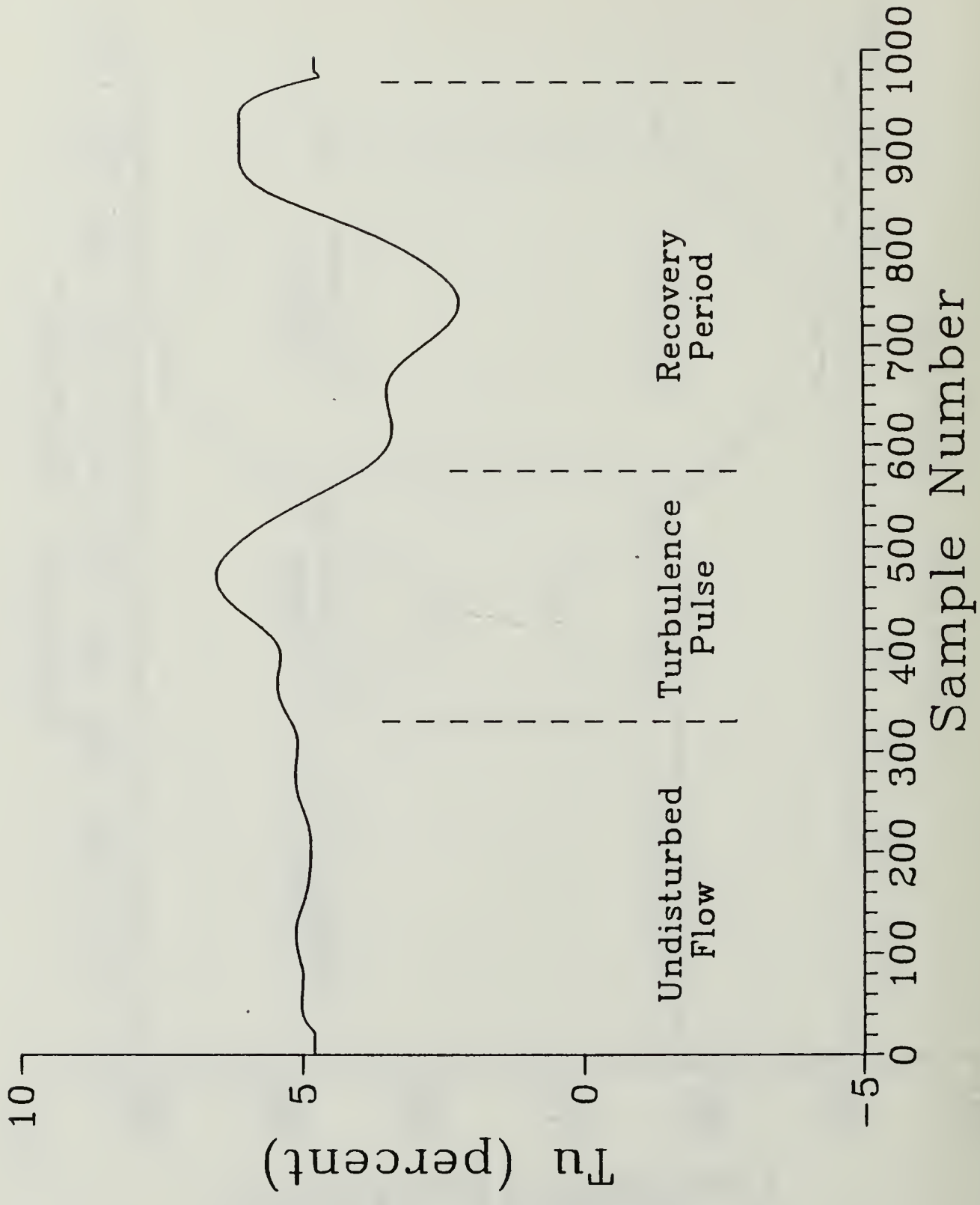

Figure 25. **Smoothed Mean Turbulence for Test Case A:** (Fc = 360 Hz, Fs = 50 KHz)

4. Spectral Analysis

Spectral analysis of the time-varying, periodic signals was conducted using program ENSPSDAV.FOR described in Chapter II. ENSPSDAV performs spectral analysis on a user selectable 256 sample-wide window of the pulse passage cycle time history. In theory, spectral analysis can only be accomplished on a discrete (digitized) time series of infinite length. In practice, the window width, or number of samples, can be reduced through the application of special techniques to the Fast Fourier Transform--the compromise being loss of frequency resolution with reduction in window width. The 256 sample-wide window used in this investigation was selected as the best balance of these factors. Each flow regime fits into the window and the resulting frequency resolution is 190 Hz. The reader must keep in mind that the output data from ENSPSDAV represents the average taken over the entire window. Thus, dynamic changes that occur in the flow regime over the window period will be lost in the resulting average.

Figure 26 and Figure 27 show the output from program ENSPSDAV for the turbulence pulse regime of Test Case A. Figure 26 displays the velocity spectrum of the signal. The vertical scale is a dB measurement of the relative turbulence energy with 0 dB representing the highest magnitude component of the signal. The horizontal scale is frequency in Hz plotted out to the Nyquist frequency. Each 10 dB reduction in the velocity spectrum represents a 10 fold reduction in power level. For example, the power level at 4,500 Hz (-20 dB) is 1/100 the level of the highest magnitude component. The mean has been removed from the signal[6] so that only the spectrum above 0 Hz is analyzed. It is important to note that the spectrum display provides no information about the absolute power contained in the spectrum, but only displays power levels relative to the highest magnitude in the spectrum. Figure 27 displays the total (cumulative) power distribution plotted with regard to frequency. The total power curve asymptotically approaches the value of the total power in the spectrum. The shape of this curve is indicative of the power distribution within the spectrum. The sharp knee observed in this plot indicates that the low frequency components of the signal contain most of the spectral power with very little power in the higher frequency components.

C. FREE STREAM ANALYSIS

The results of the free stream analysis are presented for flow at 95 ft/sec with all equipment removed from the test section. Figure 28 is a plot of velocity response over

---

6 The mean is removed for all the velocity spectrum and total power distribution plots in this report.

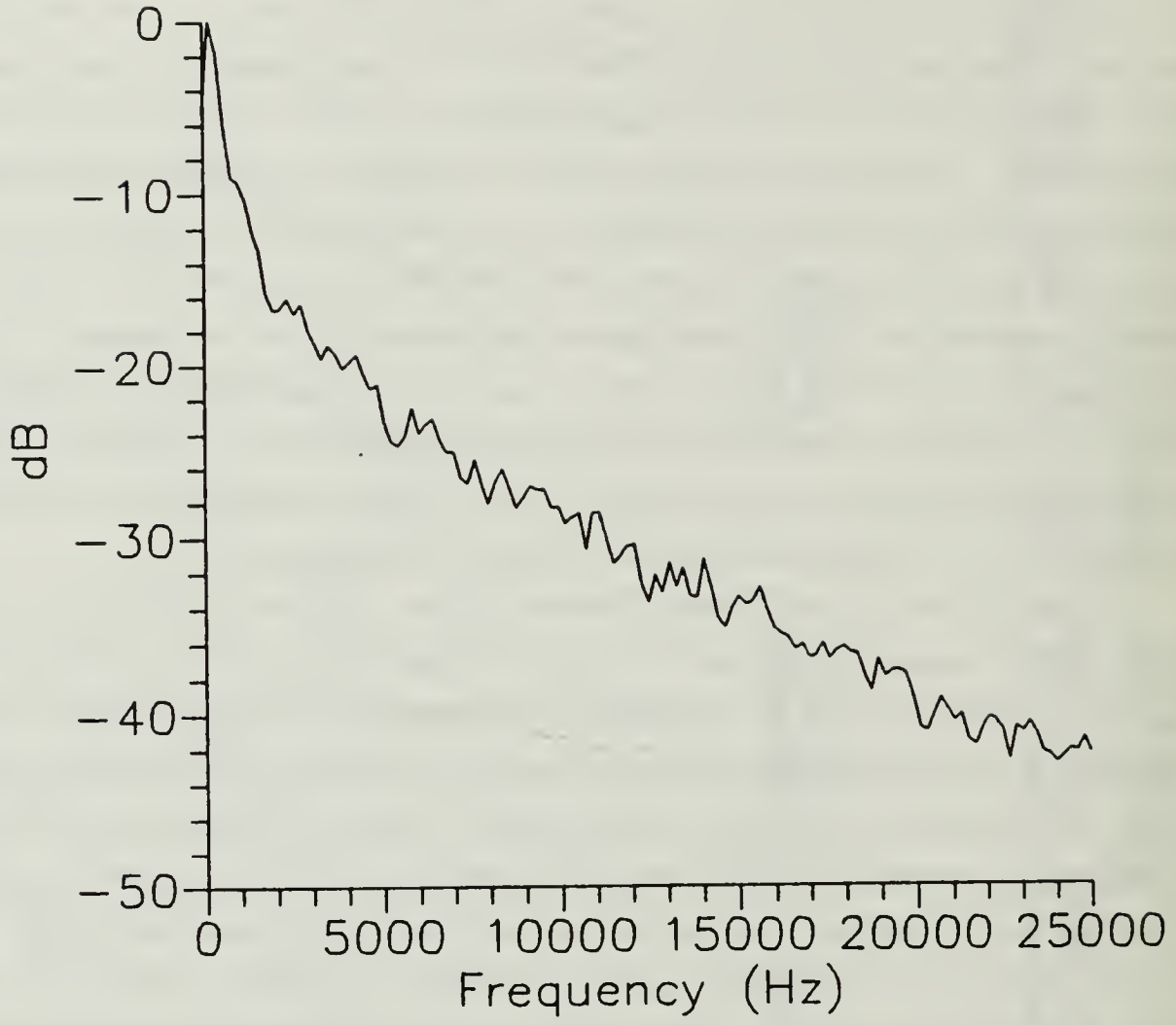

Figure 26. Velocity Spectrum for Test Case A, Turbulence Pulse

1000 samples. The signal is flat with a high frequency turbulent component of small amplitude superimposed on the mean. The free stream turbulence was calculated at 0.182% by the data analysis methods of this investigation. This figure compares favorably with the free stream turbulence intensity of 0.23% observed by Roane [Ref. 12: p. 41] at a velocity of 116.4 ft/sec. The slightly lower value of free stream turbulence observed here is not unexpected due to the slower free stream velocity.

Figure 29 shows the velocity spectrum of the free stream. The curve shows a sharp drop in intensity with increasing frequency indicating that the major frequency components are at the lower frequencies.

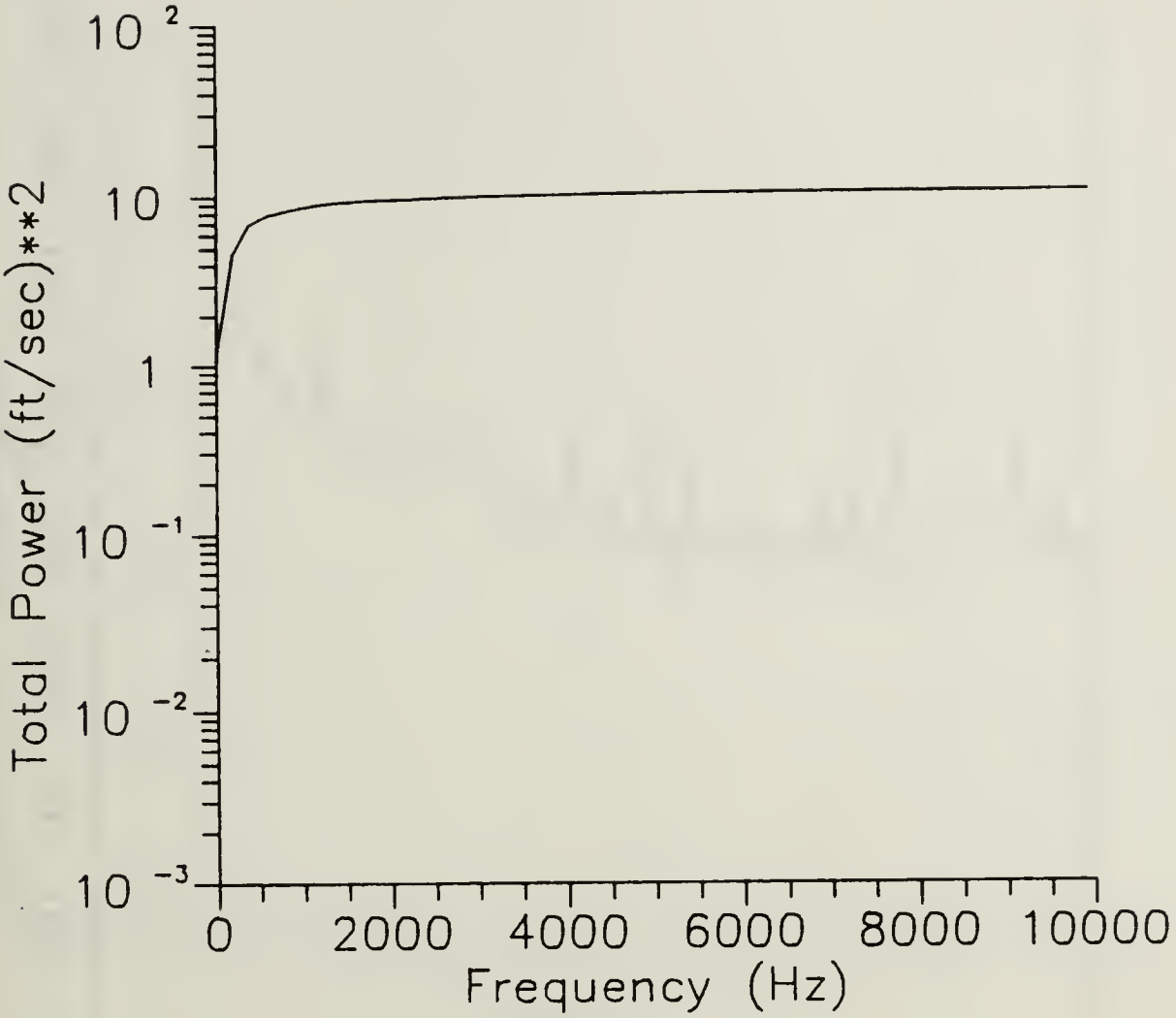

Figure 27. Total Power Distribution for Test Case A, Turbulence Pulse

The total power distribution of the free stream is depicted in Figure 30. The rapid rise and sharp knee of this curve confirm the concentration of power in the lower frequencies. The frequency components above 2 KHz provide little additional power as shown by the flatness of the curve above this point.

D. TURBULENCE PULSE ANALYSIS

The turbulence pulse was examined at three positions (4″, 6″, and 8″) downstream of the spinning rod with the wing and wingmount assembly removed. The smoothed mean velocity time histories for the three positions are shown in Figure 31. The plots show a nearly symmetric velocity deficit trace at all three positions. Pulse duration is roughly 250 samples or 5 milliseconds and the deficit maxima are constant at -20 ft/sec.

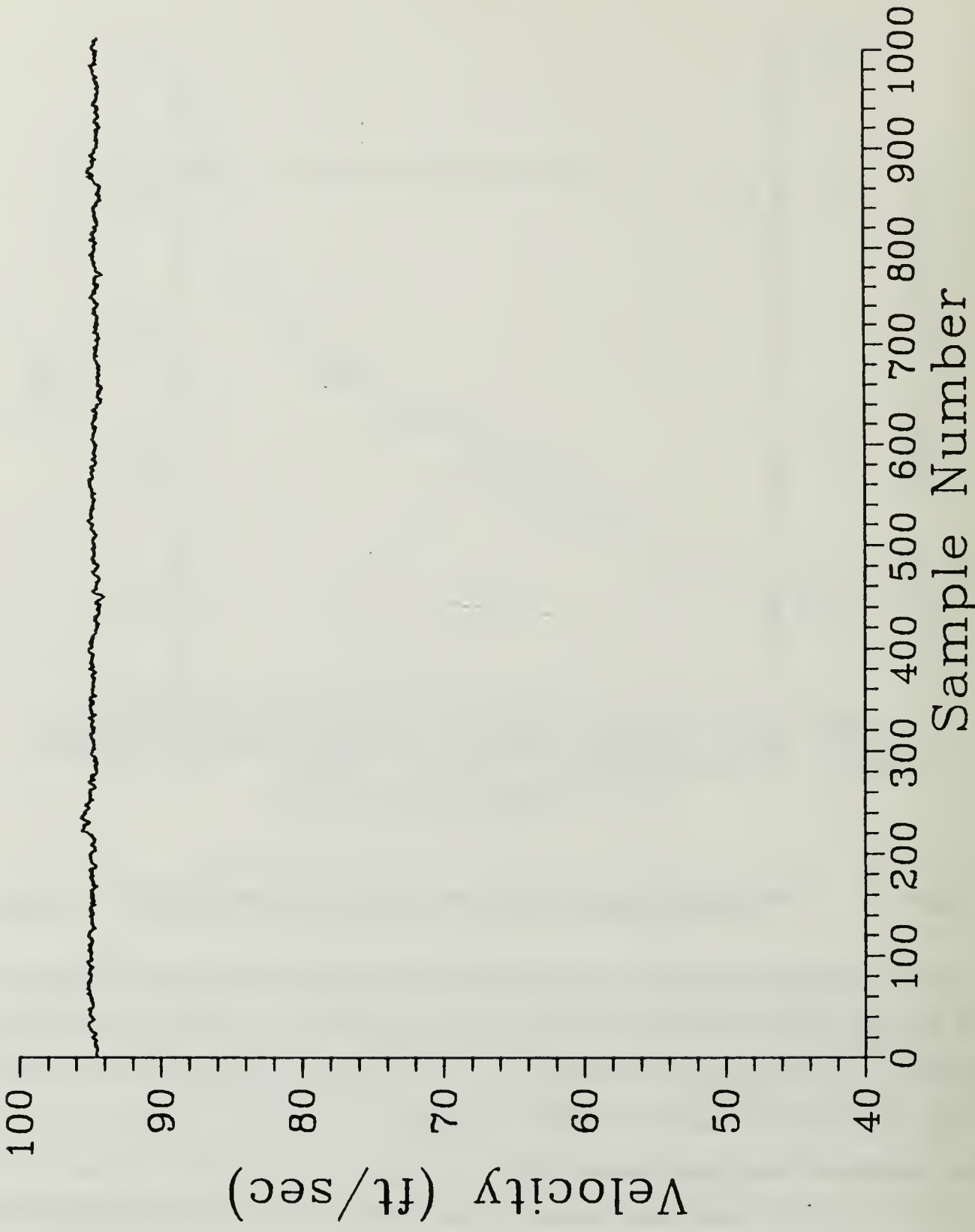

Figure 28. Test Section Free Stream Flow: (Fs = 50 KHz)

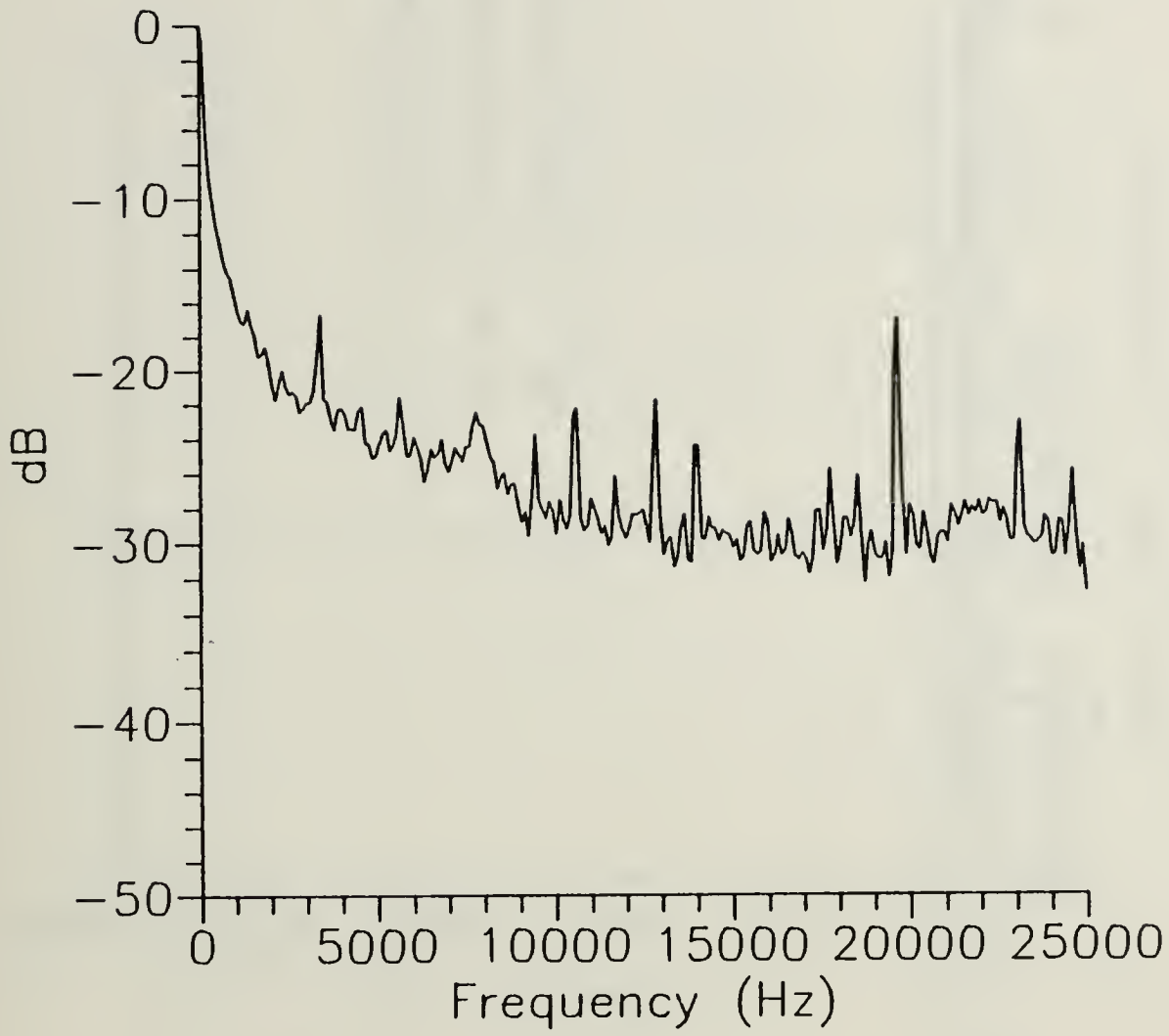

Figure 29. Free Stream Velocity Spectrum

The width of the deficit appears to increase slightly with increasing distance downstream. The velocity deficit trace observed for the spinning rod is very similar to that generated by a stationary cylinder in steady cross flow. This similarity shows that spinning the rod does not significantly alter the classical response of the cylinder.

Figure 32 is the plot of the smoothed mean turbulence traces of the turbulence pulse at the same positions. The pulse is intensely turbulent with a peak value of 10.5%. The turbulence traces coincide with the velocity traces; however, the turbulence traces become somewhat non-symmetric downstream. In addition, the turbulence appears to anticipate or lead the velocity deficit by up to 60 samples or 1.2 milliseconds. Most notably, the turbulence magnitude decreases quite rapidly with distance downstream.

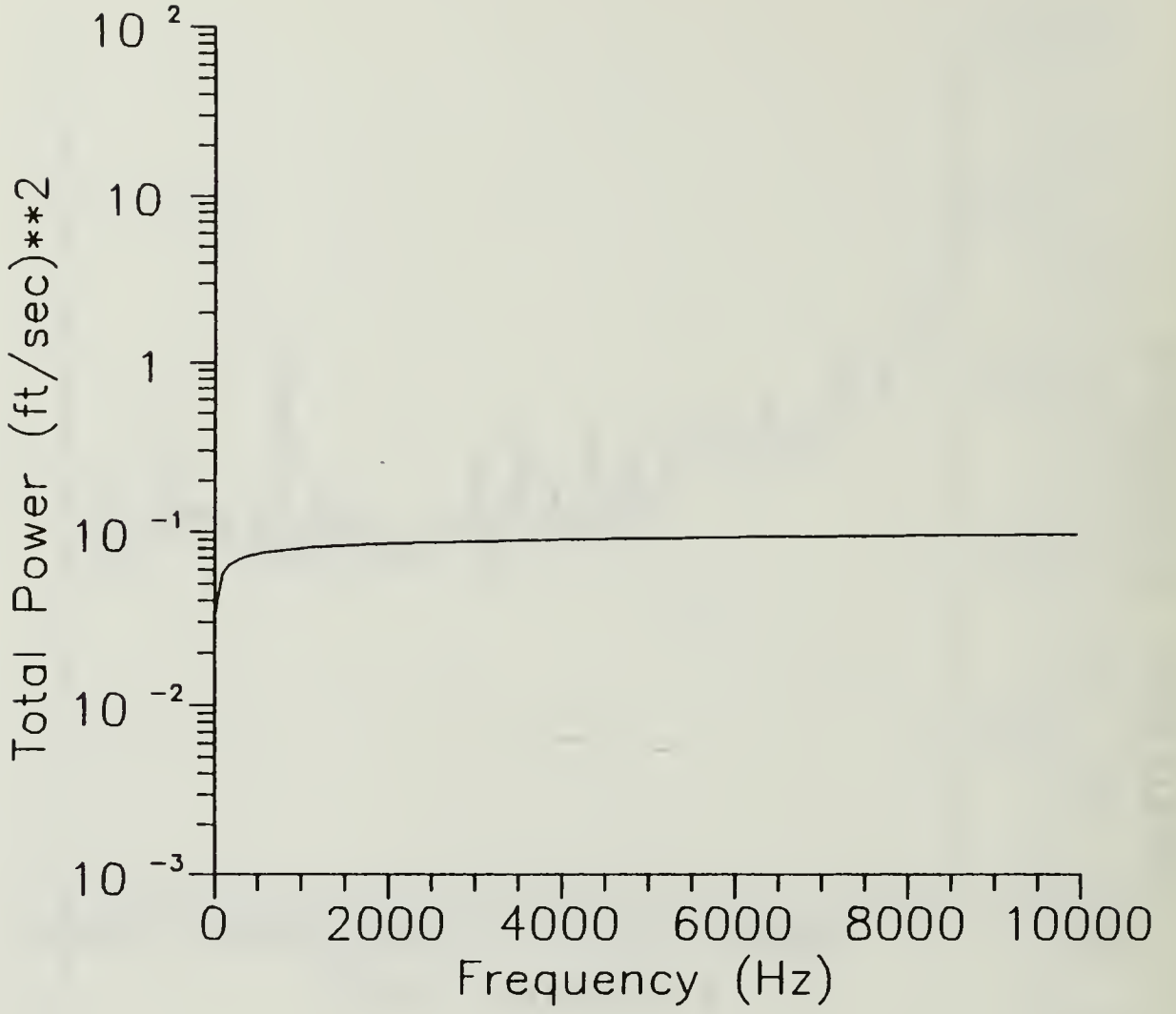

Figure 30. Free Stream Total Power Distribution

This decay is not unexpected and is generally attributed to dissipation of the high frequency turbulence components due to viscosity [Ref. 15: p. 48].

Figure 33 shows the velocity spectra of the turbulence pulse regime and the undisturbed flow regime taken at 4" downstream from the spinning rod. The turbulence pulse trace decays more rapidly and to a lower level than the undisturbed flow trace. Additionally, the undisturbed flow trace levels out at approximately -20 dB for frequencies above 5 KHz while the turbulence pulse trace bottoms out at -42 dB. These plots show the turbulence pulse to be a low frequency dominated event while the undisturbed flow regime has components at much higher frequencies.

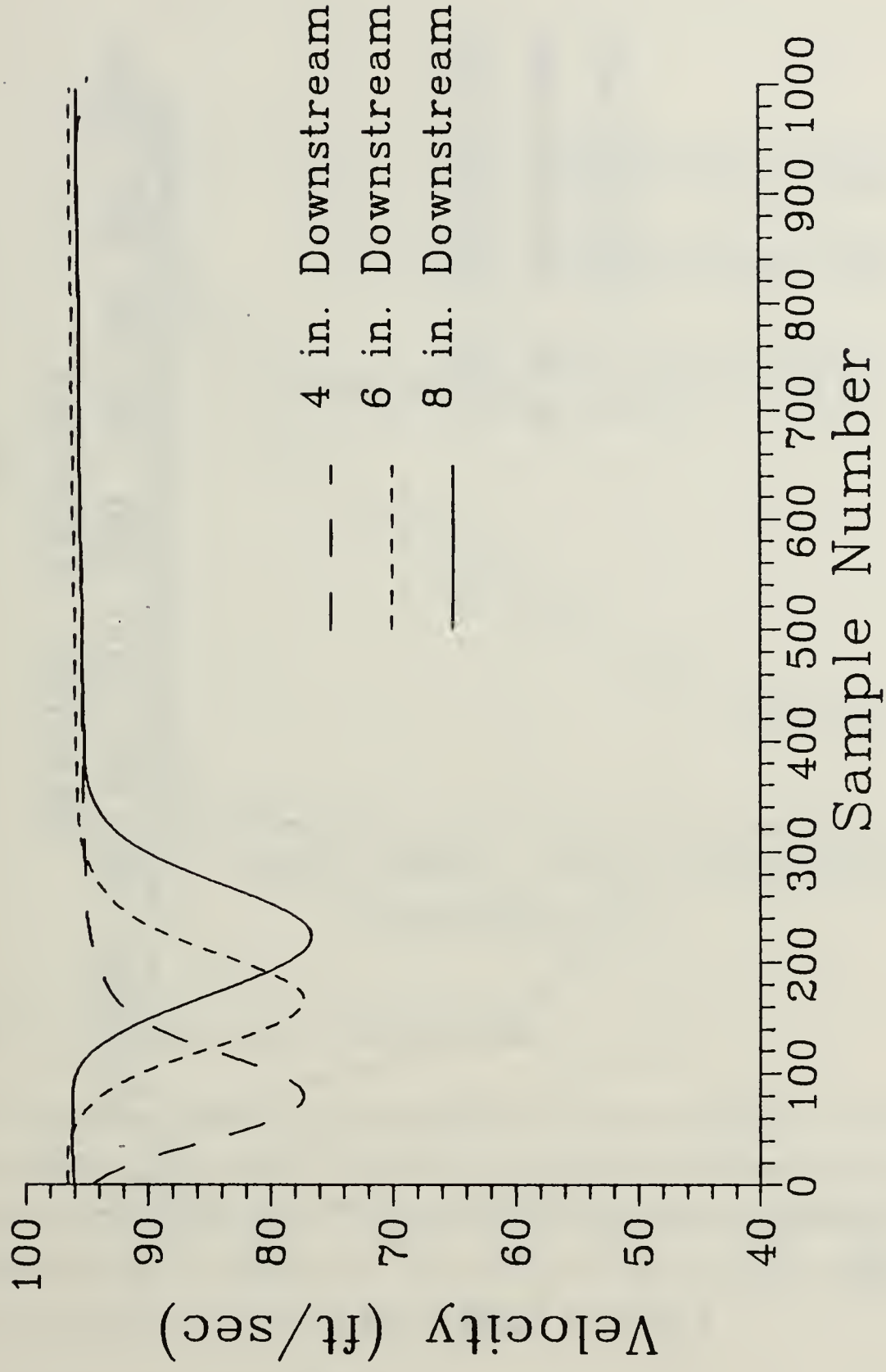

Figure 31. Turbulence Pulse Mean Velocity: (Fs = 50KHz)

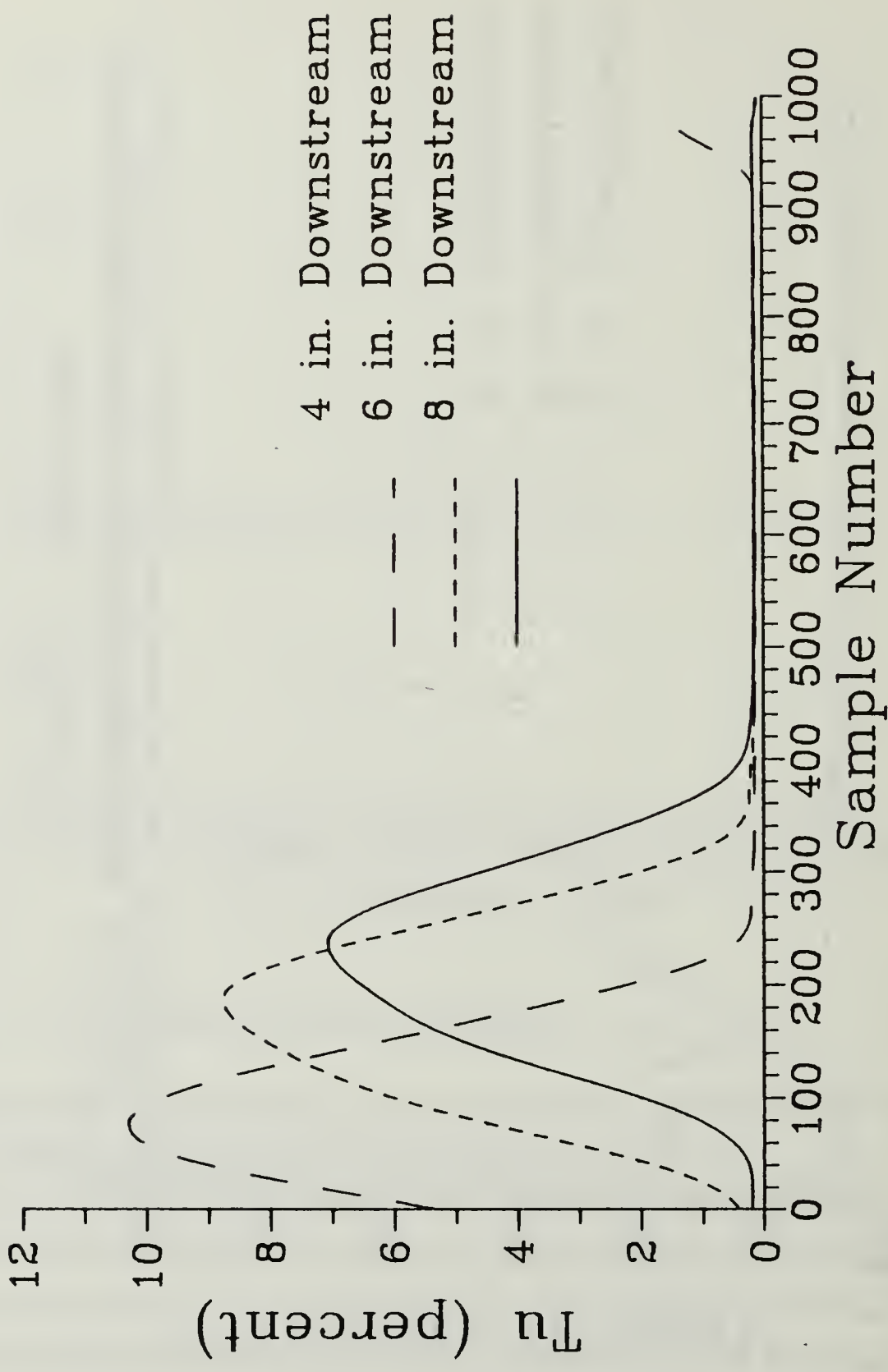

Figure 32. Turbulence Pulse Mean Turbulence: (Fs = 50 KHz)

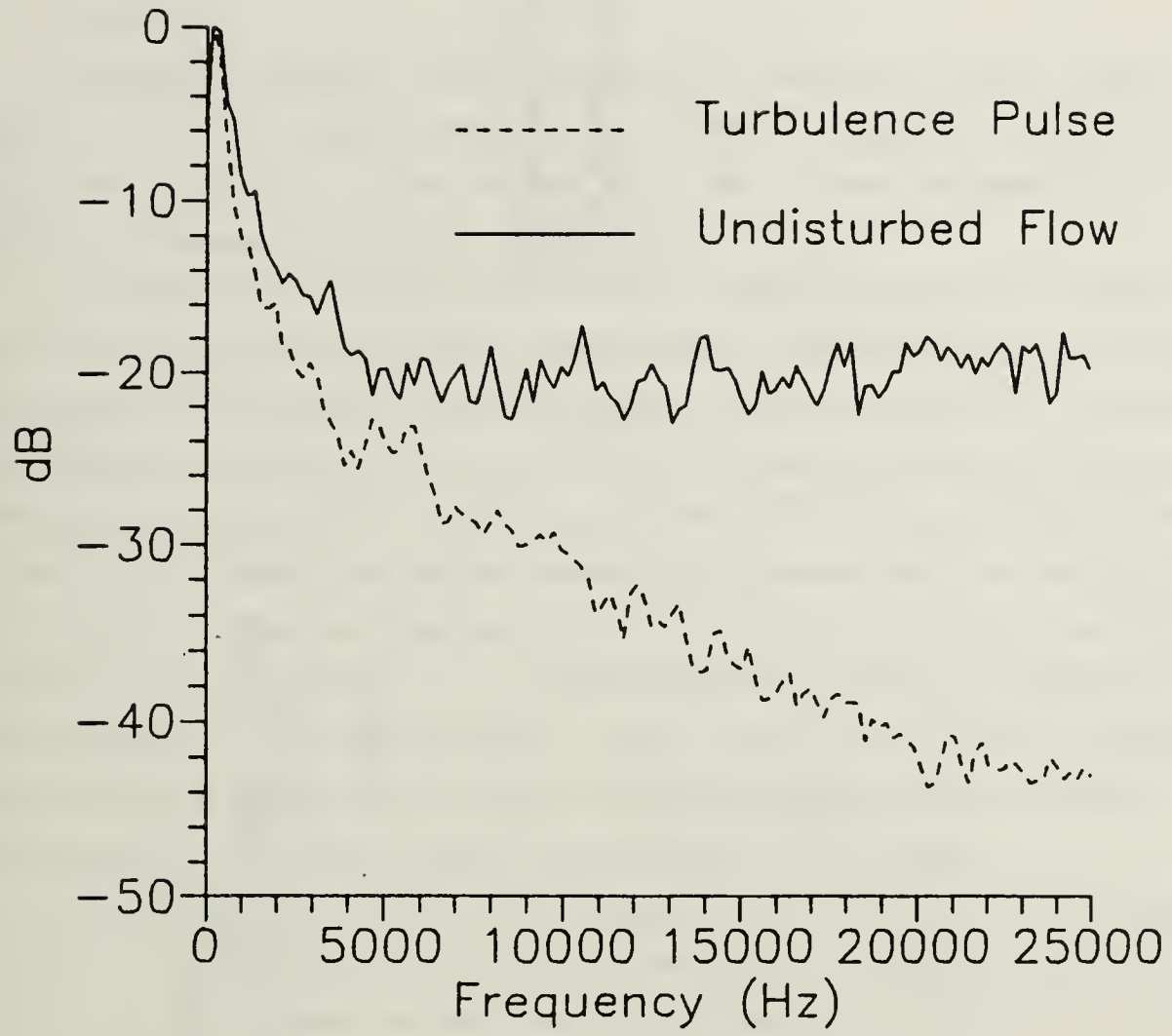

Figure 33. Turbulence Pulse Velocity Spectrum

The total power curves for the two regimes are plotted in Figure 34. The intensity of the turbulence pulse is clearly shown here; the pulse power is 4 orders of magnitude greater than the undisturbed flow. The rapid rise and sharp knee of the pulse trace also confirms the intense, low frequency nature of the turbulence pulse. Very little power is added by the frequency components above 1 KHz.

E. BOUNDARY LAYER ANALYSIS

The response of the boundary layer to periodic turbulence was investigated at three locations on the upper surface of the wing: 30% chord, 50% chord, and 70% chord. These three locations were chosen as the natural steady-state (undisturbed) flow was

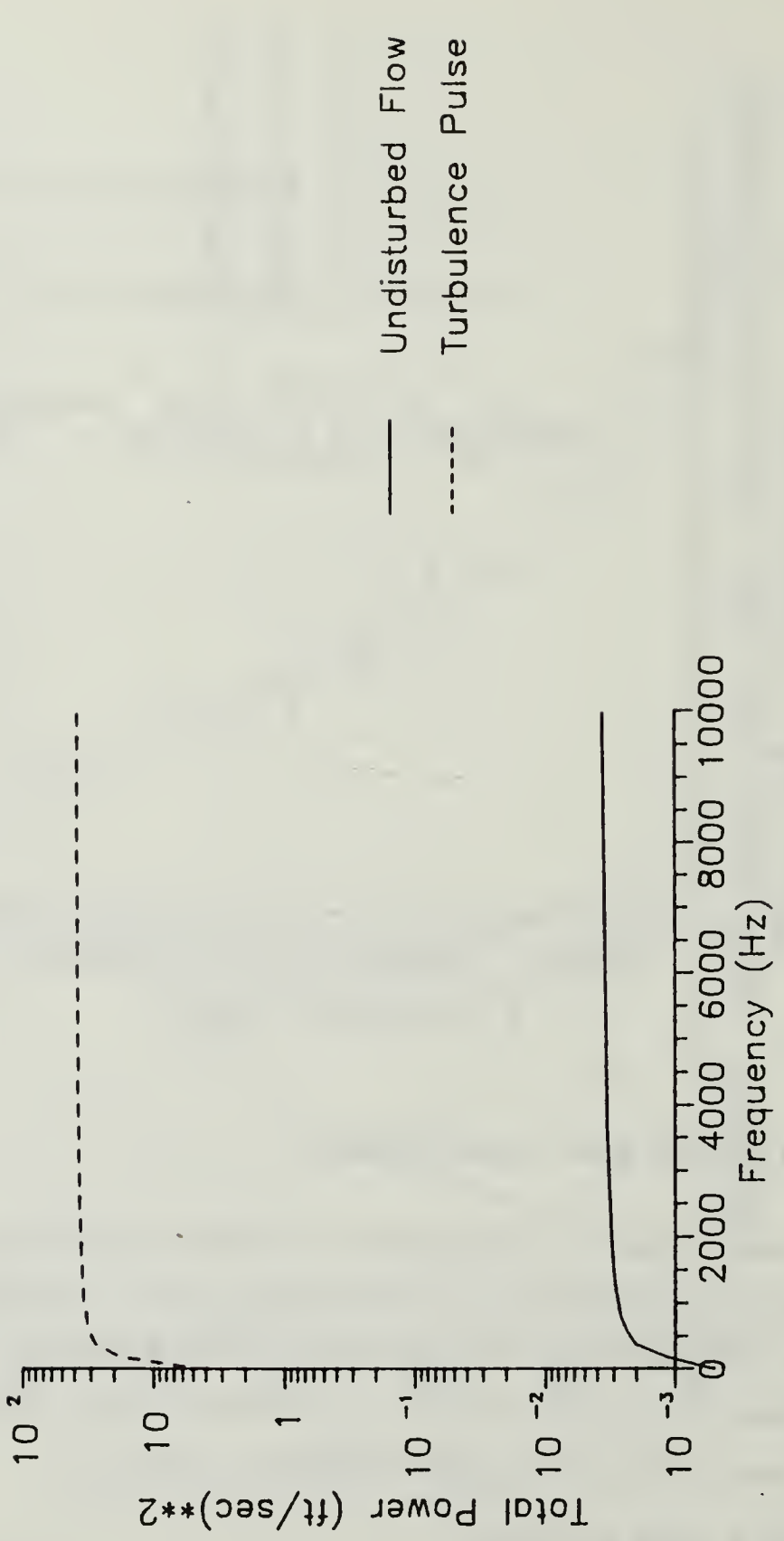

Figure 34. Turbulence Pulse Total Power Distribution

laminar at 30% chord, transitional/turbulent at 50% chord, and fully turbulent at 70% chord.

1. **30% Chord**

The ensemble-average velocity and turbulence profiles are shown in Figure 35. These plots consist of a series of time-sequenced profiles, or "snapshots", taken at several points in the time history. These profiles depict the dynamic characteristics of the boundary layer throughout one pulse passage cycle.

The profiles show that the flow at 30% chord transitions from undisturbed laminar flow with very little turbulence (sample 100); to highly turbulent flow with a nearly constant level of turbulence at the turbulence pulse center (sample 275); and back again to laminar flow (sample 550). It is interesting to note how quickly and uniformly the boundary layer responds to the turbulence pulse. The turbulence profiles show a nearly uniform turbulence increase and corresponding decrease with the passing of the turbulence pulse. At the same time, the velocity profiles transition quickly from laminar to turbulent and back to laminar in step with the turbulence pulse. The velocity increase observed near the surface of profile 350 is unusual. The velocity increase occurs just after the turbulence pulse and is still evident in the following profile (sample 400). The possible reasons for this behavior will be examined later in this section.

The smoothed mean velocity time histories and the smoothed mean turbulence time histories of the pulse passage cycle are shown in Figure 36 and Figure 37 respectively. These traces represent the time histories at increasing vertical distances (y) above the wing surface. The bottom trace shows the flow history taken closest to the wing surface (near-surface region) while the top trace depicts external flow outside of the boundary layer.

The velocity and turbulence traces in the external flow region are typical of the response observed downstream of the periodic turbulence generator (Figure 31 and Figure 32); i.e., a symmetric, bell-shaped pulse followed by an immediate return to the free stream or undisturbed state.

The velocity time history traces show a velocity deficit of 11 ft/sec in the external flow due to the turbulence pulse. This deficit increases as the surface is approached until very close to the wing. Quite near the surface, the velocity deficit decreases significantly and is followed by a sharp velocity increase just after the turbulence pulse. This velocity increase remains for some time and is slow to dissipate. The turbulence traces, on the other hand, show that the turbulence intensity of the pulse is

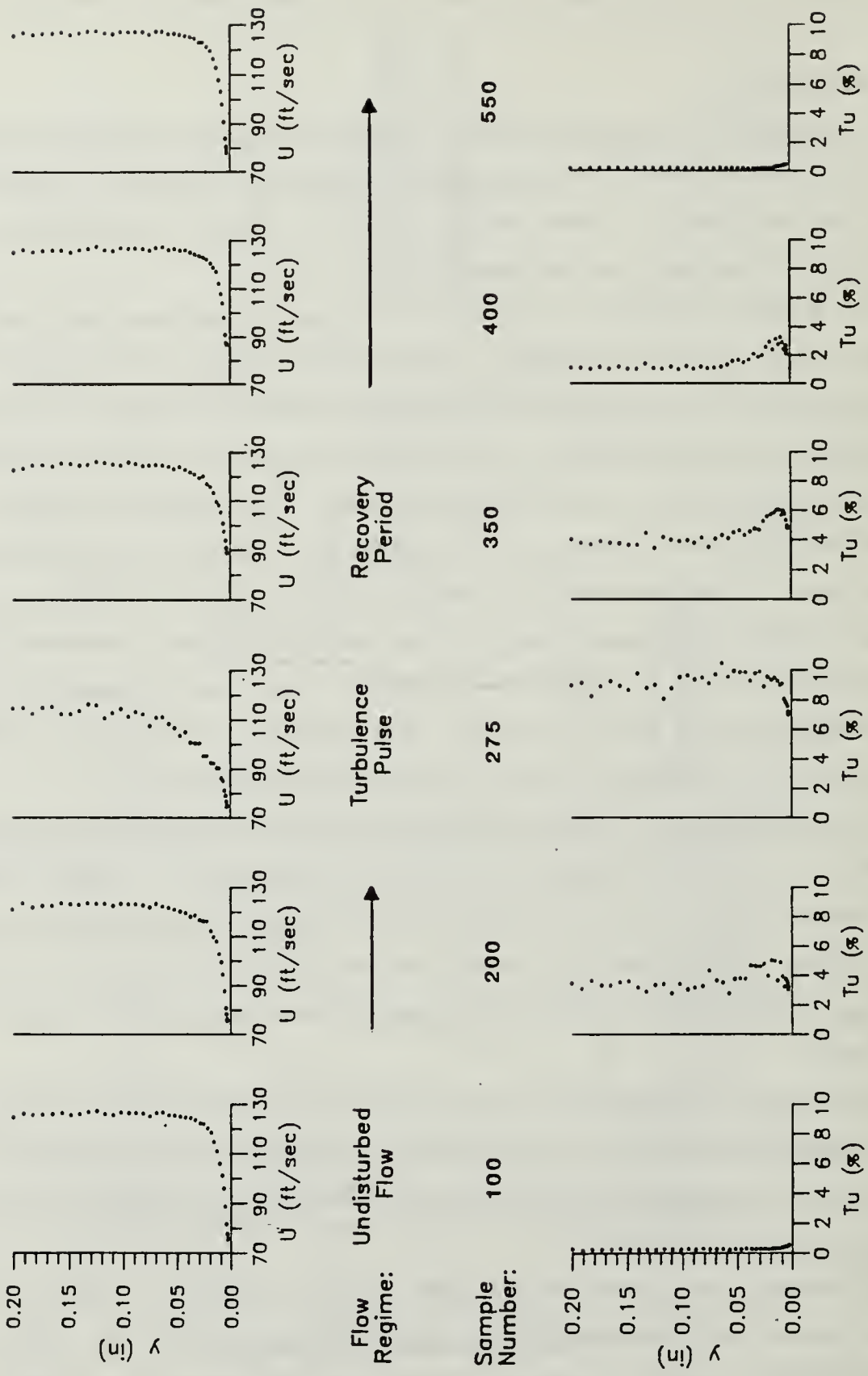

Figure 35. Ensemble Average Profiles, 30% Chord

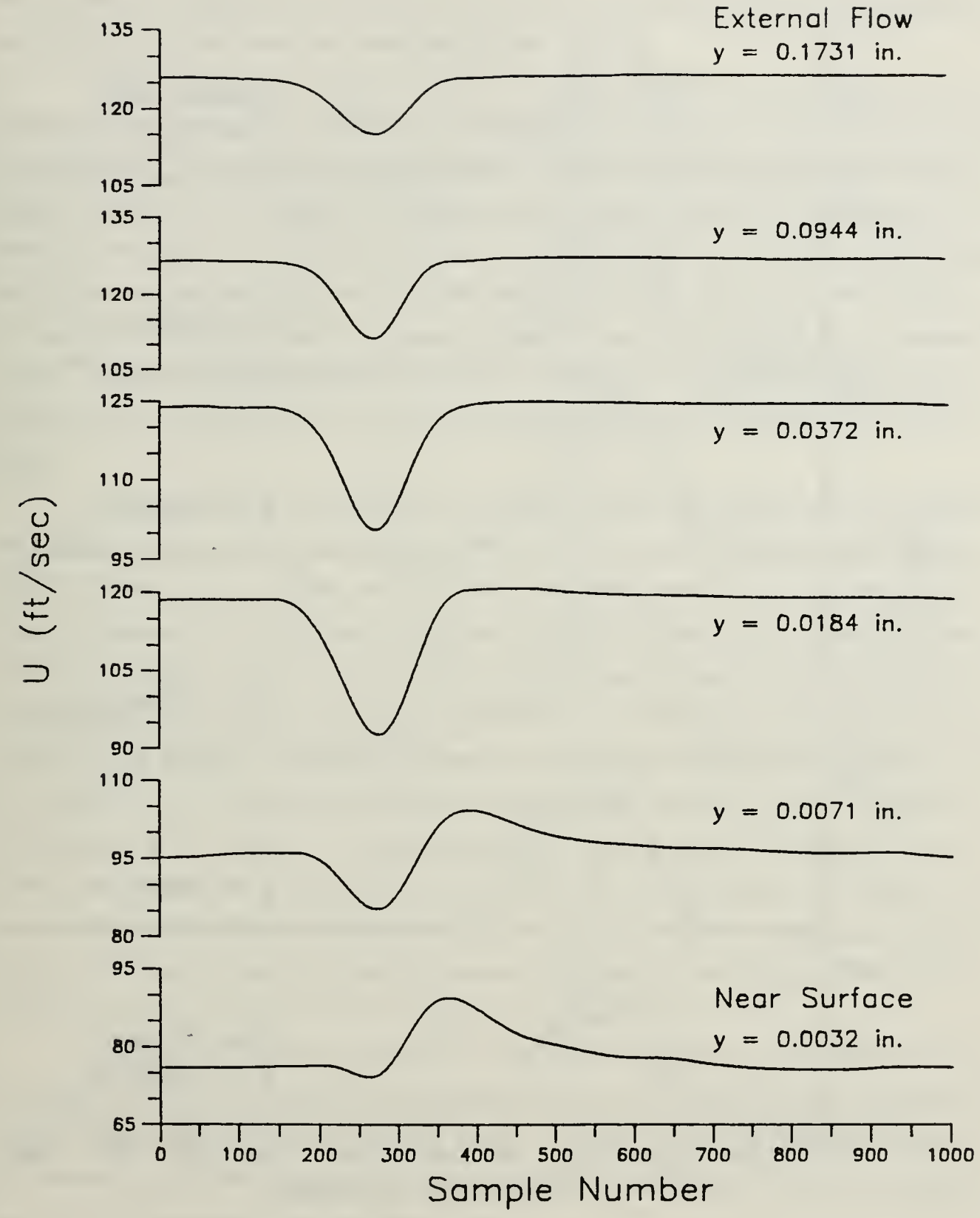

Figure 36. Mean Velocity Time Histories in the Boundary Layer, 30% Chord: (Fs = 50 KHz)

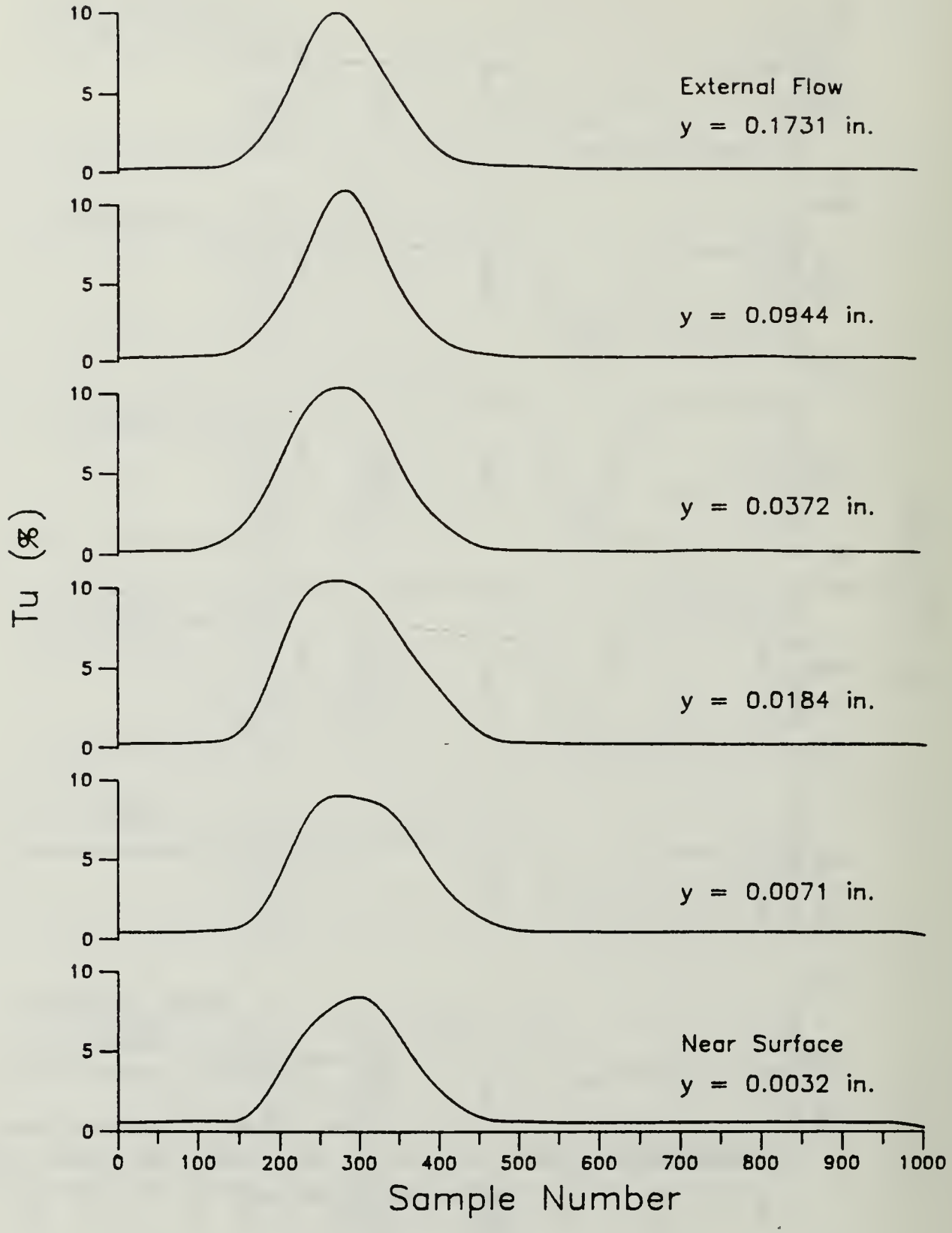

Figure 37. Mean Turbulence Time Histories in the Boundary Layer, 30% chord: (Fs = 50 KHz)

felt uniformly throughout the boundary layer with only a slight reduction in magnitude and stretching of the pulse very near the surface.

Figure 38 through Figure 42 show the velocity spectrum and total power distribution plots for the three major flow regimes (undisturbed flow, turbulence pulse, and recovery period) at points in the boundary layer. Recall that the velocity spectrum plot display is relative to the highest component in the spectrum while the total power distribution plot depicts the cumulative actual power with regard to frequency. Recall also that the mean has been removed from the spectral analysis. Hence, power changes in the mean due to mean velocity increases or deficits are not reflected in the spectral curves. One must view the mean velocity and turbulence time histories along with the profiles and the spectral plots as a group in order to understand the boundary layer behavior.

Notice how little the turbulence pulse affects the spectral distribution very near the surface in Figure 38. The velocity spectra for the undisturbed flow and recovery period regimes are very similar and the total power distribution curves for the two regimes are comparable in shape and magnitude. In addition, there is no unusual recovery period in this region. The turbulence pulse comes and goes without affecting the spectral characteristics of the flow very near the surface. Higher in the boundary layer, Figure 40 and Figure 41, the high frequency components become more significant in the undisturbed flow and recovery period regimes while the total power contained in both regimes drops sharply. This indicates more spectral power (turbulence) is contained in the boundary layer very near the surface than in the intermediate regions or even in the external flow region. Note: The author is unable to explain the unusual shapes of the undisturbed flow velocity spectra in Figure 41 and Figure 42 or the apparent increase in undisturbed flow total power in Figure 42.

Together, the velocity spectra and total power distribution plots show that the flow recovers very quickly from the turbulence pulse and the pulse does not significantly affect the characteristics of the recovery period. In other words, the undisturbed flow and recovery period velocity spectra and total power distribution curves are virtually identical at all positions in the boundary layer.

The author believes an understanding of the mechanics operating in the boundary layer at this chord location is essential in understanding the more complex responses observed at 50% and 70% chord. The discussion that follows is the author's interpretation of the operating mechanics.

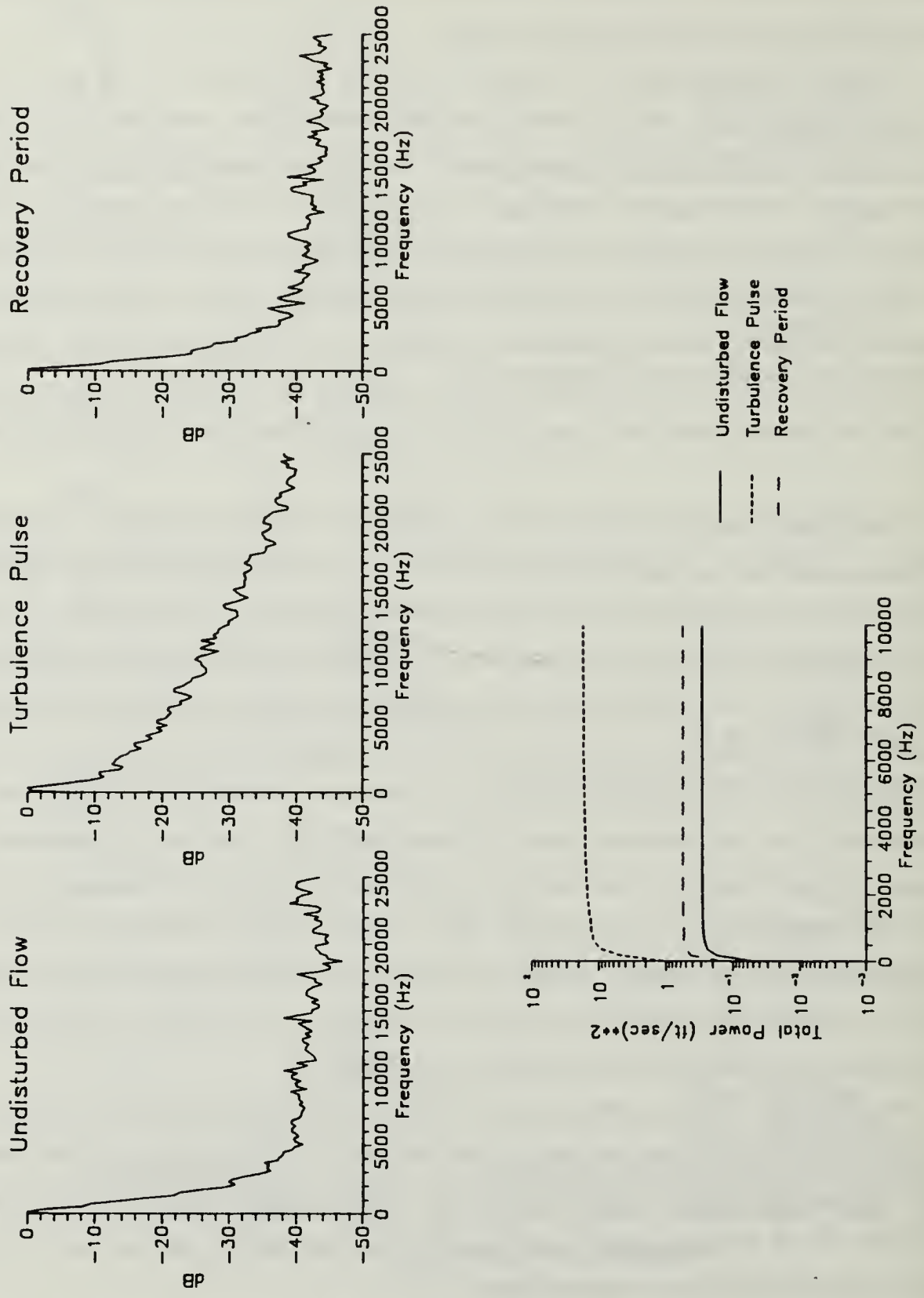

Figure 38. Velocity Spectra and Total Power Distribution, 30% Chord, y = 0.0032″

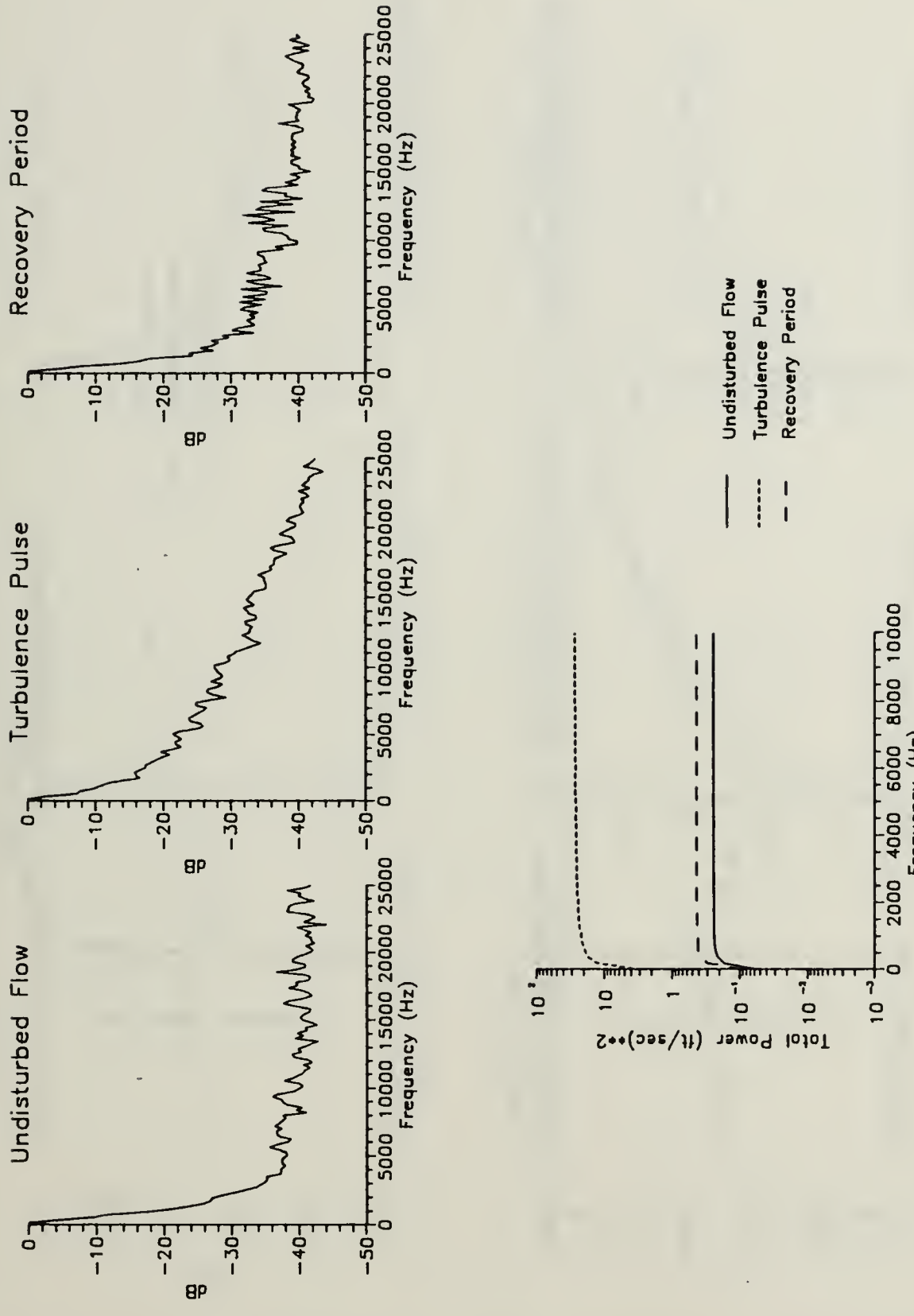

Figure 39. Velocity Spectra and Total Power Distribution, 30% Chord, y = 0.0071″

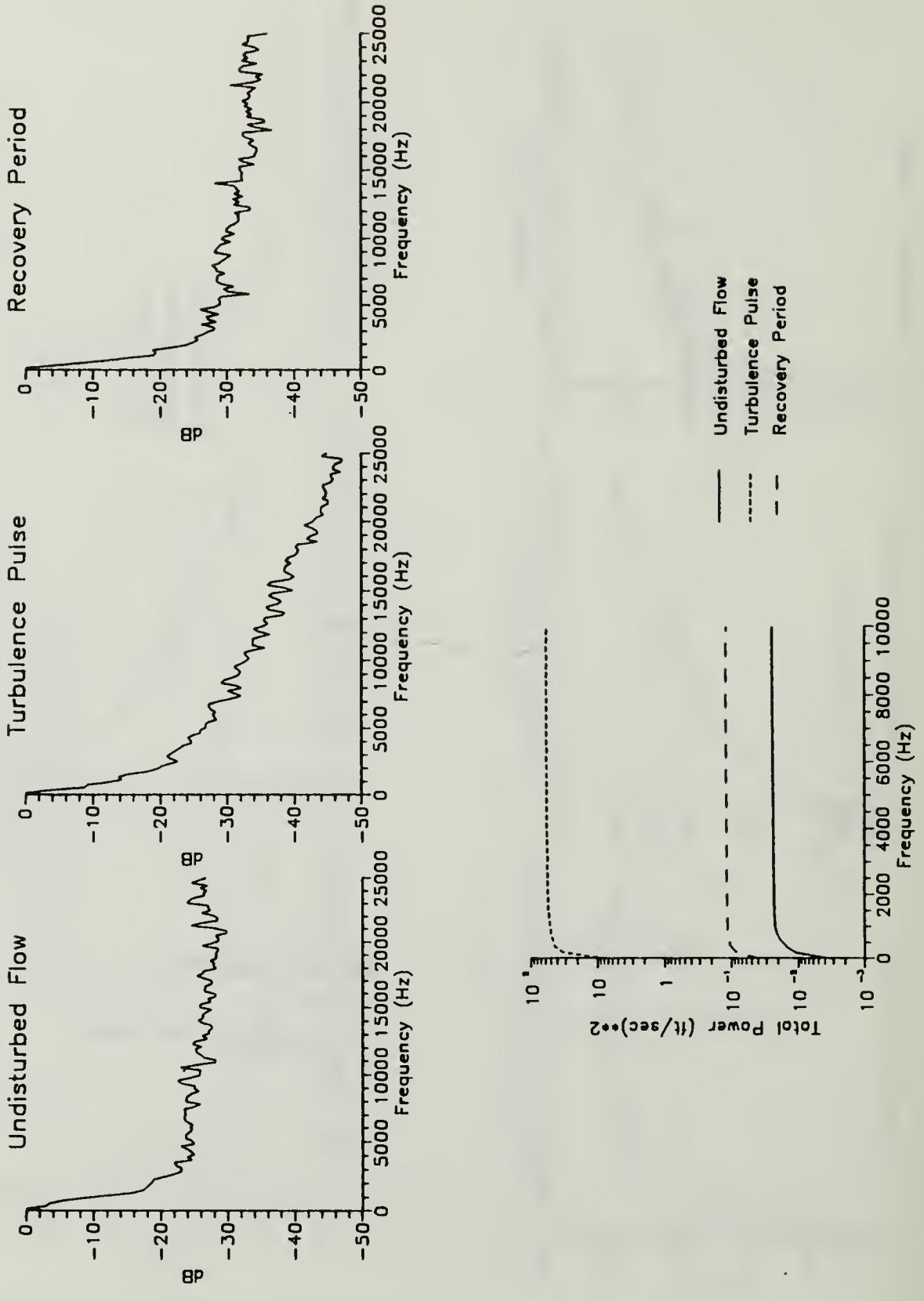

Figure 40. Velocity Spectra and Total Power Distribution, 30% Chord, y = 0.0184″

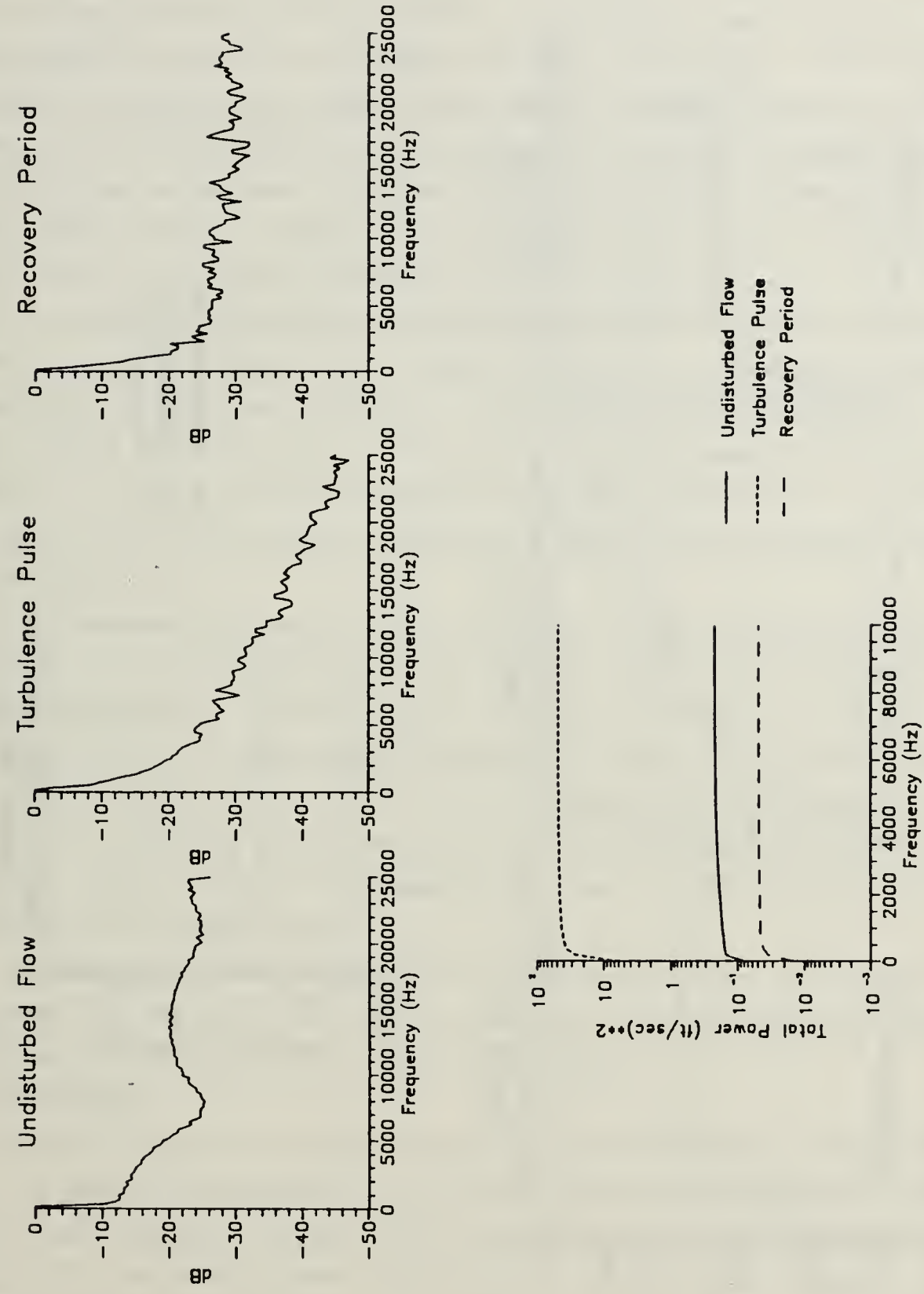

Figure 41. Velocity Spectra and Total Power Distribution, 30% Chord, y = 0.0372″

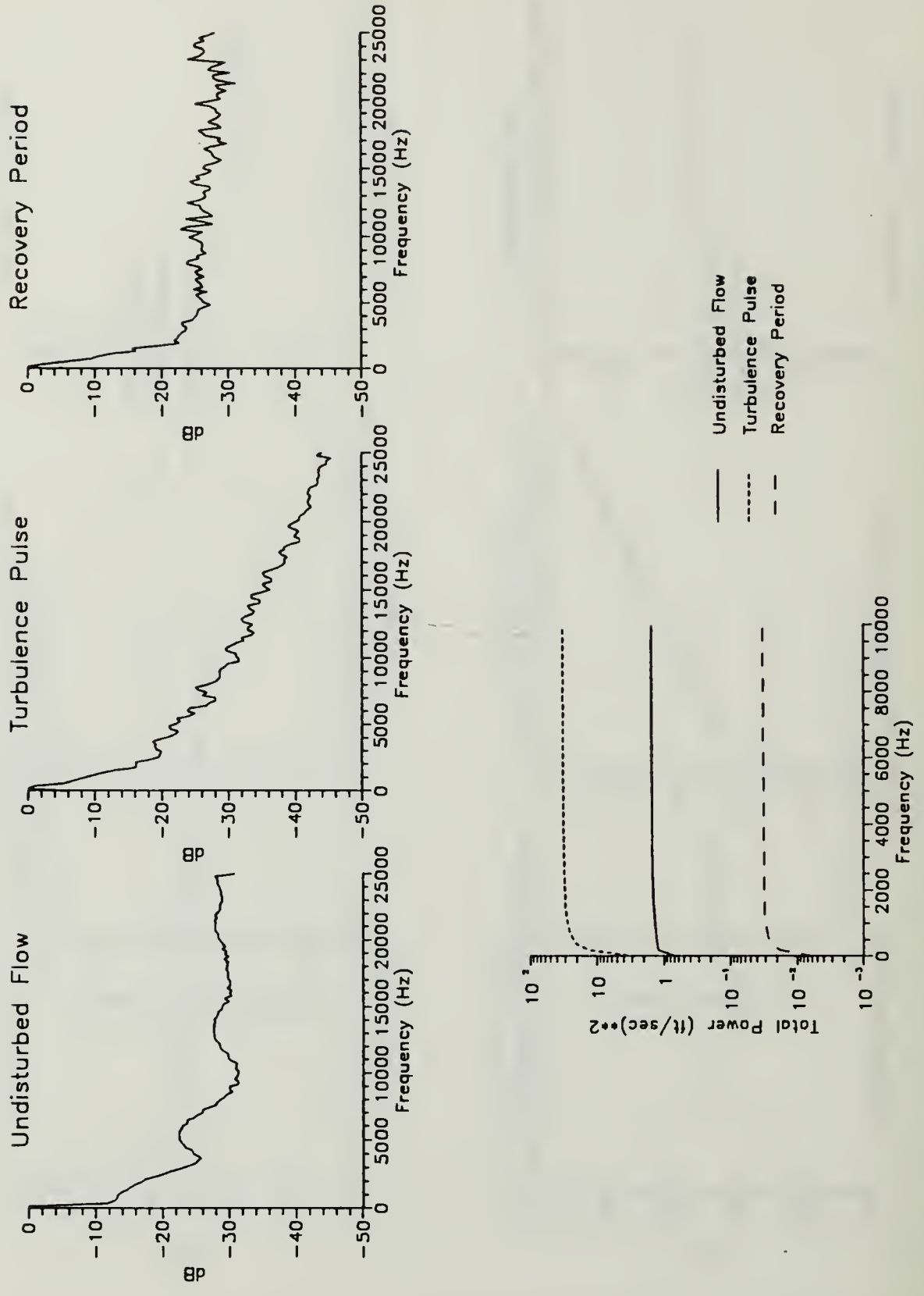

Figure 42. Velocity Spectra and Total Power Distribution, 30% Chord, y = 0.0944″

The data show a normally laminar flow being uniformly disturbed by a strong, highly turbulent pulse from the external flow. The boundary layer responds to the passing pulse by momentarily transitioning to extremely turbulent flow. Once the pulse has passed, the boundary layer rapidly returns to low turbulence laminar flow. Note however, that the velocity time history graph (Figure 36) shows that the mean velocity quite near the surface increases in response to the turbulence pulse. Furthermore, this velocity increase remains in evidence for a considerable period after the velocity profile returns to laminar. The cause of this velocity increase is important.

The turbulence time histories show there is considerable turbulence and mixing throughout the entire boundary layer in response to the pulse. This seems to indicate that momentum transfer down through the boundary layer is possibly responsible for the velocity increase near the surface. The velocity time histories seem to support this supposition with regard to observed characteristics of the velocity deficit. The growth of the velocity deficit as the surface is approached is consistent with momentum transfer down through the layer.

The boundary layer region very near the wing surface cannot transfer momentum due to the solid wing boundary. Thus, the near-surface region absorbs all the transferred momentum as a velocity increase. This is evidenced by the sharp decrease of the velocity deficit and rapid velocity increase, or flow acceleration, just following the pulse. These two phenomena are clearly observed in the bottom two velocity time histories. Finally, the velocity increase remains in the near-surface region due to the positive velocity gradient ($\frac{dU}{dy}$) in the boundary layer and is slowly dissipated by the viscous effects of the laminar layer.

In summary, the velocity increase in the near-surface region of the boundary layer appears to be the result of a downward transfer of momentum within the boundary layer induced by the high turbulence of the turbulence pulse.

2. 50% Chord

Figure 43 shows the ensemble average velocity and turbulence profiles at 50% chord. The boundary layer response at this position is quite unlike the simple laminar-turbulent-laminar response observed at 30% chord. To begin with, the undisturbed flow at sample 150 is transitional/turbulent with 5% to 6% turbulence near the surface. The flow becomes extremely turbulent at sample 350 with a high level of turbulence across the entire profile. During the recovery period, the flow becomes what appears to be fully laminar by sample 650; the turbulence is extremely low over the entire region and the boundary layer thickness has decreased from around 0.08 inches at sample 150 to 0.04

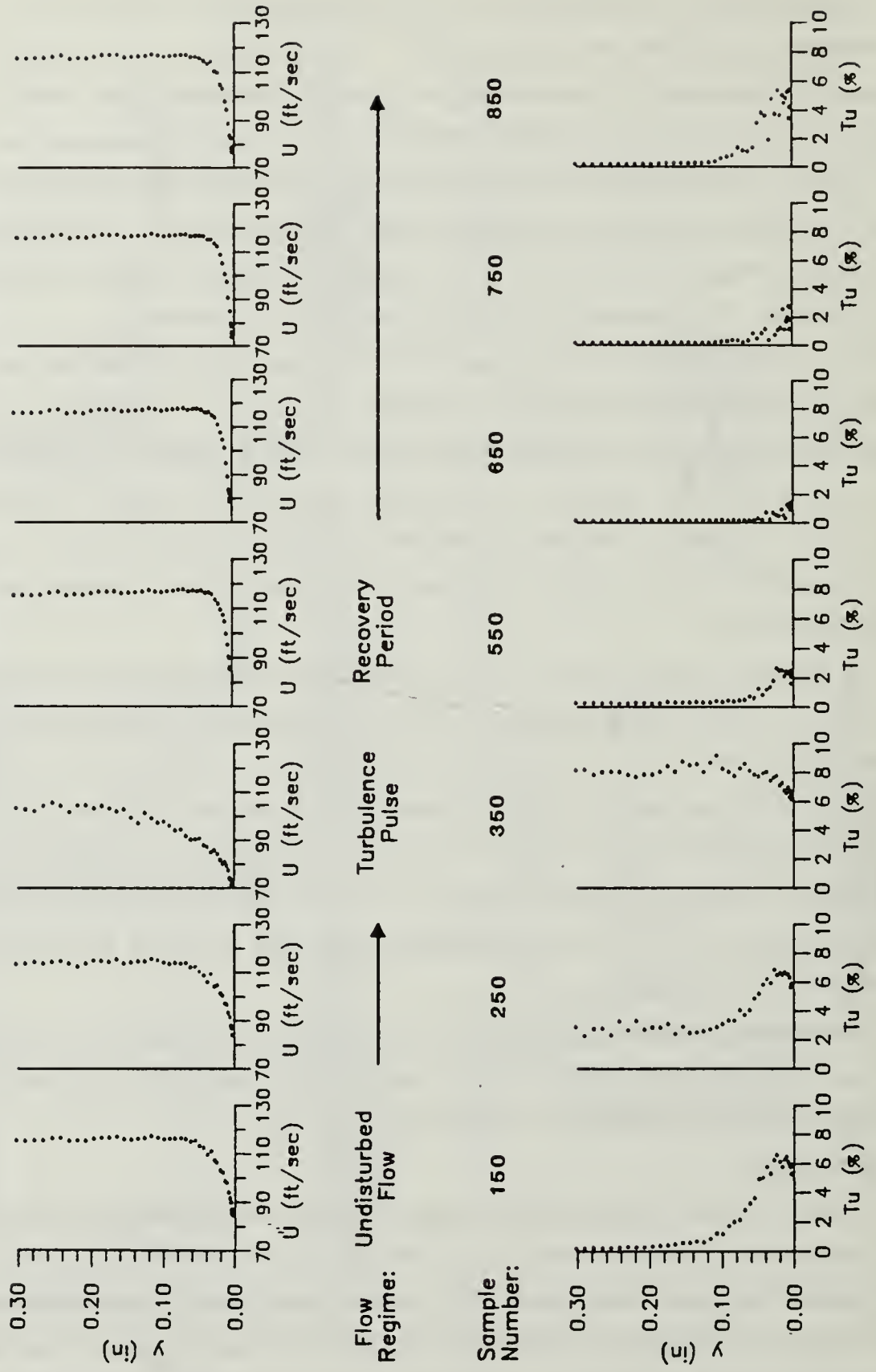

Figure 43. Ensemble Average Profiles, 50% Chord

inches. Samples 750 and 850 show the flow returning to the original transitional/turbulent state as evidenced by increasing levels of turbulence in the near surface region.

The smoothed velocity time histories (Figure 44) clearly show the influence of the velocity deficit over the entire boundary layer. The corresponding smoothed turbulence time histories (Figure 45), however, do not show any turbulence penetration into the near-surface region. Apparently the high level of natural near-surface turbulence overshadows the effects of the turbulence pulse. The apparent answer to this dilemma lies in the velocity spectra and total power distribution plots of the undisturbed flow regime and the turbulence pulse regime near the surface.

Shown in Figure 46 are the velocity spectra and total power distribution curves taken near the bottom of the boundary layer. This figure corresponds to the near-surface region of the mean velocity and mean turbulence traces. The undisturbed flow total power trace is quite broad banded with significant power contributions from the frequency components up to 4 KHz due to the high levels of turbulence generated near the surface. The turbulence pulse, on the other hand, is a low frequency dominated phenomenon having no significant spectral power components above 1 KHz. Thus, while the turbulence intensity of the undisturbed flow and turbulence pulse are almost equal in magnitude, the spectral makeup of each regime varies greatly. The distinct nature of the turbulence pulse makes it felt throughout the turbulent near-surface layers. The effect of the turbulence pulse on the undisturbed flow is clearly seen in this figure. The undisturbed flow spectrum is altered by the turbulence pulse such that the recovery period spectrum resembles the turbulent pulse spectrum.

Figure 47 through Figure 51 depict the changes in the velocity spectra and total power distribution at increasing vertical distances in the boundary layer. Near the surface (Figure 46), the turbulence pulse clearly alters the recovery period spectrum by removing the high frequency components contained in the undisturbed flow regime. In the middle of the boundary layer (Figure 49), the recovery period spectrum begins to resemble that of the undisturbed flow showing the decreasing impact of the turbulence pulse on the flow. Finally, in the external-flow region (Figure 51), the undisturbed flow and recovery spectra match, indicating that the effects of the turbulence pulse are purely transient. Of interest are the very large spikes in the spectra of the recovery period plots for $y < 0.1250$ inches. The author speculates that these are Tollmien-Schlichting waves generated during the laminar to turbulent transition.

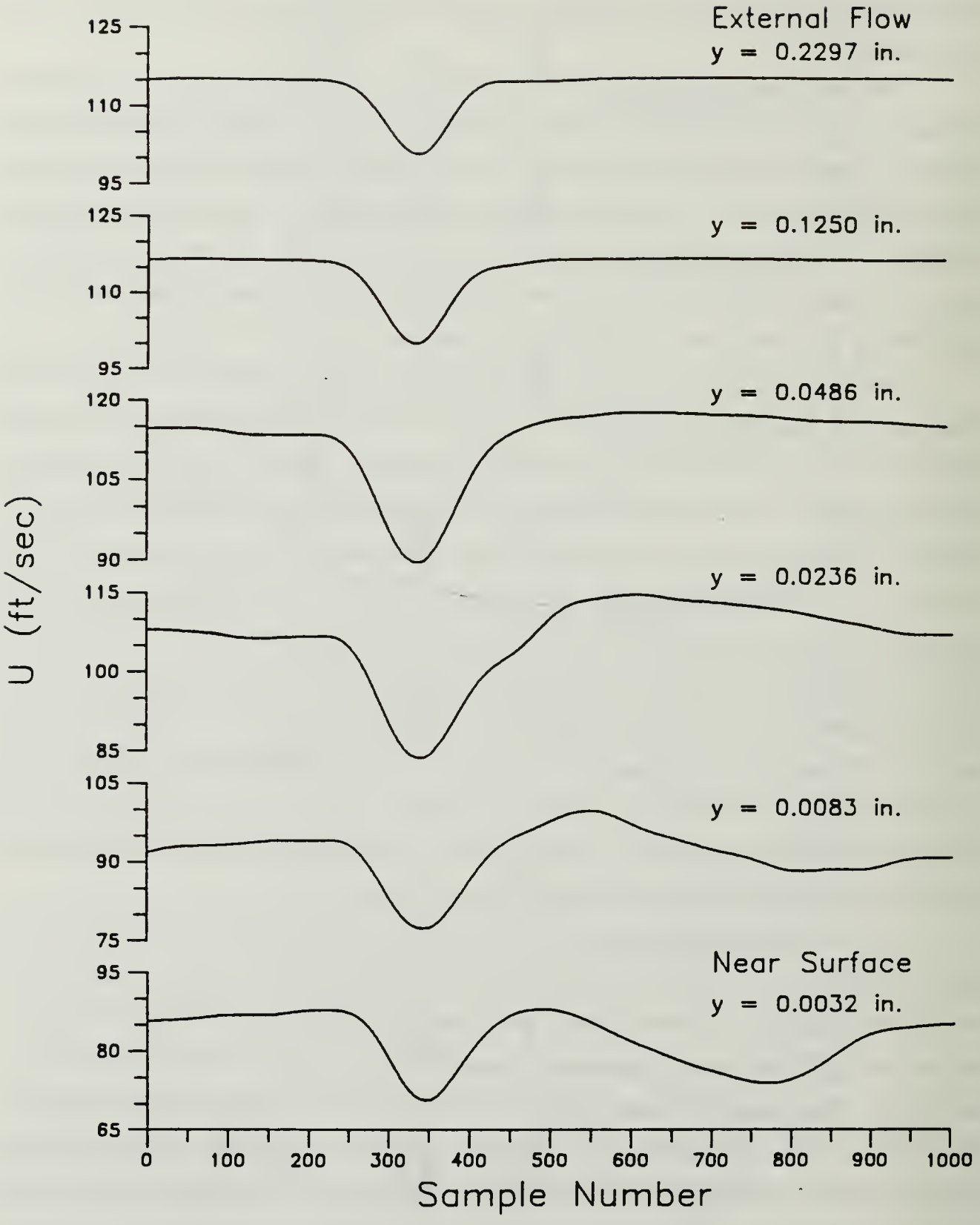

Figure 44. Mean Velocity Time Histories in the Boundary Layer, 50% Chord: (Fs = 50 KHz)

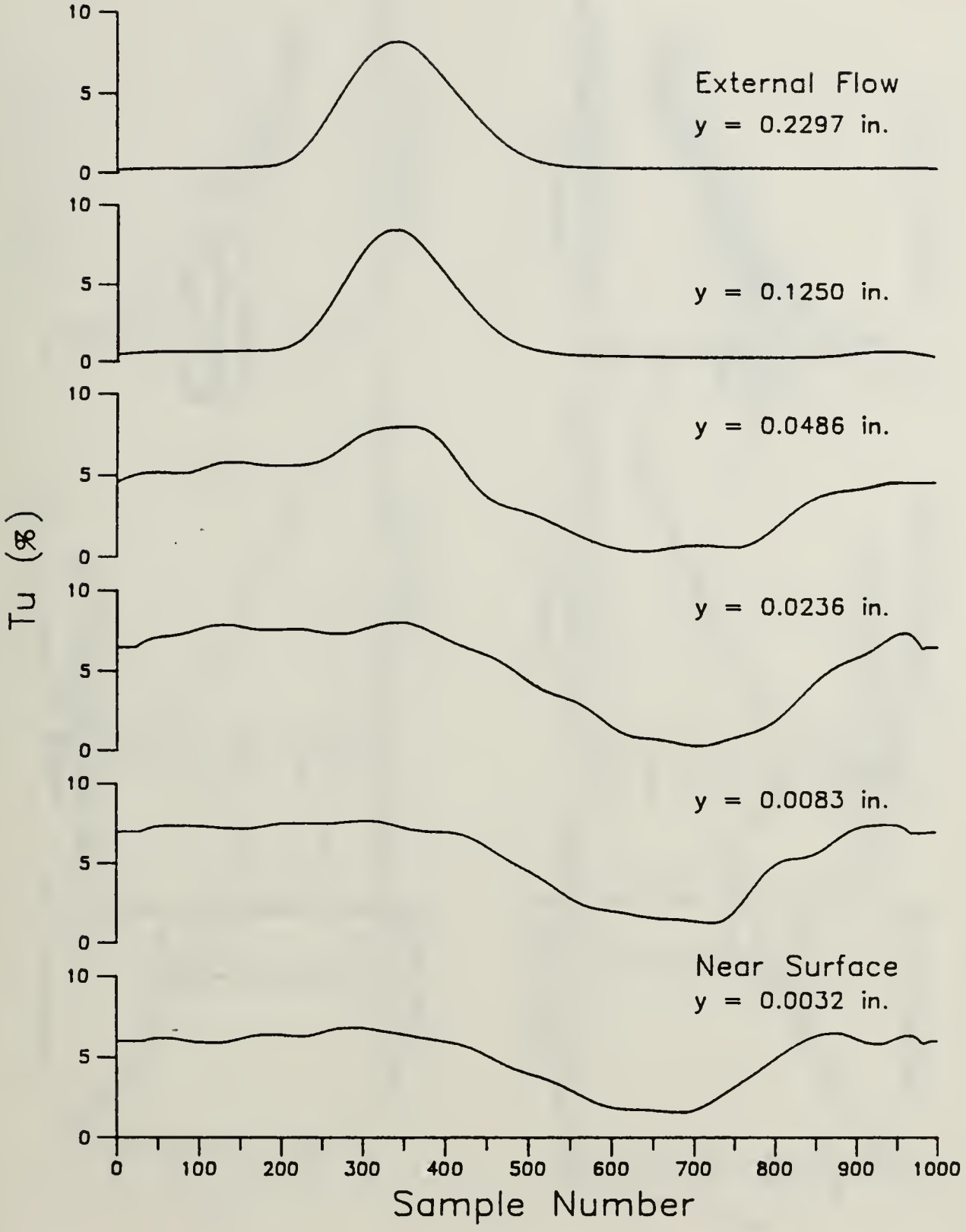

Figure 45. Mean Turbulence Time Histories in the Boundary Layer, 50% Chord: (Fs = 50 KHz)

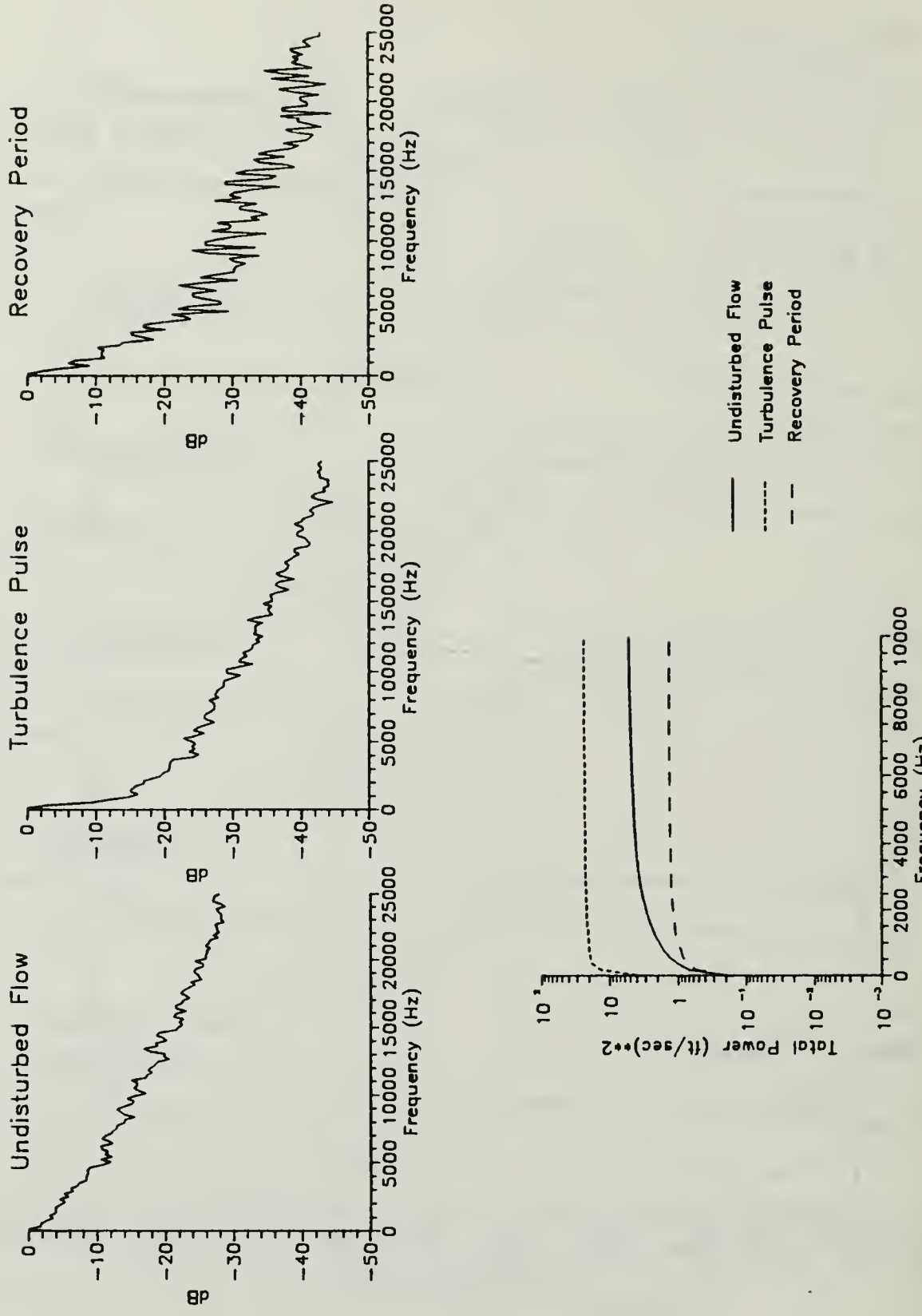

Figure 46. Velocity Spectra and Total Power Distribution, 50% Chord, y = 0.0032″

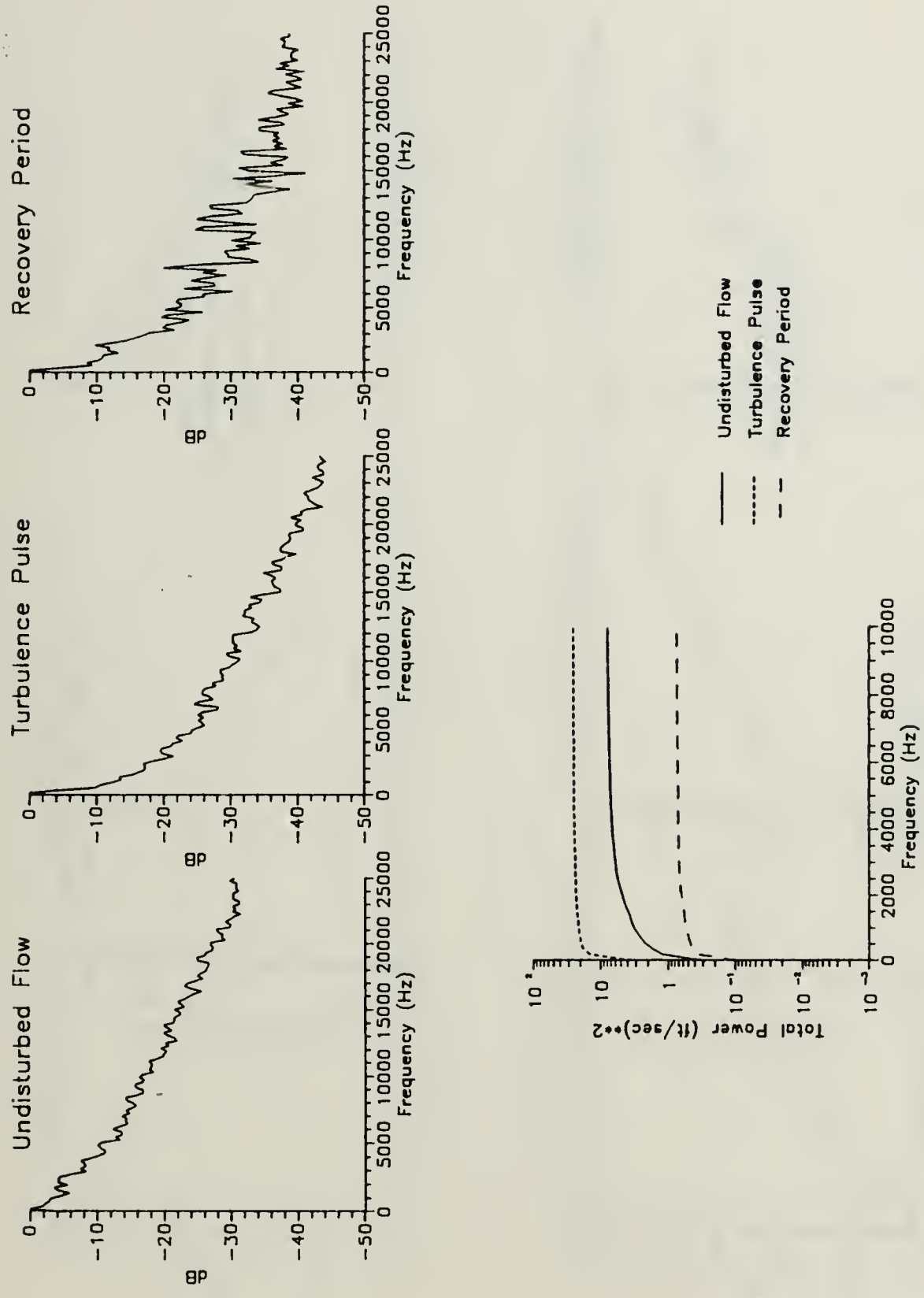

Figure 47. Velocity Spectra and Total Power Distribution, 50% Chord, y = 0.0083″

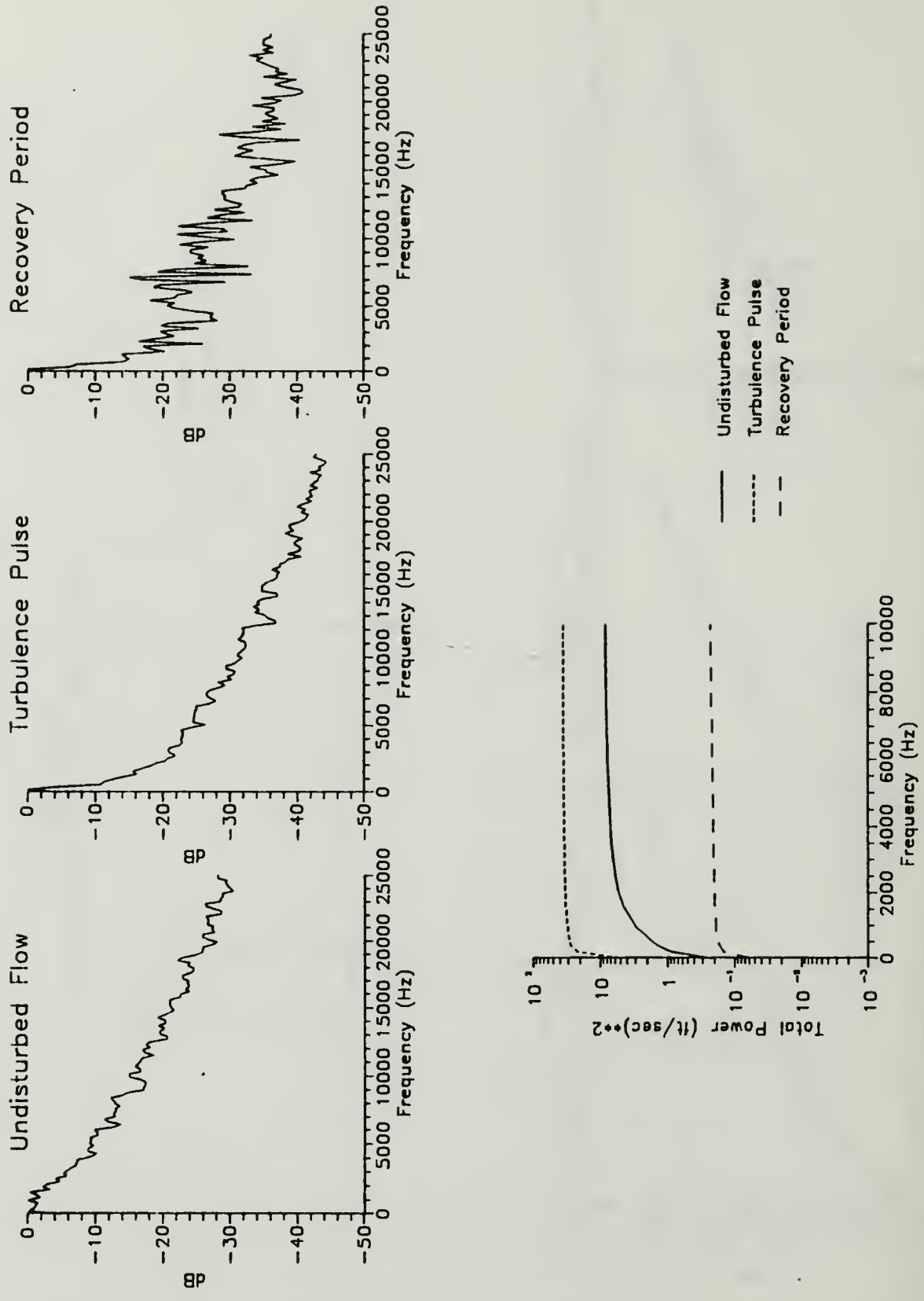

Figure 48. Velocity Spectra and Total Power Distribution, 50% Chord, y = 0.0236″

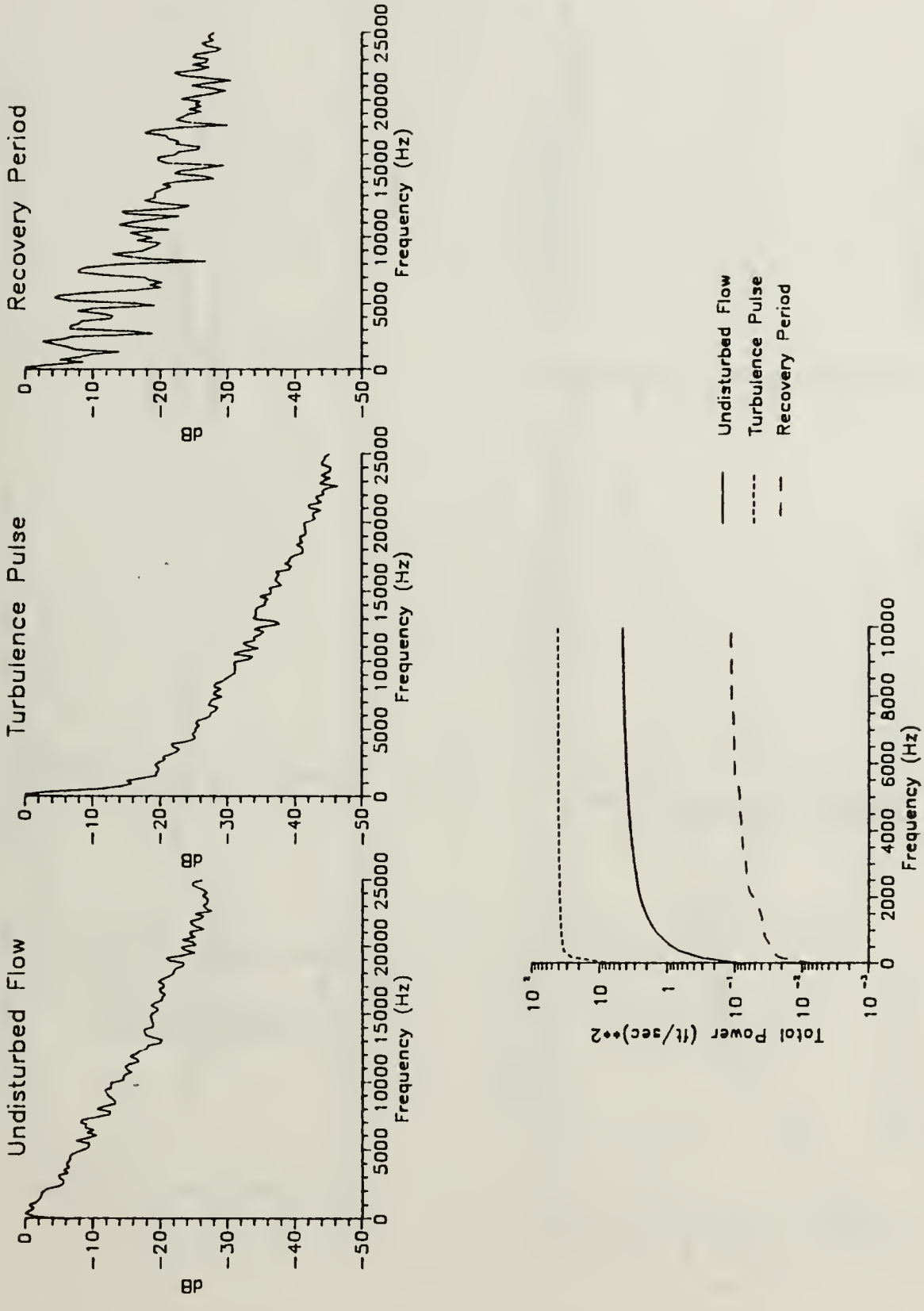

Figure 49. Velocity Spectra and Total Power Distribution, 50% Chord, y = 0.0486"

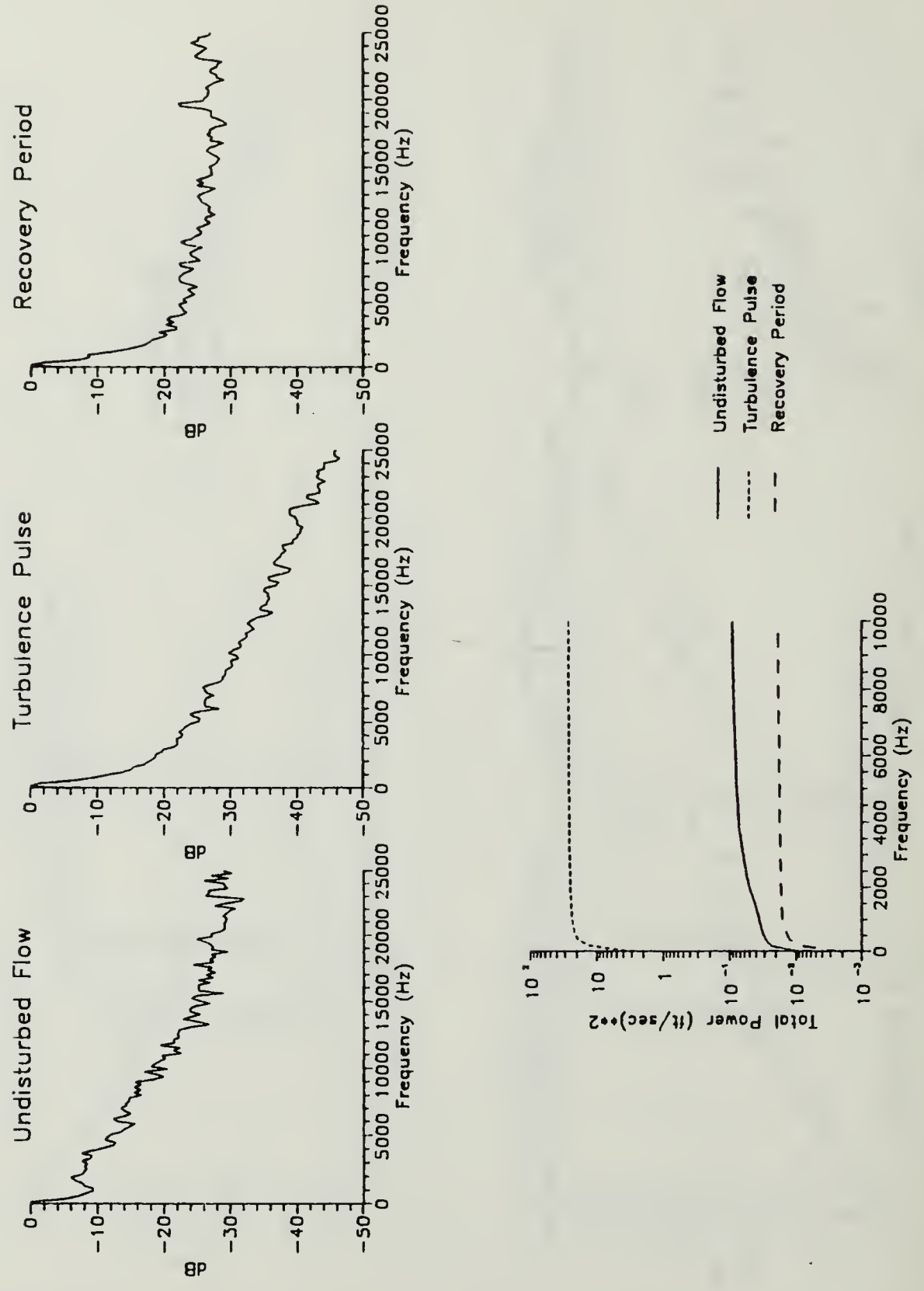

Figure 50. Velocity Spectra and Total Power Distribution, 50% Chord, y = 0.1250″

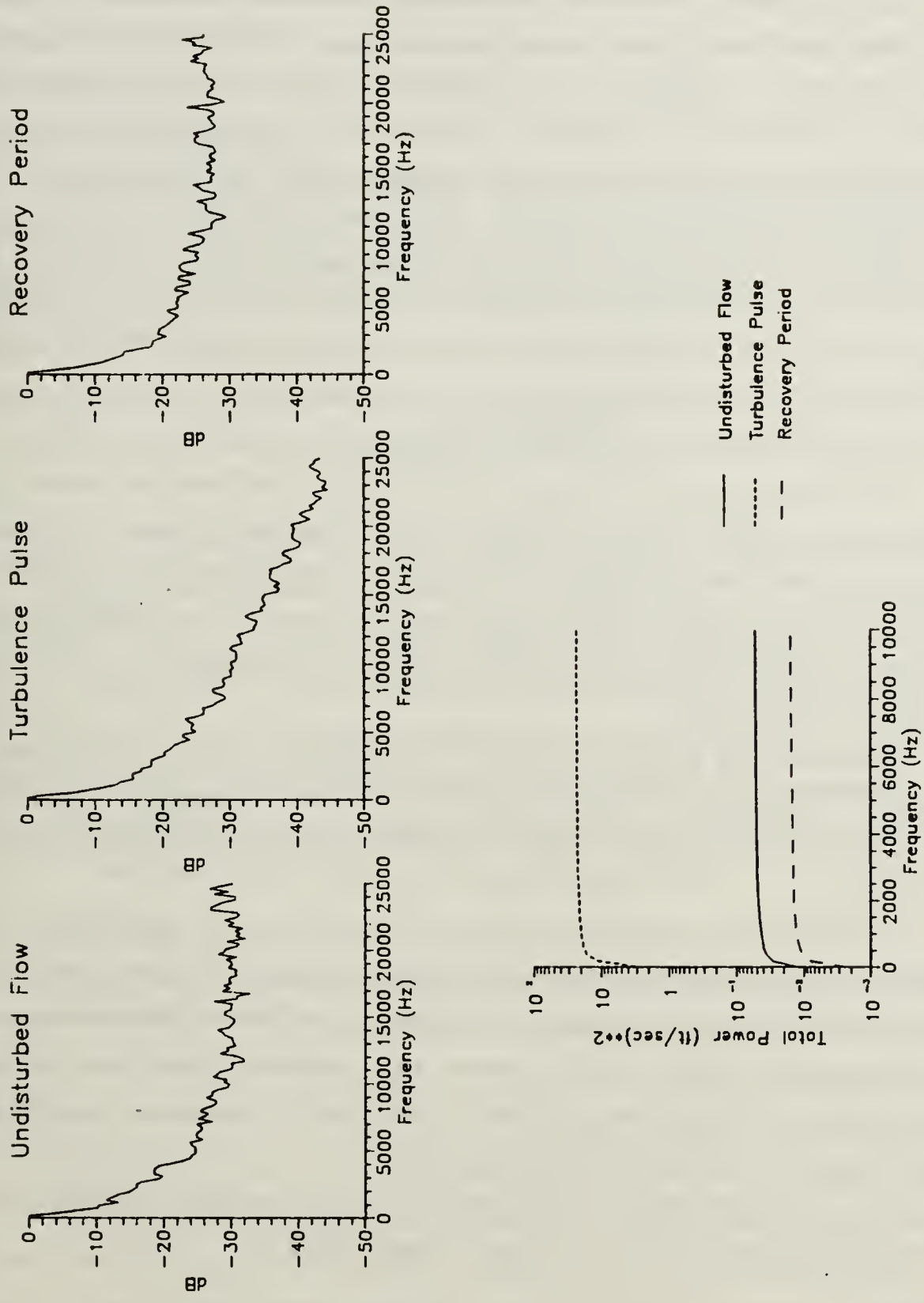

Figure 51. Velocity Spectra and Total Power Distribution, 50% Chord, y = 0.2297″

The total power distribution plots show trends similar to the velocity spectra curves. Near the surface (Figure 46), the turbulent power is quite high for all three flow regimes. Although the turbulent pulse does not affect the recovery period power level, the frequency distribution of the power is clearly altered by the turbulence pulse. The undisturbed flow curve rises slowly to the asymptote while the recovery period curve rises sharply and levels off very quickly. Near the middle of the boundary layer (Figure 48 and Figure 49), the recovery period turbulence power is much lower than that of the free stream. This shows that there is a definite recovery process operating in this region as the flow is energized back to the free stream condition. In the external-flow region (Figure 51), the undisturbed flow and recovery period cumulative power are nearly equal indicating that the effects of the turbulence pulse are purely transitory.

The reverse-transition to laminar flow (variously called reversion, inverse or reverse transition, relaminarization, and laminarization) observed in Figure 43 is identical to the phenomenon observed by Howard [Ref. 6] for a wing immersed in propeller wash. It appears that the turbulence pulse triggers some mechanism in the boundary layer to laminarize the inherently turbulent boundary layer in this investigation as the propeller wash did in Howard's work.

Narasimha and Sreenivasan, in their comprehensive survey of relaminarizing flows, identified four major reversion mechanisms: reversion by dissipation; reversion in stably stratified flows; reversion in highly accelerated flows; and relaminarization by rotation. [Ref. 16]

Laminarization by sudden acceleration of the flow in the near surface region appears to be the mechanism at work in this instance. Analysis of the turbulence pulse regime of Figure 44 reveals instantaneous accelerations of 8,000 to 10,000 ft/sec^2 are felt by the flow near the surface. The flow appears to be accelerated both by the turbulence pulse itself during recovery from the velocity deficit and by momentum transfer down through the boundary layer (see previous section).

One of the most widely used parameters that have proven to predict the onset and course of laminarization of a turbulent boundary layer is:

$$K = \frac{\nu}{U_e^2(x)} \frac{dU_e(x)}{dx} \tag{10}$$

where K is the acceleration parameter, $U_e(x)$ is the edge free stream velocity, ν the kinematic viscosity, and $\frac{dU_e(x)}{dx}$ the instantaneous velocity derivative. K, as used in

Equation 10, is purely a free stream parameter that carries no information at all about the boundary layer itself. Numerous investigators have proposed that values of K greater than 2 x 10^{-6} to 3.5 x 10^{-6} will give rise to laminarization in low speed incompressible flows. [Ref. 16]

In this investigation, the accelerated flow is observed in the boundary layer and in the external free stream as well. For this reason, the author chose to evaluate K locally within the boundary layer as a means of predicting laminarization. Applied in this manner, K becomes:

$$K = \frac{\nu}{U^2(x,y)} \frac{dU(x,y)}{dx} \tag{11}$$

where U(x,y) is the local ensemble average velocity at height y in the boundary layer.

Values of the acceleration parameter, K, range from 2.2 x 10^{-6} at the near-surface region to 1.7 x 10^{-6} in the upper regions of the boundary layer at 50% chord using local velocity values. The value calculated near the surface is clearly sufficient to induce laminarization of the turbulent boundary layer at this position. It is interesting to note that K is much higher at 30% chord where it remains fairly constant at 4.4 x 10^{-6} over the entire boundary layer region; but K does not play a significant role at 30% chord other than hastening the return to naturally laminar flow.

3. 70% Chord

The ensemble average velocity and turbulence profiles plotted in Figure 52 show yet entirely different characteristics than observed at 30% and 50% chord. The undisturbed flow is fully turbulent with a high level of turbulence spanning the entire boundary layer region (sample 200). The turbulence pulse flattens the velocity profile while inducing high turbulence (6% - 8%) uniformly over the vertical region (samples 350 and 410). During recovery, the velocity profiles become laminar like (sample 720) as the turbulence decreases in the middle and upper regions of the boundary layer. The turbulence traces appear transitional/turbulent in the recovery regime. Sample 850 shows the flow becoming fully turbulent again with the boundary layer height increasing and with increasing turbulence in the lower and middle section of the boundary layer.

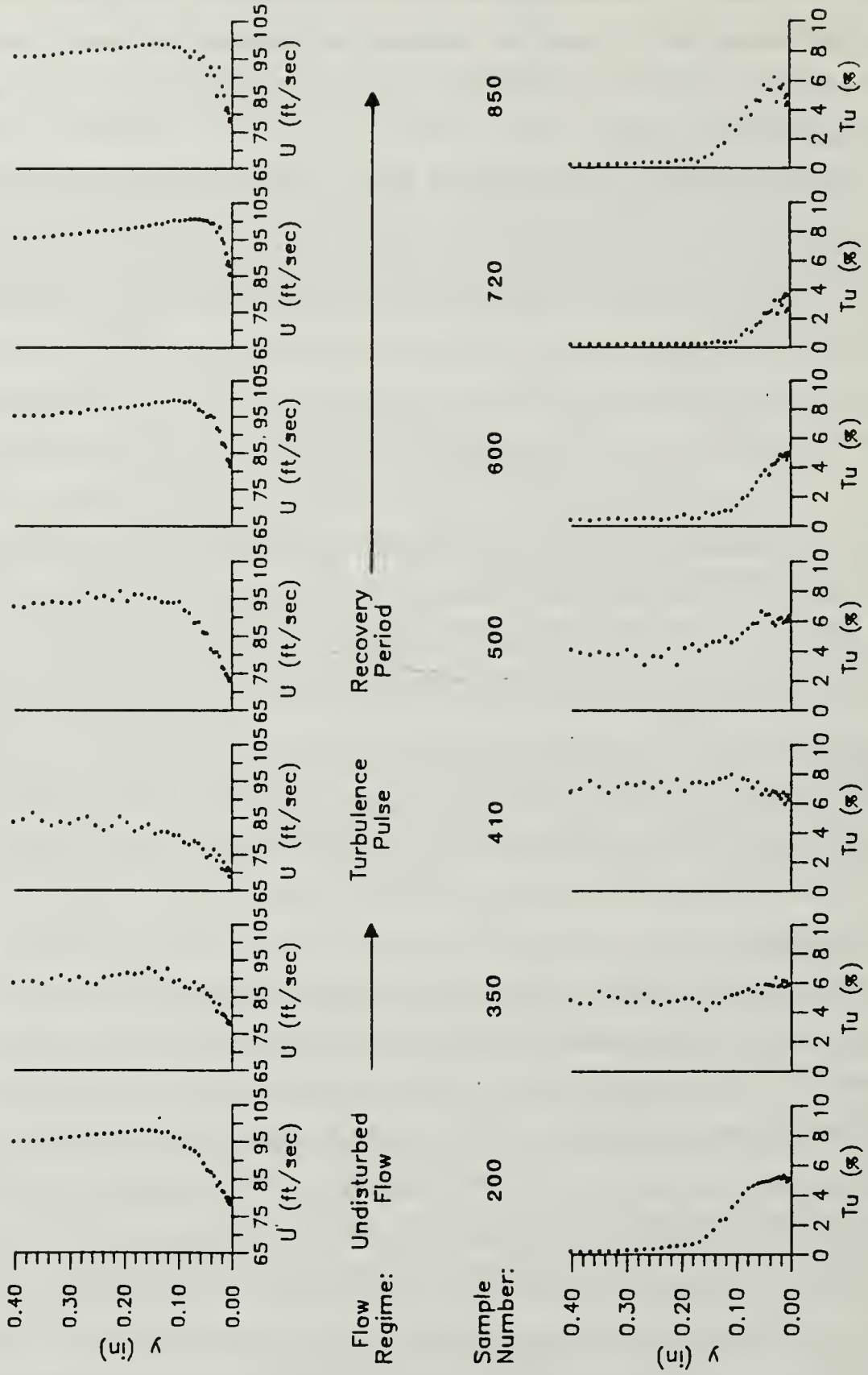

Figure 52. Ensemble Average Profiles, 70% Chord

Note that the turbulence level near the surface remains high and fairly constant throughout the period. Clearly the laminarization process is at work here also, but the effects are greatly reduced.

The smoothed velocity time histories plotted in Figure 53 show that the velocity deficit is felt throughout the boundary layer. The velocity deficit grows near the mid-layer and decreases again near the surface. Of interest in the velocity time histories is the nature of the velocity increase following the turbulence pulse. The velocity increase is much higher at 70% chord than at the previous wing locations. Note also the long recovery period and slow rise and decay time associated with the velocity increase.

Figure 54 shows the smoothed turbulence time histories. Notice the high turbulence levels that persist in the near-surface regions during the entire period. The trace at y = 0.0702 inches would tend to indicate that the turbulence pulse affects the mid-layer region more than the near-surface region at this chord location.

The velocity spectra and total power distribution graphs are shown in Figure 55 through Figure 60. In the near-surface region (Figure 55 through Figure 57), the turbulence pulse mainly affects the velocity spectrum of the recovery period while total power remains high and nearly equal over the three flow regimes. Toward the middle of the layer (Figure 58 and Figure 59), the total power levels of the undisturbed flow and recovery period regimes drop and the velocity spectra align more closely. It is interesting to note that the total power of the recovery period is less than that for the undisturbed flow in the middle boundary layer region. This indicates that there is a definte recovery process at work here. In the external-flow region (Figure 60), the turbulence pulse does not affect the velocity spectrum of the recovery period. Here the power curves for the undisturbed flow and recovery period regimes are very low magnitude and equal.

The local acceleration parameter (K) from Equation 11, varies from 1.3×10^{-6} near the surface to 1.9×10^{-6} at the middle of the boundary layer. The low value of K near the surface indicates that this region should not laminarize. This is borne out by the data; the near-surface region is dominated by high turbulence and the mean velocity responds very slowly to the turbulence pulse. Conversely, the middle boundary layer region, with a value of K close to that necessary for laminarization, has a laminar-like response: a sharp drop in turbulence following the turbulence pulse with a corresponding sharp velocity increase.

Apparently the turbulence pulse prompts the middle boundary layer toward laminar flow but the pulse is unable to fully penetrate into the thick, highly turbulent

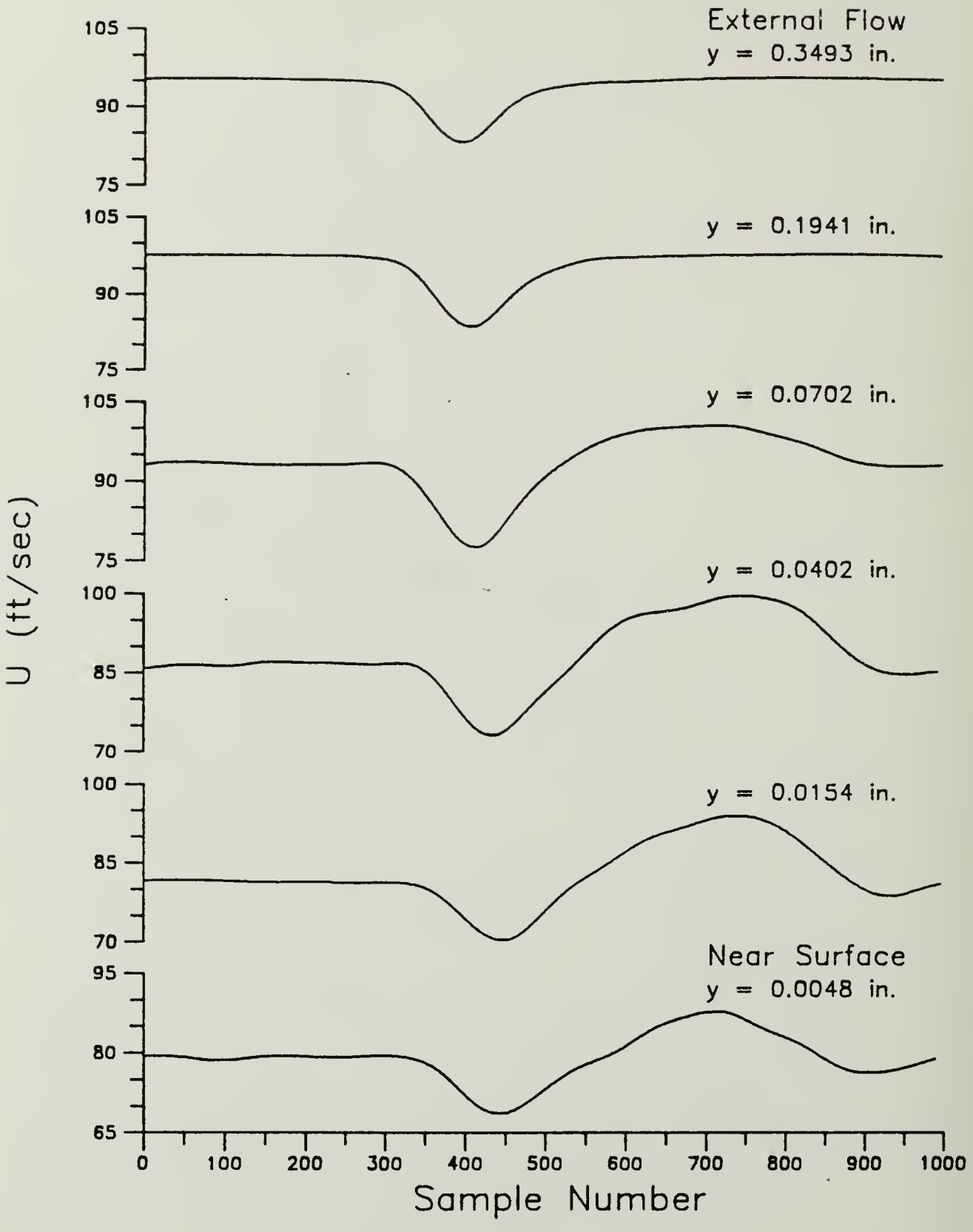

Figure 53. Mean Velocity Time Histories in the Boundary Layer, 70% Chord: (Fs = 50 KHz)

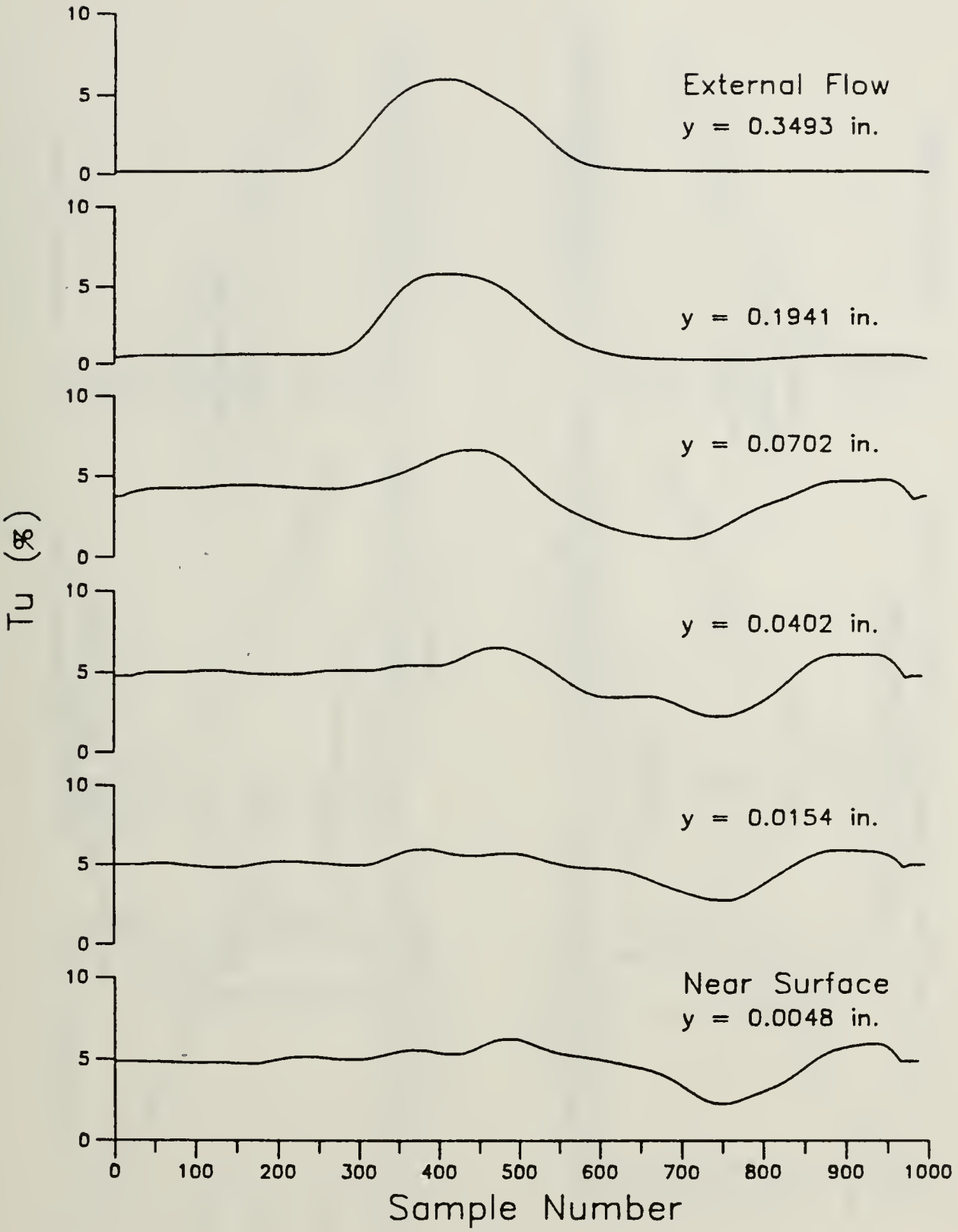

Figure 54. Mean Turbulence Time Histories in the Boundary Layer, 70% Chord: (Fs = 50 KHz)

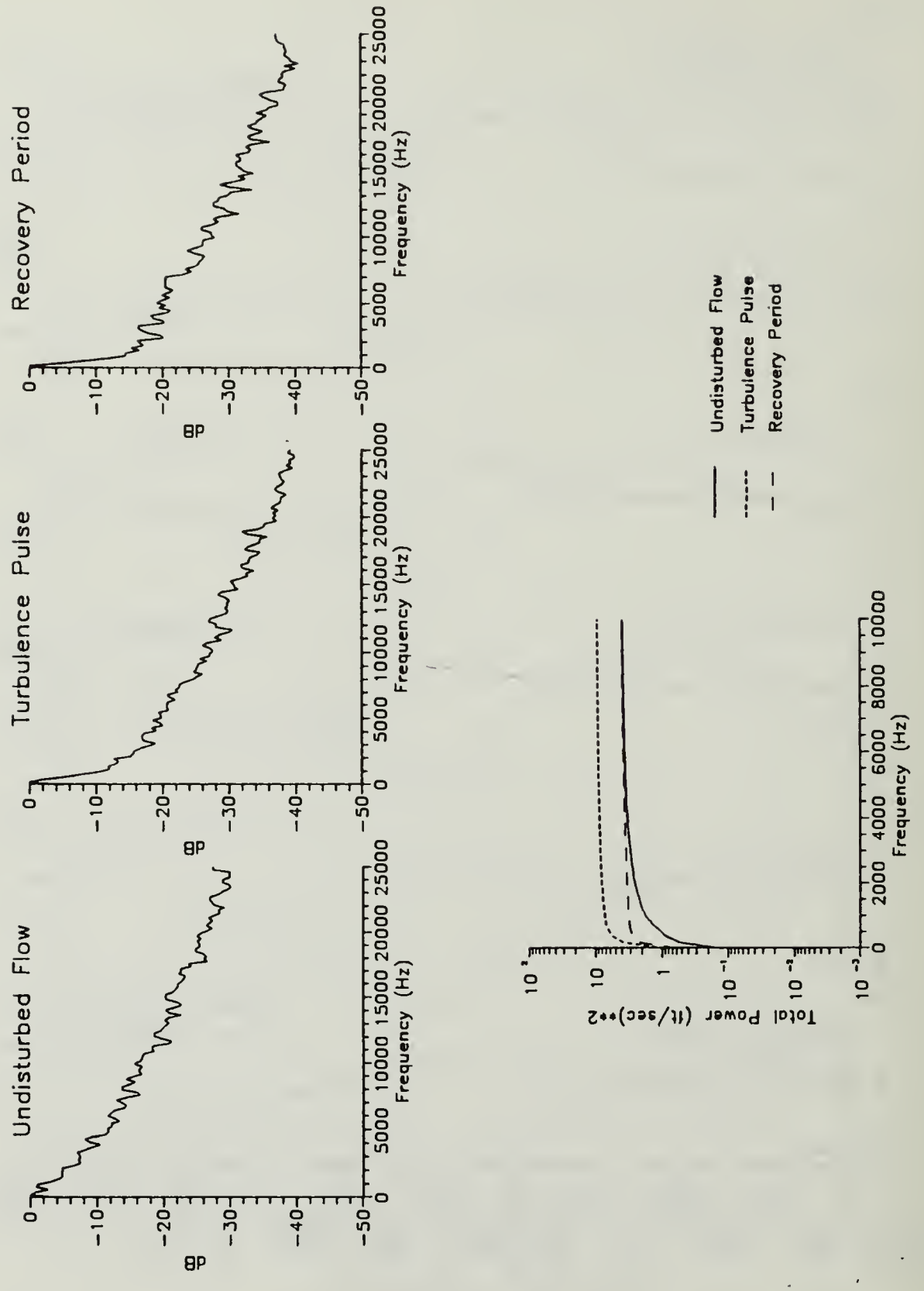

Figure 55. Velocity Spectra and Total Power Distribution, 70% Chord, y = 0.0048″

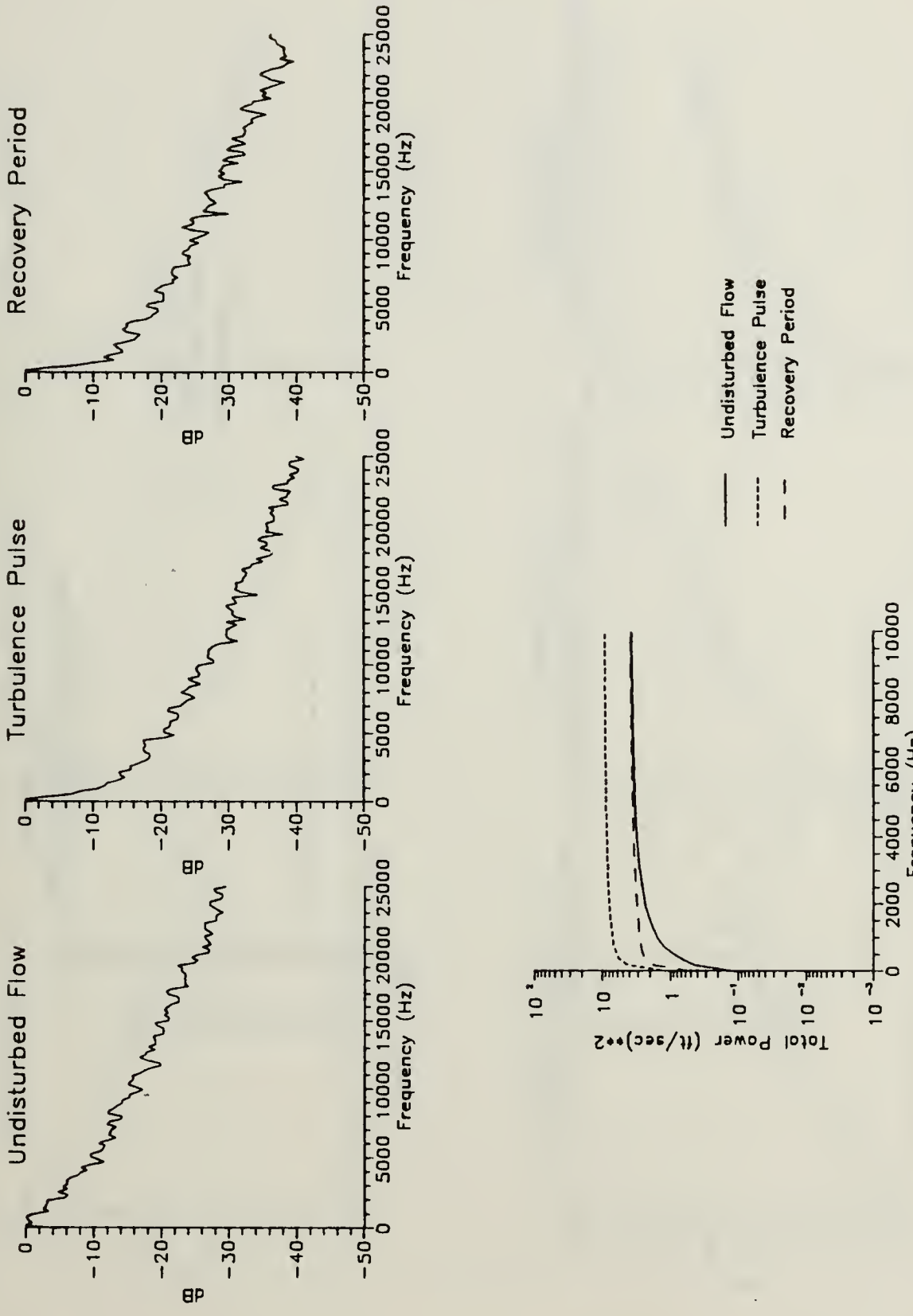

Figure 56. Velocity Spectra and Total Power Distribution, 70% Chord, y = 0.0154″

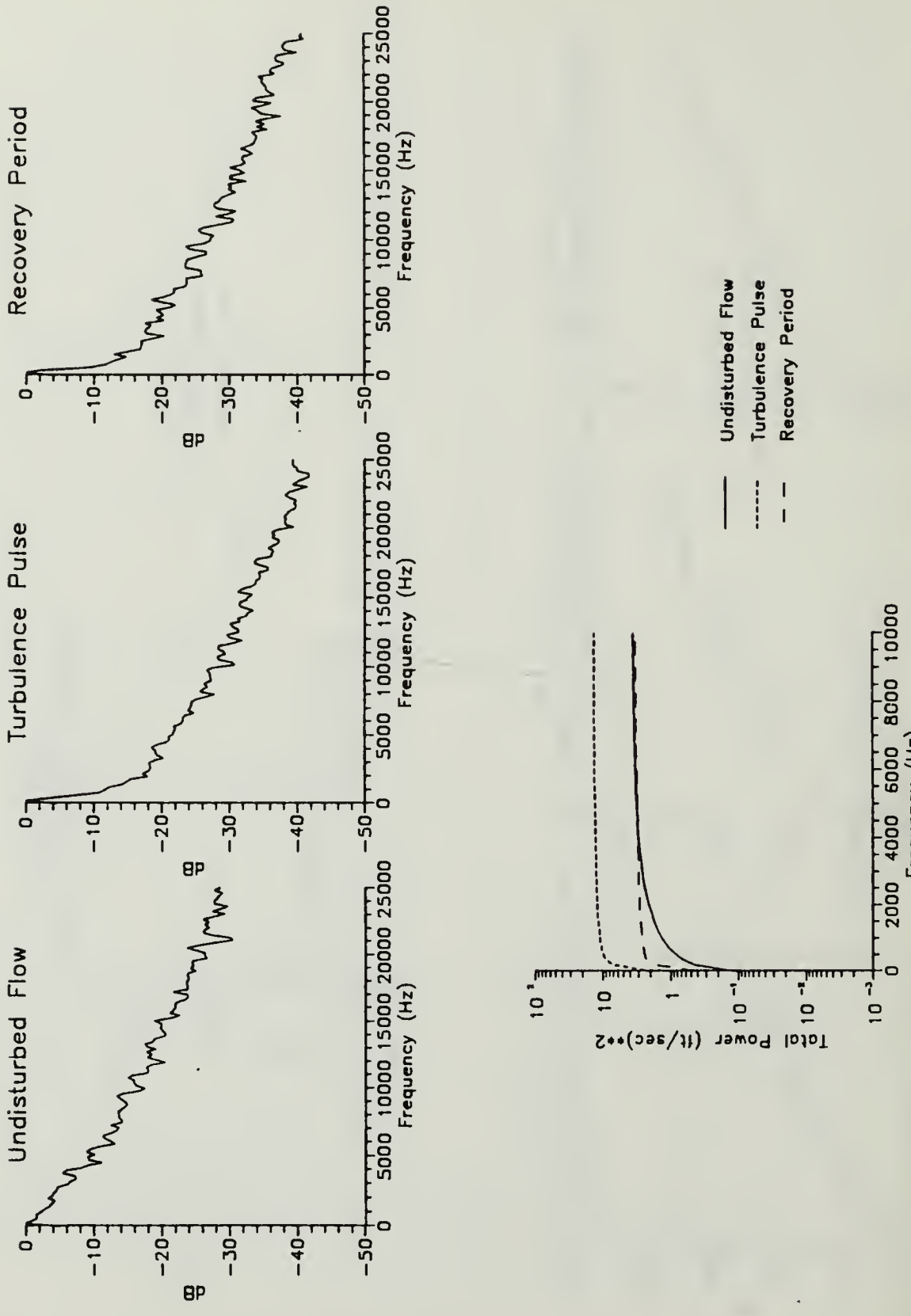

Figure 57. Velocity Spectra and Total Power Distribution, 70% Chord, y = 0.0402″

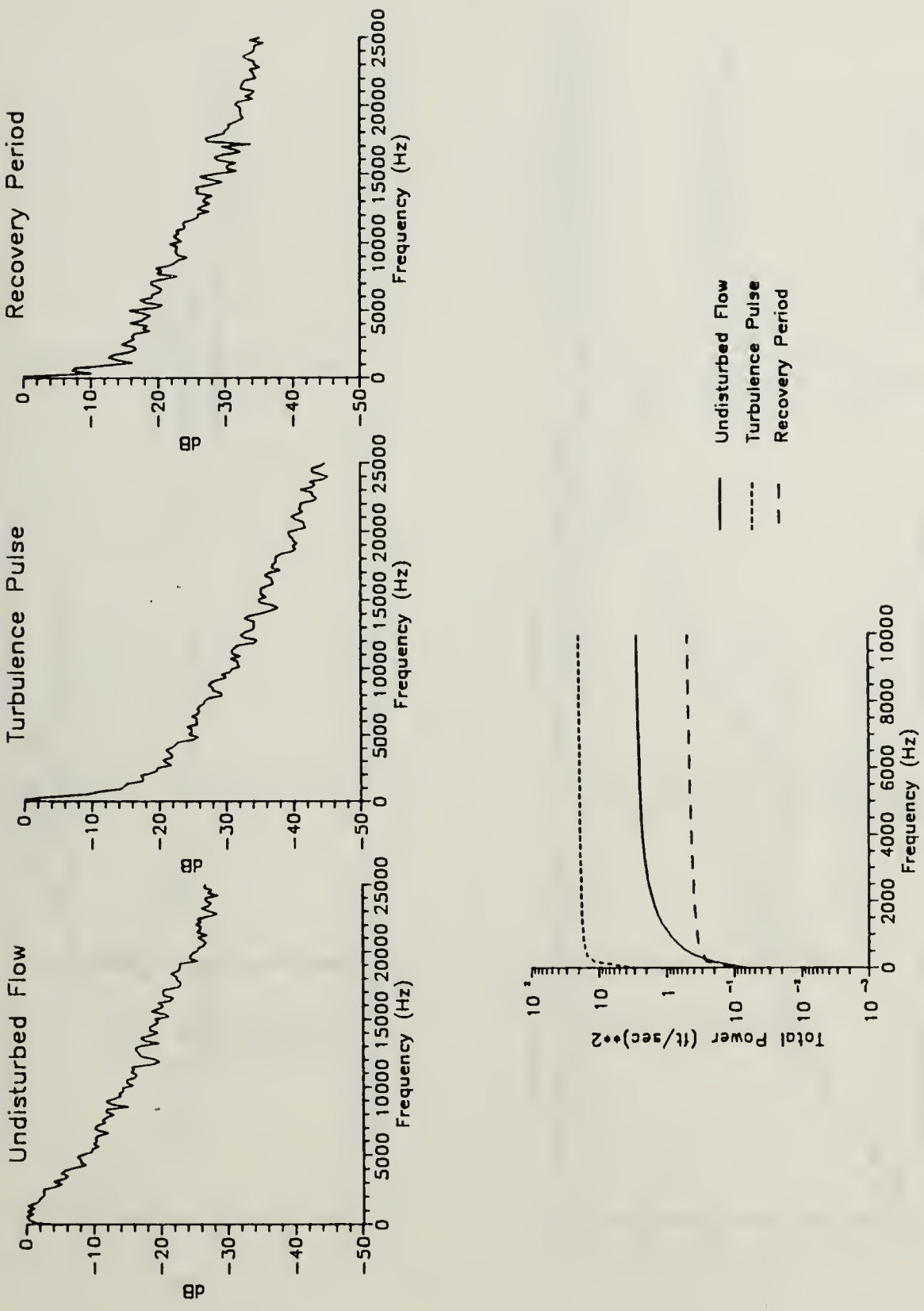

Figure 58. Velocity Spectra and Total Power Distribution, 70% Chord, y = 0.0702″

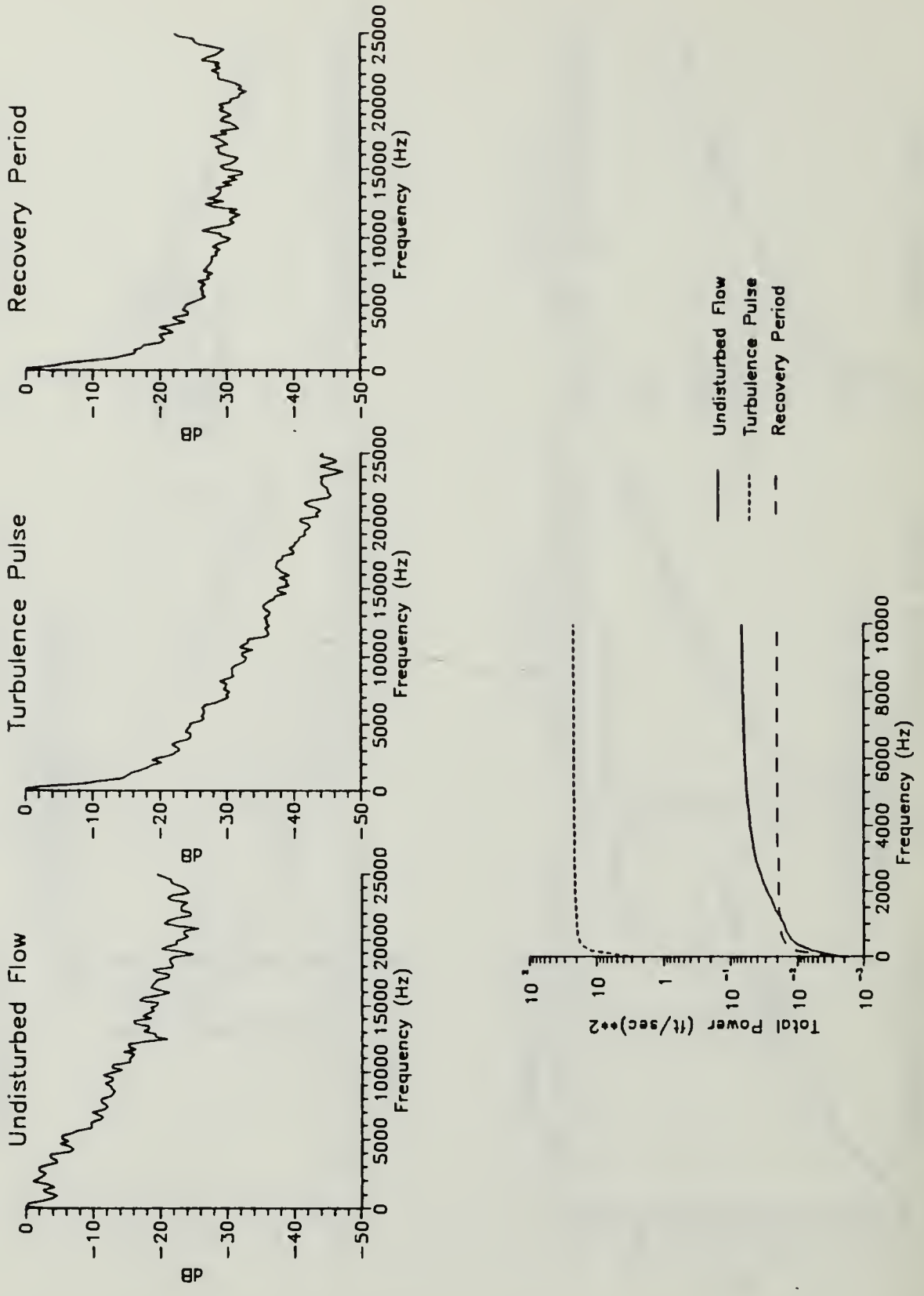

Figure 59. Velocity Spectra and Total Power Distribution, 70% Chord, y = 0.1941″

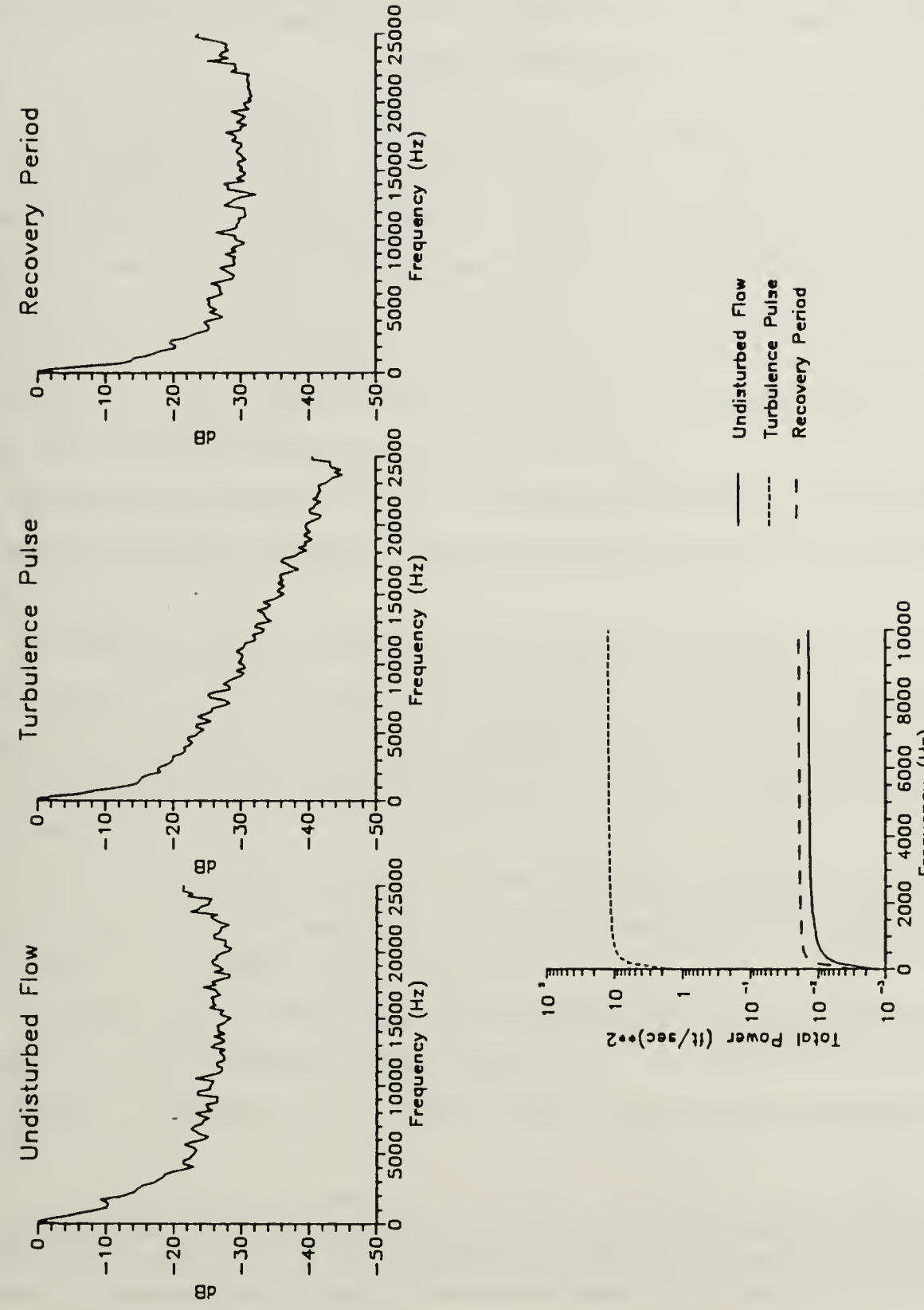

Figure 60. Velocity Spectra and Total Power Distribution, 70% Chord, y = 0.3493″

near-surface region. Regardless, the turbulence pulse appears able to prompt a laminar-like response at this chord location, contrary to what one would intuitively expect.

V. CONCLUSIONS

The time-varying effects of periodic free stream turbulence have been investigated on a wing boundary layer at three representative chord locations (laminar, transitional turbulent, and turbulent) on the wing. An experimental method was developed and tested to generate non-thrusting, uniform periodic turbulence pulses in the external flow over the test wing. Although the turbulence pulses were restricted to one test condition, 50 pulses per second and a turbulence intensity of near 10%, they demonstrated the dynamic character of the boundary layer subjected to single-event turbulence. The results of this investigation are detailed below.

The turbulence pulse was a short (5 millisecond), high intensity (10.5% Tu), low frequency dominated (no significant spectral components above 1 KHz), non-thrusting event.

The turbulence pulse was shown to fully penetrate the boundary layer at all three chord locations. It was observed that the turbulence pulse suppressed the high frequency spectral components in the recovery period regime. Actual penetration was less near the surface in the turbulent flow region of the wing, but the effects of the pulse were still quite evident.

The boundary layer time-response showed a distinct transition from undisturbed (laminar, transitional, or turbulent) flow to highly turbulent flow when subjected to the turbulence pulse at all three chord locations.

The recovery process leading back to undisturbed flow was highly dependent on the nature of the undisturbed flow as shown below:

Laminar: Quick boundary layer response with a rapid return to undisturbed laminar flow.

Transitional/Turbulent: Slower boundary layer response than in the laminar region. Laminarization was evident during the recovery process followed by a slow return to undisturbed transitional/turbulent flow. The boundary layer thickness was decreased during the recovery period, and the turbulence intensity dropped to 1/6 of its normal undisturbed value near the surface.

Turbulent: Slow boundary layer response. Laminarization is quite evident in the mid and upper portions of the boundary layer and evident to a lesser degree near the surface. There was a marked decrease in boundary layer thickness during the recovery period in this region before returning to the undisturbed turbulent value.

Laminarization appears to be mainly prompted by rapid acceleration of the flow internal to the boundary layer. The internal flow is accelerated both by the turbulence pulse itself during recovery from the velocity deficit and by momentum transfer down through the boundary layer. The velocity time-history traces show that the small velocity deficit associated with the turbulence pulse in external flow is amplified in the middle boundary layer region due to momentum transfer down through the layer. The near-surface flow experiences a rapid velocity increase as a result of the momentum transfer.

The total spectral power content of the flow regimes (undisturbed, flow, turbulence pulse, and recovery period) was more dependent on vertical position in the boundary layer than on chord location. Near the surface, the total power of all three regimes was very high and nearly equal even though the spectral distribution of the power varied considerably. The middle boundary layer region, on the other hand, is characterized by a high power turbulence pulse, medium power level undisturbed flow, and a low power recovery period. The very low power level observed in the recovery period shows that the turbulence pulse drives the flow to a very low turbulent energy state. Laminarization occurs as there is insufficient spectral power to support turbulent flow at this point. The flow slowly gains power and transitions back to the undisturbed flow regime as the steady state characteristics once again prevail. At the edge of the boundary layer, the power level of the turbulence pulse remains quite high while the power levels of the undisturbed flow and recovery regimes are low and nearly equal.

VI. RECOMMENDATIONS

This investigation demonstrated the stabilizing nature of periodic turbulence on the transitional and turbulent regions of the wing. The study was done at a single low angle of attack at three representative chord locations (laminar, transitional, and turbulent). Further experimental work should be done at additional chord locations and at higher angles of attack to further study the stabilizing effect of periodic turbulence on attached boundary layers and on flow near separation.

More research also needs to be undertaken to better understand the mechanism at work in the laminarization process. Future studies should investigate the individual pulse passage cycles in greater detail to determine if ensemble-averaging techniques adequately represent the highly dynamic laminarization process, or if statistical methods or a single pulse passage cycle analysis would be more instructive.

Data collection was extremely time consuming with the present configuration. The following modifications should be implemented for future investigations:

Store and process all data in binary integer format rather than in ASCII real format. This will reduce the mass data storage requirement by a factor of nine and also greatly reduce data transfer and processing time.

Expand the random access memory of the data acquisition computer so that the data collection and traverser control software routines can be managed by one personal computer. This will allow for full automation of the test sequence.

Use a hot-film probe instead of a hot-wire probe in the NPS low speed wind tunnel to avoid contamination induced drift problems.

Decrease the digitizing rate. This investigation has shown that little useful spectral information is contained in the frequencies above 10 KHz. As such, the sampling rate could easily be reduced to 20 KHz with no loss of meaningful data. This step alone will reduce mass storage by 60% with a comparable reduction in data handling and processing time.

Future research should also be directed toward investigating the effect of periodic or single-event turbulence on an airfoil near stall or in post-stall flight with regard to loss of attached flow and loss of control. Questions to be answered include:

What is the effect of the observed stabilizing phenomena on flow near separation?

Can the results be worked to an advantage at high angles of attack with regard to aircraft supermaneuverability or controllability? This is important as augmented lift from dynamic-stall maneuvering will have limited application unless the pilot can maintain control to transition quickly from one maneuvering state to another.

Directly related areas of interest include continued studies of the effects of wind gusts, ship airwake turbulence, missile wake, and aircraft wake on aircraft stability and controllability. Future studies of canard wake/airfoil interaction at high lift seem pertinent, especially in relation to the continuing supermaneuverability studies at NPS.

APPENDIX A. AIRFOIL COORDINATES

UPPER		LOWER	
x/c	y/c	x/c	y/c
1.000	.0000	1.000	.0000
.990	.0008	.990	-.0002
.980	.0015	.980	-.0005
.970	.0022	.970	-.0008
.960	.0030	.960	-.0010
.950	.0039	.950	-.0011
.940	.0050	.940	-.0011
.930	.0064	.930	-.0009
.920	.0080	.920	-.0007
.910	.0100	.910	-.0003
.900	.0121	.900	.0000
.890	.0142	.890	.0006
.850	.0220	.880	.0010
.800	.0310	.850	.0023
.750	.0400	.800	.0042
.700	.0483	.750	.0056
.650	.0561	.700	.0066
.600	.0635	.650	.0071
.550	.0704	.600	.0072
.500	.0766	.550	.0067
.450	.0816	.540	.0065
.400	.0858	.530	.0063
.350	.0894	.520	.0061
.300	.0918	.510	.0059
.250	.0927	.500	.0056
.240	.0926	.490	.0053
.230	.0923	.480	.0050
.220	.0919	.470	.0047
.210	.0914	.460	.0044
.200	.0907	.450	.0040
.190	.0900	.440	.0036
.180	.0888	.430	.0031
.170	.0876	.420	.0027
.160	.0862	.410	.0022
.155	.0854	.400	.0018
.150	.0846	.390	.0013
.145	.0837	.380	.0009
.140	.0828	.370	.0004
.135	.0818	.360	.0000
.130	.0808	.340	-.0008
.125	.0797	.320	-.0015
.120	.0785	.300	-.0020
.115	.0773	.280	-.0025
.110	.0760	.260	-.0029
.105	.0746	.240	-.0032
.100	.0731	.220	-.0034

.095	.0716	.210	-.0035
.090	.0700	.200	-.0034
.085	.0684	.180	-.0033
.080	.0666	.150	-.0030
.075	.0647	.100	-.0016
.070	.0628	.080	-.0008
.060	.0585	.060	-.0000
.050	.0537	.050	.0002
.040	.0481	.040	.0003
.030	.0415	.030	.0000
.020	.0335	.025	-.0002
.015	.0286	.020	-.0008
.010	.0233	.015	-.0016
.005	.0169	.010	-.0008
		.005	.0020

APPENDIX B. DATA SAMPLE SPACING

Sample Number	30% Chord (in)	50% Chord (in)	70% Chord (in)
01	0.0032	0.0032	0.0048
02	0.0033	0.0034	0.0060
03	0.0038	0.0041	0.0075
04	0.0046	0.0051	0.0095
05	0.0057	0.0064	0.0122
06	0.0071	0.0083	0.0154
07	0.0087	0.0106	0.0192
08	0.0107	0.0132	0.0236
09	0.0130	0.0163	0.0286
10	0.0156	0.0197	0.0342
11	0.0184	0.0236	0.0427
12	0.0217	0.0278	0.0469
13	0.0251	0.0324	0.0541
14	0.0288	0.0374	0.0619
15	0.0330	0.0428	0.0702
16	0.0372	0.0486	0.0790
17	0.0418	0.0547	0.0884
18	0.0467	0.0612	0.0982
19	0.0518	0.0680	0.1086
20	0.0572	0.0751	0.1194
21	0.0628	0.0826	0.1307
22	0.0687	0.0904	0.2425
23	0.0748	0.0986	0.1547
24	0.0811	0.1071	0.1674
25	0.0877	0.1158	0.1805
26	0.0944	0.1250	0.1941
27	0.1014	0.1343	0.2080
28	0.1087	0.1440	0.2223
29	0.1162	0.1538	0.2371
30	0.1238	0.1640	0.2521
31	0.1316	0.1743	0.2676
32	0.1396	0.1850	0.2833
33	0.1477	0.1958	0.2994
34	0.1560	0.2070	0.3157
35	0.1644	0.2182	0.3324
36	0.1731	0.2297	0.3493
37	0.1818	0.2413	0.3665
38	0.1906	0.2531	0.3839
39	0.1996	0.2651	0.4016
40	0.2087	0.2722	------
41	------	0.2894	------
42	------	0.3017	------

APPENDIX C. PROGRAM TRAVERSE

```
100 REM ********** PROGRAM TRAVERSE.BAS **********
110 REM
120 REM THIS PROGRAM, WRITTEN BY D. KINDELSPIRE AND MODIFIED BY R. RENOUD
130 REM (SEP 88) CONTROLS THE VELMEX 8300 3-D TRAVERSER.  THE INITIAL
140 REM PORTION OF THE PROGRAM IS DEDICATED TO OPERATOR-SELECTABLE OPTIONS
150 REM (I.E. MOTOR VELOCITY, MOTOR ACCELERATION, ETC.) AVAILABLE FOR
160 REM EACH MOTOR.  DEFAULT MOTOR VALUES FOR EACH OPTION ARE PROVIDED
170 REM IN THE PROGRAMMING AND THE OPERATOR CAN SELECT THE DEFAULTS FOR
180 REM ALL MOTORS WITH ONE KEYSTROKE.  THEW PROGRAM GIVES THE OPERATOR
190 REM A CHOICE OF MANUAL INPUT (MEANING ONE MOTOR MOVEMENT FOR EACH
200 REM INPUT WITH INPUT IN INCHES) OR COMPUTER-CONTROLLED MOVEMENT
210 REM THROUGH THE BOUNDARY LAYER.  THE SINE FUNCTION-BASED ALGORITHIM
220 REM USED TO COMPUTE THE MOTOR MOVEMENTS THROUGH THE BOUNDARY LAYER
230 REM GIVES MOVEMENT COMMANDS IN INCREMENTS OF THE MINIMUM MOTOR
240 REM MOVEMENT STEP SIZE (0.000125 INCHES).
250 REM
260 REM ************************************************************************
1000 REM
1010 REM     OPEN THE COM PORT AND INITIALIZE THE MOTOR SETTINGS
1020 OPEN "com1:1200,n,8,1,rs,cs,ds,cd" FOR RANDOM AS #1
1030 REM SET MOTOR DEFAULT VALUES
1040 DATA 1000,1000,1000,2,2,2,0.000125,0.000125,0.000125
1050 READ V1, V2, V3, R1, R2, R3, C1, C2, C3
1060 DIM Z(100), Z1(100), HWV(100), RMS(100), VEL(100), NDVEL(100), VRMS(100)
1070 PI = 3.141592654#
1080 PRINT
1090 PRINT "*****************************************************"
1100 PRINT "** USER MUST SELECT 'CAPS LOCK' FUNCTION **"
1110 PRINT "*****************************************************"
1120 REM          DISPLAY MOTOR DEFAULT SETTINGS
1130 PRINT "              ***************************************"
1140 PRINT "           INITIALIZED VALUES FOR ALL MOTOR SETTINGS:"
1150 PRINT "                VELOCITY = 1000 STEPS/SEC"
1160 PRINT "                RAMP(MOTOR ACCELERATION) = 2  (6000 STEPS/SEC
1170 PRINT "                DEFAULT INCREMENTAL UNITS ARE INCHES"
1180 PRINT "              ***************************************"
1190 PRINT
1200 PRINT "DO YOU WANT TO INPUT YOUR OWN INCREMENT EACH TIME OR HAVE THE"
1210 PRINT "COMPUTER COMPUTE MOVEMENTS THROUGH A BOUNDARY LAYER FOR YOU ?"
1220 PRINT
1230 PRINT "         ********** NOTE **********"
1240 PRINT "FOR COMPUTED BOUNDARY LAYER MOVEMENT, YOU MUST KNOW:"
1250 PRINT "     1. WHICH MOTOR WILL MOVE THE APPROPRIATE DIRECTION."
1260 PRINT "     2. HOW THICK (IN INCHES) IS THE B.L."
1270 PRINT "     3. HOW MANY DATA COLLECTION POINTS DO YOU WANT IN THE B.L."
1280 PRINT "         ***********************************"
1290 PRINT
1300 PRINT "NOTE!! USE MANUAL CONTROL TO INITIALIZE PROBE POSITION BEFORE"
1310 PRINT "           SELECTING COMPUTER CONTROLLED MOVEMENT.     "
1320 PRINT
1330 INPUT "MANUAL CONTROL OR COMPUTER CONTROL (ENTER 'MAN' or 'CP')"; CON$
```

```
1340 IF CON$ = "CP" THEN 3130
1350 REM  OPTION TO CHANGE DEFAULT SETTINGS OF VELOCITY OR ACCELERATION RAMP
1360 PRINT
1370 PRINT
1380 PRINT " DO YOU WANT TO CHANGE THE VELOCITY OR ACCELERATION RAMP"
1390 PRINT "        DEFAULT SETTINGS? (Y or N)"
1400 PRINT
1410 PRINT "IF 'NO', THIS PROGRAM WILL THEN LET YOU DEFINE THE"
1420 PRINT "DISTANCE YOU WANT TO MOVE (IN INCHES). IF 'YES',"
1430 PRINT "YOU CAN CHANGE ANY OR ALL OF THE DEFAULT SETTINGS FOR ANY MOTOR."
1440 PRINT
1450 PRINT
1460 PRINT
1470 INPUT "DO YOU WANT TO CHANGE ANY OF THE DEFAULT SETTINGS? (Y or N)"; D$
1480 IF D$ = "Y" THEN 1520
1490 IF D$ = "N" THEN 2150
1500 REM
1510 REM   ***** OPERATOR SELECTED MOTOR VARIABLES *****
1520 PRINT
1530 PRINT
1540 INPUT "WHICH DEFAULT VALUE? (ENTER '1'FOR VELOC OR '2' FOR ACCEL RAMP)"; L
1550 ON L GOTO 1620, 1860
1560 PRINT "DO YOU WANT TO CHANGE THE DEFAULT VELOCITY? (Y OR N)"
1570 INPUT V$
1580 IF V$ = "Y" THEN 1620
1590 PRINT "DO YOU WANT TO CHANGE THE DEFAULT ACCELERATION RAMP? (Y or N)"
1600 IF R$ = "Y" THEN 1920
1610 IF R$ = "N" THEN 1380
1620 PRINT
1630 PRINT
1640 INPUT "WHICH MOTOR VELOCITY DO YOU WISH TO CHANGE? (1,2, or 3)"; J
1650 ON J GOTO 1660, 1760, 1810
1660 PRINT
1670 PRINT
1680 INPUT "ENTER DESIRED VELOCITY OF MOTOR #1"; V1
1690 PRINT
1700 PRINT
1710 PRINT
1720 PRINT "DO YOU WANT TO CHANGE VELOCITY OF ANOTHER MOTOR? (Y OR N)"
1730 INPUT V$
1740 IF V$ = "Y" THEN 1620
1750 IF V$ = "N" THEN 1360
1760 PRINT
1770 PRINT
1780 INPUT "ENTER DESIRED VELOCITY OF MOTOR 2"; V2
1790 PRINT
1800 GOTO 1710
1810 PRINT
1820 PRINT
1830 INPUT "ENTER DESIRED VELOCITY OF MOTOR #3"; V3
1840 PRINT
1850 GOTO 1710
1860 PRINT
1870 PRINT
1880 INPUT "WHICH MOTOR ACCEL RAMP DO YOU WANT TO CHANGE? (1, 2, or 3)"; K
1890 ON K GOTO 1900, 1990, 2050
```

```
1900 PRINT
1910 PRINT
1920 INPUT "ENTER DESIRED ACCELERATION RAMP OF MOTOR #1"; R1
1930 PRINT
1940 PRINT
1950 PRINT "DO YOU WANT TO CHANGE THE ACCEL RAMP OF ANOTHER MOTOR? (Y or N)?"
1960 INPUT RM$
1970 IF RM$ = "Y" THEN 1860
1980 IF RM$ = "N" THEN 1380
1990 PRINT
2000 PRINT
2010 INPUT "ENTER DESIRED ACCELERATION RAMP OF MOTOR #2"; R2
2020 PRINT
2030 PRINT
2040 GOTO 1930
2050 PRINT
2060 PRINT
2070 INPUT "ENTER DESIRED ACCELERATION RAMP OF MOTOR #3"; R3
2080 PRINT
2090 PRINT
2100 GOTO 1930
2110 REM
2120 REM DEFINE DISTANCE TO MOVE MOTOR
2130 PRINT
2140 PRINT
2150 PRINT
2160 REM INITIALIZE MOTOR INCREMENTS TO ZERO
2170 I1 = 0
2180 I2 = 0
2190 I3 = 0
2200 PRINT
2210 PRINT " ********************************************************************************"
2220 PRINT " **      DEFINE WHICH MOTOR YOU WANT TO MOVE                                   **"
2230 PRINT " **                                                                            **"
2240 PRINT " **        NOTE!!!  A POSITIVE ('+') INCREMENT TO A MOTOR                      **"
2250 PRINT " **      MOVES TRAVERSER AWAY FROM THAT PARTICULAR MOTOR                       **"
2260 PRINT " **                                                                            **"
2270 PRINT " **  -- MOTOR #1 MOVES THE PROBE UPSTREAM AGAINST THE FLOW                     **"
2280 PRINT " **  -- MOTOR #2 MOVES THE PROBE TOWARD THE ACCESS WINDOW                      **"
2290 PRINT " **  -- MOTOR #3 MOVES THE PROBE VERTICALLY DOWNWARD                           **"
2300 PRINT " ********************************************************************************"
2310 PRINT
2320 PRINT
2330 INPUT "WHICH MOTOR DO YOU WANT TO MOVE? (1,2, or 3)"; L
2340 ON L GOTO 2350, 2460, 2530
2350 PRINT
2360 PRINT
2370 PRINT "HOW FAR DO YOU WANT TO MOVE MOTOR #1?"
2380 PRINT " ********** (ENTER DISTANCE IN INCHES) **********"
2390 INPUT I1
2400 PRINT
2410 PRINT
2420 PRINT "DO YOU WANT TO MOVE ANOTHER MOTOR ALSO? (Y or N)?"
2430 INPUT C$
2440 IF C$ = "Y" THEN 2300
2450 IF C$ = "N" THEN 2600
```

```
2460 PRINT
2470 PRINT
2480 PRINT "HOW FAR DO YOU WANT TO MOVE MOTOR #2?"
2490 PRINT " ********** (ENTER DISTANCE IN INCHES) **********"
2500 INPUT I2
2510 PRINT
2520 GOTO 2410
2530 PRINT
2540 PRINT
2550 PRINT "HOW FAR DO YOU WANT TO MOVE MOTOR #3?"
2560 PRINT " ********** (ENTER DISTANCE IN INCHES) **********"
2570 INPUT I3
2580 PRINT
2590 GOTO 2400
2600 PRINT
2610 PRINT
2620 REM DISPLAY OPERATOR SELECTED MOTOR VARIABLES
2630 PRINT " ****************************************"
2640 PRINT
2650 PRINT "SUMMARY OF OPERATOR INPUTS:"
2660 PRINT "         MOTOR #1   VELOCITY = "; V1
2670 PRINT "                    ACCELERATION RAMP = "; R1
2680 PRINT "                    INCREMENTAL DISTANCE = "; I1; "INCHES"
2690 PRINT "         MOTOR #2   VELOCITY = "; V2
2700 PRINT "                    ACCELERATION RAMP = "; R2
2710 PRINT "                    INCREMENTAL DISTANCE = "; I2; "INCHES"
2720 PRINT "         MOTOR #3   VELOCITY = "; V3
2730 PRINT "                    ACCELERATION RAMP = "; R3
2740 PRINT "                    INCREMENTAL DISTANCE = "; I3; "INCHES"
2750 PRINT
2760 PRINT " ****************************************"
2770 PRINT
2780 PRINT
2790 PRINT "DO YOU WANT TO CHANGE ANY OF THESE VALUES? (Y or N)"
2800 PRINT
2810 PRINT "ENTER 'N' TO START MOTOR MOVEMENT.  ENTER 'Y' TO RETURN"
2820 PRINT "TO VARIABLE SELECTION SUBROUTINE."
2830 INPUT V$
2840 IF V$ = "Y" THEN 1360
2850 GOSUB 3060
2860 PRINT
2870 PRINT
2880 INPUT "DO YOU WANT TO INPUT ANOTHER MANUAL MOTOR MOVEMENT (Y or N)"; M$
2890 IF M$ = "Y" THEN 2140
2900 PRINT
2910 PRINT "DO YOU WANT TO INPUT COMPUTER CONTROLLED MOTOR MOVEMENT?"
2920 PRINT "       ********** NOTE!!! ********** "
2930 PRINT " ALL PREVIOUS MOTOR INCREMENT INPUTS HAVE BEEN ZEROIZED."
2940 PRINT "PROGAM WILL LET YOU CHOOSE MANUAL OR CP-CONTROLLED B.L. MOVEMENT."
2950 PRINT "******* (IF 'NO', THE PROGRAM WILL END). *******"
2960 PRINT
2970 INPUT "DO YOU WANT COMPUTER CONTROLLED MOTOR MOVEMENT (Y or N)"; N$
2980 IF N$ = "Y" THEN 1220
2990 PRINT
3000 PRINT
3010 PRINT
```

```
3020 PRINT "     ************************************"
3030 PRINT "          THE PROGRAM HAS ENDED."
3040 PRINT "     ************************************"
3050 END
3060 REM   ********* MOTOR MOVEMENT SUBROUTINE **********
3070 PRINT #1, "&": PRINT #1, "E"; "C1="; C1; ":C2="; C2; ":C3="; C3
3080 PRINT #1, "I1="; I1; ":V1="; V1; ":R1="; R1;
3090 PRINT #1, ":I2="; I2; ":V2="; V2; ":R2="; R2
3100 PRINT #1, "I3="; I3; ":V3="; V3; ":R3="; R3; ":@"
3110 RETURN
3120 REM   ************************************************************
3130 PRINT
3140 REM ********* COMPUTER CONTROLLED BOUNDARY LAYER MOVEMENT *********
3150 PRINT
3160 PRINT
3170 PRINT "     ************************************************"
3180 PRINT "     **              NOTE !!!                      **"
3190 PRINT "     ** COMPUTER CONTROLLED BOUNDARY LAYER **"
3200 PRINT "     **   MOVEMENT IS PROGRAMMED WITH A    **"
3210 PRINT "     ** DEFAULTED NEGATIVE MOTOR INCREMENT **"
3220 PRINT "     **  (i.e. MOTOR #3 WILL MOVE UPWARD   **"
3230 PRINT "     **  BY ENTERING A (+) B.L. DISTANCE). **"
3240 PRINT "     ************************************************"
3250 PRINT
3260 REM SET INITIAL BL HEIGHT AND NUMBER OF DATA POINTS TO ZERO
3270 N = 0
3280 BL = 0
3290 PRINT
3300 INPUT "ENTER ESTIMATED INITIAL POINT DISTANCE ABOVE SURFACE (INCHES)"; ZIP
3310 PRINT
3320 INPUT "WHAT IS THE B.L. THICKNESS (IN INCHES) THAT YOU WANT TO MEASURE"; BL
3330 PRINT
3340 INPUT "HOW MANY DATA POINTS DO YOU WANT TO SAMPLE IN THE B.L."; N
3350 PRINT
3360 INPUT "WHICH MOTOR WILL MOVE YOU THROUGH THE B.L. (1,2, or 3)"; MN
3370 ON MN GOTO 3380, 3730, 4090
3380 PRINT
3390 PRINT
3400 REM  MOTOR 1 CP-CONTROLLED MOTOR MOVEMENT
3410 Z(0) = 0
3420 I1 = 0
3430 I2 = 0
3440 I3 = 0
3450 FOR J = 1 TO N
3460 Z(J) = BL * (1 - SIN((PI / 2) * (1 + (J - 1) / (N - 1))))
3470 STP = CINT((Z(J) - Z(J - 1)) / .000125) * .000125
3480 Z(J) = Z(J - 1) + STP
3490 I1 = -STP
3500 PRINT
3510 PRINT
3520 PRINT "   ****************************"
3530 PRINT
3540 PRINT "   DATA POINT "; J
3550 PRINT
3560 GOSUB 3060
3570 PRINT
```

```
3580 PRINT
3590 IF J = N THEN 3620
3600 INPUT "PRESS 'ENTER' FOR NEXT MOVEMENT"; MOVE$
3610 NEXT J
3620 PRINT "ALL MOVEMENTS COMPLETE"
3630 PRINT
3640 PRINT
3650 PRINT "YOU WANT TO REPOSITION TRAVERSER FOR ANOTHER MOVEMENT (Y OR N)?"
3660 PRINT
3670 PRINT "IF 'Y', THE PROGRAM WILL TAKE YOU TO MANUAL CONTROL SUBROUTINE."
3680 PRINT "IF 'N', THE PROGRAM WILL END."
3690 PRINT
3700 INPUT "ANOTHER MOVEMENT"; R$
3710 IF R$ = "Y" THEN 1290
3720 IF R$ = "N" THEN 2990
3730 PRINT
3740 PRINT
3750 REM CP-CONTROLLED MOTOR MOVEMENT FOR MOTOR 2
3760 Z(0) = 0
3770 I1 = 0
3780 I2 = 0
3790 I3 = 0
3800 FOR J = 1 TO N
3810 Z(J) = BL * (1 - SIN((PI / 2) * (1 + (J - 1) / (N - 1))))
3820 STP = CINT((Z(J) - Z(J - 1)) / .000125) * .000125
3830 Z(J) = Z(J - 1) + STP
3840 I2 = -STP
3850 PRINT
3860 PRINT
3870 PRINT
3880 PRINT "   ****************************"
3890 PRINT
3900 PRINT "   DATA POINT "; J
3910 PRINT
3920 GOSUB 3060
3930 PRINT
3940 PRINT
3950 IF J = N THEN 3980
3960 INPUT "PRESS ENTER FOR NEXT MOVEMENT"; MOVE$
3970 NEXT J
3980 PRINT "ALL MOVEMENTS COMPLETED"
3990 PRINT
4000 PRINT
4010 PRINT "YOU WANT TO REPOSITION TRAVERSER FOR ANOTHER MOVEMENT (Y OR N)?"; R$
4020 PRINT
4030 PRINT "IF 'Y', THE PROGRAM WILL TAKE YOU TO MANUAL CONTROL SUBROUTINE."
4040 PRINT "IF 'N', THE PROGRAM WILL END."
4050 PRINT
4060 INPUT "ANOTHER MOVEMENT"; R$
4070 IF R$ = "Y" THEN 1290
4080 IF R$ = "N" THEN 2990
4090 PRINT
4100 PRINT
4110 REM CP-CONTROLLED MOTOR MOVEMENT FOR MOTOR 3
4120 Z(0) = 0
4130 I1 = 0
```

```
4140 I2 = 0
4150 I3 = 0
4160 FOR J = 1 TO N
4170 Z(J) = BL * (1 - SIN((PI / 2) * (1 + (J - 1) / (N - 1))))
4180 STP = CINT((Z(J) - Z(J - 1)) / .000125) * .000125
4190 Z(J) = Z(J - 1) + STP
4200 I3 = -STP
4210 PRINT
4220 PRINT
4230 PRINT
4240 PRINT "   **************************"
4250 PRINT
4260 PRINT "   DATA POINT "; J
4270 PRINT
4280 GOSUB 3060
4290 PRINT
4300 PRINT
4310 IF J = N THEN 4340
4320 INPUT "PRESS 'ENTER' FOR NEXT MOTOR MOVEMENT"; MOVE$
4330 NEXT J
4340 PRINT "ALL MOVEMENTS COMPLETED"
4350 PRINT
4360 PRINT
4370 PRINT "YOU WANT TO REPOSITION TRAVERSER FOR ANOTHER MOVEMENT (Y OR N)?"; R$
4380 PRINT
4390 PRINT "IF 'Y', THE PROGRAM WILL TAKE YOU TO MANUAL CONTROL SUBROUTINE."
4400 PRINT "IF 'N', THE PROGRAM WILL END."
4410 PRINT
4420 INPUT "ANOTHER MOVEMENT"; R$
4430 IF R$ = "Y" THEN 1290
4440 IF R$ = "N" THEN 2990
4450 END
```

APPENDIX D. PROGRAM HWCAL

```
100 REM ********************** PROGRAM HWCAL.BAS ***********************************
110 REM
120 REM This program is used to calibrate the hot wire in the low speed wind
130 REM tunnel.  The hotwire is calibrated against a pitot/static probe
140 REM located in the free stream adjacent to the hotwire.  Pitot/static
150 REM output (delta P) is in cm of water.  Hotwire output from the IFA-100
160 REM is digitally read by a Metrabyte 16f A to D board controlled by
170 REM Labtech Notebook software.  Suggested A to D speed is 1000 Hz with a
180 REM period of 1.01 sec.  The first 1000 data points are used by this
190 REM program.  The program output file is directly compatable with
200 REM "Grapher" for plotting calibration curves and determining
210 REM conversion equations.
220 REM
230 REM ************************************************************************

240 REM ************************************************************************
250 REM
260 REM VARIABLES:
270 REM     dp  :  Pitot/static probe delta P (cm water)
280 REM     hwv :  Hotwire voltage (volts)
290 REM     vfps:  Tunnel velocity (feet per second)
300 REM     ofi :  Output file name
310 REM
320 REM ************************************************************************
1000 DIM DP(20), HWV(20)
1010 R = 53.3: REM gas constant for air
1020 G = 32.174
1030 CLS : PRINT "Enter output file name": INPUT ; OFI$
1040 OPEN OFI$ FOR OUTPUT AS #2
1050 PRINT #2, "'cm water'", "'hwv'", "'vfps'","'vhpw .5'"
1060 I = 1
1070 PRINT : PRINT "Enter cm of water for calibration point "; I
1080 INPUT ; DP(I)
1090 PRINT : HWV(I) = 0
1100 REM Execute A to D conversion of hotwire using Labtech Notebook "go"
1110 SHELL " nb go"
1120 REM Labtech Notebook writes output file to data.prn
1130 OPEN "c: nb data data.prn" FOR INPUT AS #1
1140 FOR J = 1 TO 1000
1150 INPUT #1, HWV
1160 HWV(I) = HWV(I) + HWV
1170 NEXT J
1180 CLOSE #1
1190 HWV(I) = HWV(I) / 1000
1200 CLS : PRINT "hvw for point "; I; " = "; HWV(I)
1210 INPUT "another calibration point (y/n)"; C$
1220 IF C$ = "n" THEN GOTO 1250
1230 I = I + 1
1240 GOTO 1070
1250 CLS : INPUT "Enter ambient temperature (Deg F)"; T
1260 T = T + 460
```

```
1270 INPUT "Enter barometric pressure (in. Hg)"; P
1280 PRINT "Wait - Writing Output Data File"
1290 P = P / 29.92 * 14.7 * 144
1300 RO = P / (R * T * G)
1310 FOR J = 1 TO I
1320 VFPS = SQR(2 * DP(J) * 2.048 / RO)
1330 PRINT #2, DP(J), HWV(J), VFPS, HWV(J) 2, SQR(VFPS)
1340 NEXT J
1350 CLOSE #2
1360 CLS : INPUT "Another calibration run (y/n)"; C$
1370 IF C$ = "y" THEN GOTO 1000
1380 PRINT "BYE"
1390 END
```

APPENDIX E. PROGRAM BLDATA

```
100 REM ****************** PROGRAM BLDATA.BAS ************************************
110 REM
111 REM This driver program controls the analog-to-digital data acquisition
112 REM process using the software package LABTECH NOTEBOOK in conjunction
113 REM with the Metrabyte 16f A to D card.
140 REM This progarm allowes the user to enter the number of data points
150 REM for the run.  It initiates the data collection by running LABTECH
160 REM NOTEBOOK program "go" directly from the nb directory via dos
170 REM command.  This control program also generates incremental names for
180 REM the data files.
190 REM
200 REM ************************************************************************************
1000 CLS
1010 INPUT "Enter number of data points for this wing position (1-99)"; N
1020 IF (N < 1) OR (N > 99) GOTO 1010
1030 REM *** generating string segments for data file names
1040 B$ = MID$(STR$(1), 2): REM string number "1"
1050 E$ = MID$(STR$(N), 2): REM ending string number "n"
1060 X$ = "XXXXXX"
1070 EX$ = ".DAT"
1080 CLS
1090 PRINT "Data files will be incremented from:"
1100 PRINT (X$ + B$ + EX$); "  To  "; (X$ + E$ + EX$)
1110 PRINT
1120 PRINT "Enter common data file id (XXXXXX) for this run
1125 PRINT "(Six characters maximum - no extension"
1130 INPUT F$
1140 IF LEN(F$) > 6 OR LEN(F$) < 1 GOTO 1120
1150 CLS
1160 PRINT N; "Data files will be generated and incremented as follows:"
1170 PRINT (F$ + B$ + EX$); "  To  "; (F$ + E$ + EX$)
1180 PRINT
1190 INPUT "Are the number of points and file names ok (y n)"; C$
1200 IF C$ = "n" GOTO 1000
1210 IF C$ = "y" GOTO 1230
1220 GOTO 1190
1230 CLS
1240 FOR I = 1 TO N
1250 PRINT : PRINT "ready for point "; I; " of "; N; " points": PRINT
1260 PRINT "Insert New Data Disk in Drive A"
1270 PRINT "Strike any key when ready"
1280 BEEP
1290 C$ = INKEY$: IF C$ = "" GOTO 1290
1300 REM *** generating incremented data file name
1310 IF (I > 10) OR (I = 10) THEN I$ = MID$(STR$(I), 2)
1320 IF (I < 10) THEN I$ = (MID$(STR$(0), 2) + MID$(STR$(I), 2))
1330 FI$ = (F$ + I$ + EX$)
1340 PRINT "Doing A to D conversion and writing data file "; FI$
1350 SHELL "cd nb": REM DOS command to ensure system in nb subdirectory
1360 SHELL "go": REM executing labtech notebook via DOS from NB subdir
1370 R1$ = "ren A: DATA.PRN "
```

```
1380 R2$ = R1$ + FI$
1390 SHELL R2$
1400 NEXT I
1410 INPUT "Another run"; C$
1420 IF C$ = "y" GOTO 1000
1430 PRINT "BYE"
1440 END
```

APPENDIX F. PROGRAM CONVERT

```
      PROGRAM CONVERT
C*****************************************************************************
C
C  THIS PROGRAM CONVERTS THE RAW HOT-WIRE VOLTAGE AND POSITION SENSOR
C  VOLTAGE INTO VELOCITY DATA AN A SYNCHRONIZATION PULSE.  INPUT DATA
C  IS IN ASCII INTEGER FORM WITH THE INTEGER VALUES 0 TO 4095 REP-
C  RESENTING 0 TO 5 VOLTS.  THE BAR SENSOR VOLTAGE WAS PROCESSED TO
C  RETURN A  VALUE OF 2 AT THE EXACT CENTER OF THE POSTION SENSOR
C  PULSE AND A 0 ELSEWHERE.  THE HOT-WIRE VOLTAGE TO VELOCITY CONVER-
C  SION CONSTANTS ARE OBTAINED FROM THE HOT-WIRE CALIBRATION DATA
C  FROM PROGRAM HWCAL.BAS.
C
C*****************************************************************************
C
      REAL HWV, PROP, A, B, PPROP, TIC
      CHARACTER*12 INFILE, OUTFILE, CHOICE*2
      INTEGER I,J,K
      DIMENSION DAT (50000,2)
      A = 0
      B = 0
C
5     PRINT '(/A )',' ENTER THE INPUT DATA FILE NAME:'
      READ (*,'(A)') INFILE
C
      PRINT '(/A )', ' ENTER THE OUTPUT DATA FILE NAME:'
      READ (*,'(A)') OUTFILE
C
      OPEN (10, FILE=INFILE, STATUS = 'OLD')
      OPEN (11, FILE=OUTFILE, STATUS = 'NEW')
C
      PRINT '(/A )', ' CONVERSION FROM HWV TO VELOCITY IS OF THE FORM:'
      PRINT '(/A )', ' VEL = (A * HWV**2 + B) ** 2'
      PRINT '(/A/)',  ' . . . '
      WRITE (*,*) ' A = ', A
      WRITE (*,*) ' B = ', B
      PRINT '(/A/)', ' CHANGE A OR B (Y/N) ? '
      READ (*,'(A)') CHOICE
      IF (CHOICE .EQ. 'N') GOTO 7
      PRINT '(/A )', ' A = '
      READ (*,*) A
      PRINT '(/A )', ' B = '
      READ (*,*) B
C
7     PPROP=0
      PRINT '(/A/)', ' READING DATA INTO ARRAY - WAIT'
      DO 10 J = 1, 50000
      READ (10, *, END=50, ERR=50) HWV, PROP
      DAT (J,1) = HWV
      DAT (J,2) = PROP
10    CONTINUE
```

```
C
50    CONTINUE
      PRINT '(/A/)', ' DOING DATA CONVERSION - WAIT SOME MORE'
      DO 20 I = 1, J-1
      DAT (I,1) = (A * (DAT (I,1) * 5. / 4095.) ** 2 + B) ** 2
      PROP = DAT (I,2) * 5. / 4095.
      TIC = 0.
      IF (PROP .GT. 1.5 .AND. PROP .LT. 2. .AND. PROP .LT. PPROP)
     +TIC = 2.
      PPROP = PROP
      DAT (I,2) = TIC
20    CONTINUE
C
      PRINT '(/A/)', ' WRITING OUTPUT FILE - ALMOST DONE!'
      DO 30 I = 1, J-1
      WRITE (11,80) DAT (I,1), DAT (I,2)
80    FORMAT (F11.4, F5.0)
30    CONTINUE
C
      WRITE (*,*) ' # OF CONVERSIONS IS :', (J-1) * 2
      CLOSE (10)
      CLOSE (11)
      WRITE (*,*) ' ANOTHER RUN (Y/N) ?'
      READ (*,'(A)') CHOICE
      IF (CHOICE .EQ. 'Y') GOTO 5
C
      END
```

LIST OF REFERENCES

1. Mueller, T.J., *Low Reynolds Number Vehicles,* AGARDograph 288, AGARD-AG-288, pp. 1-16, February 1985.

2. Meier, H.U., and Kreplin, H.P., "Influence of Freestream Turbulence on Boundary-Layer Development," *AIAA Journal,* Vol. 18, No. 7, pp. 11-15, January 1980.

3. National Aeronautics and Space Administration Final Report (NASA-CR-180638), *The Influence of Free-Stream Turbulence on Separation of Turbulent Boundary Layers in Incompressible, Two-Dimensional Flow,* by J.L. Potter, and others, pp. 1-42, 22 December 1986.

4. Kindelspire, D.W., *The Effects of Freestream Turbulence on Airfoil Boundary Layer Behavior at Low Reynolds Numbers,* Master's Thesis, Naval Postgraduate School, Monterey, CA, September 1988.

5. Brendel, M., *Experimental Study of the Boundary Layer on a Low Reynolds Number Airfoil in Steady and Unsteady Flow,* Ph.D. Dissertation, University of Notre Dame, Notre Dame, IN, May 1986.

6. Howard, Richard M., *An Investigation of the Effects of the Propeller Slipstream on a Wing Boundary Layer,* Ph.D. Dissertation, Texas A&M University, College Station, TX, May 1987.

7. Department of Aeronautics and Astronautics, *Laboratory Manual for Low-Speed Wind-Tunnel Testing,* Naval Postgraduate School, Monterey, CA, October 1983.

8. TSI Incorporated, *IFA 100 System Instruction Manual,* Revision C, St. Paul, MN, August 1987.

9. Brendat, J.S. and Piersol, A.G., *Engineering Applications of Correlation and Spectral Analysis*, John Wiley and Sons, New York, NY, 1980.

10. Johnson, D.K., *A Data Analysis System for Unsteady Turbulence Measurements*, Master's Thesis, Naval Postgraduate School, Monterey, CA, September 1988.

11. Vagt, J.D., and Fernholz, H.H., "A Discussion of Probe Effects and Improved Measuring Techniques in the Near-Wall Region of an Imcompressible Three-Dimensional Turbulent Boundary Layer," *Turbulent Boundary Layers - Experiments, Theory and Modelling*, AGARD Conference Proceedings No. 271, pp. 10-1 to 10-17, January, 1980.

12. Roane, D.P., Jr., *The Effect of a Turbulent Airstream on a Vertically Launched Missile at High Angles of Attack*, Master's Thesis, Naval Postgraduate School, Monterey, CA, December 1987.

13. Thermo-Systems Inc., *Hot Wire - Hot Film - Ion Anemometer Systems*, CAT, FORM 6560375, St. Paul, MN, 1975.

14. American Institute of Aeronautics and Astronautics, AIAA-87-1259, *Influence of a Heated Leading Edge on Boundary Layer Growth, Stability, and Transition*, by Landrum, D.B., and Macha, J.M., pp. 1-9, June 1987.

15. Bradshaw, P., *An Introduction to Turbulence and its Measurement*, Pergamon Press, New York, NY, 1971.

16. Narasimha, R., and Sreenivasan, K.R., "Relaminarization of Fluid Flows," *Advances in Applied Mechanics*, Vol. 39, pp. 246-256, Academic Press, Inc., New York, NY, 1979.

INITIAL DISTRIBUTION LIST

		No. Copies
1.	Defense Technical Information Center Cameron Station Alexandria, VA 22304-6145	2
2.	Library, Code 0142 Naval Postgraduate School Monterey, CA 93943-5002	2
3.	Chairman Department of Aeronautics and Astronautics, Code 67 Naval Postgraduate School Monterey, CA 93943-5000	2
4.	Commander Naval Air Systems Command Washington, DC 20360	1
5.	Commandant (G-PTE-1) United States Coast Guard Washington, DC 20593-0001	2
6.	NASA Langley Research Center MS 185 Technical Library Hampton, VA 23665	1
7.	NASA Ames Research Center Technical Library Moffett Field, CA 94035	1
8.	Dr. Bruce J. Holmes Head, Flight Applications Branch NASA Langley Research Center MS 247 Hampton, VA 23665	1
9.	Dr. S. J. Miley c/o Aerospace Engineering Dept. Texas A & M University College Station, TX 77843	1
10.	Mr. Thomas Momiyama Naval Air Systems Command Aircraft Division - Research and Technology Air 931 Washington, DC 20360	1

11. Mr. Harry Berman 1
Naval Air Systems Command
Aircraft Division - Research and Technology
Air 931
Washington, DC 20360

12. Mr. Donald K. Johnson 1
Air Force Flight Test Center
6520 Test Group/ENF
Edwards, AFB, CA 93523

13. Prof. R. M. Howard 10
Department of Aeronautics and Astronautics, Code 67HO
Naval Postgraduate School
Monterey, CA 93943-5000

14. LCDR Robert W. Renoud 2
USCG Aircraft Repair and Supply Center
Elizabeth City, NC 27909-5001

Thesis
R3457
c.1
Renoud
Boundary layer response to an unsteady turbulent environment.